Development of an improved ramped pyrolysis method for radiocarbon dating and application to Antarctic sediments

Simon Reeve

A thesis submitted to
Victoria University of Wellington
in partial fulfilment of the requirements for the degree of
Master of Science
in Geology

Antarctic Research Centre
Victoria University of Wellington
August 2019

Abstract

Archives of the retreat history of the Antarctic Ice Sheet since the Last Glacial Maximum (~20,000 years ago) are preserved in marine sediment cores from around the margins of Antarctica, but accurate dating methods remain elusive in many areas. Radiocarbon dating of key lithofacies transitions indicative of grounding-line retreat is problematic due to pervasive reworking issues in glacimarine sediments. Bulk sediment material can be radiocarbon dated but yields ages which are not indicative of the time of sedimentation due to the presence of reworked carbon material from pre-Last Glacial Maximum times. Consequently, development of methods to date only the autochthonous carbon component of these sediments are required to date the retreat of the Last Glacial Maximum ice sheet in Antarctica.

A new radiocarbon dating capability has been developed at Rafter Radiocarbon Laboratory (RRL), National Isotope Centre, GNS Science, Lower Hutt, in the course of this study. This has entailed designing, building and testing a ramped pyrolysis (RP) system, in which sedimentary material is heated from ambient to ~1000°C in the absence of oxygen (pyrolysed), with the carbon liberated during pyrolysis being combined with oxygen at a temperature of ~800°C to produce CO_2. The amount of CO_2 produced is measured by a gas analyser and the CO_2 is captured in a vacuum line. The method exploits the thermochemical behaviour of degraded organic carbon. Organic carbon which has been least degraded with time breaks down earliest under pyrolysis, so CO_2 captured from this fraction most closely approximates the time of deposition of the sediment. CO_2 captured at higher temperatures represents more degraded carbon-containing fractions and yields older ages.

The RP system includes a gas delivery system to deliver ultra-high purity He (carrier gas) and O_2, a furnace system in which to pyrolyse sample material and oxidise the liberated carbon, a CO_2 detection system to measure the CO_2 produced and a vacuum line system to enable simultaneous collection and processing of CO_2. The RRL system was based on the design developed by Dr Brad Rosenheim (University of South Florida (USF)), the originator of the first RP system at the National Ocean Sciences AMS Facility (Woods Hole Oceanographic Institution, Massachusetts, USA), who also provided guidance in this thesis. As part of the study, a visit to USF was undertaken, with sediment samples from Crystal Sound, Antarctic

Peninsula being processed in the USF RP system. CO_2 collected from RP processing was radiocarbon dated at RRL.

The scope of this thesis was to develop and build the RRL RP system, and numerous tests were conducted during this process and are presented in this thesis. As part of this, sediment samples from Crystal Sound were also processed on the RRL RP system, and an interlaboratory comparison was conducted on the same materials processed independently through both the USF and RRL RP systems. In the development and testing of the RRL system, numerous issues were identified and a set of operating protocols developed. Due to time constraints and the scope of this thesis, interlaboratory comparisons were limited in number, but initial results show good reproducibility, and that ramped pyrolysis captured significantly younger carbon populations in both the USF and RRL RP systems than methods using bulk sediment dating alone. Within uncertainties, the ages of the youngest and oldest splits from RP processing of the same material on both systems were indistinguishable.

Acknowledgements

Thanks to my supervisors Jocelyn Turnbull, Rob McKay and Richard Levy for consistent guidance and encouragement, and for asking the challenging questions. Without their support, the project could not have been completed. Thanks also to Tim Naish, for first setting me off on a radiocarbon path.

Special thanks are due to collaborator Brad Rosenheim, whose pioneering work with ramped pyrolysis underlies this project. Without his input, the work involved in developing an RP system at RRL would have been vastly greater. Thanks also to USF students Ryan, Theresa, Carey and Dylan, for showing me the ropes working the USF RP system.

For helping me grasp the practicalities of radiocarbon dating, thanks to the RRL team, Albert, Helen, Jenny, Jeremy, Julia, Margaret and especially Cathy, who takes up the baton with the RP system. To GNS experts who helped in numerous ways to get the RP system up and running, particularly Andy for conjuring flow control, Bruce and John for electrical savvy, and Steve, Grant and Ryan, for mechanical workings, many thanks. Keith, your glasscraft is the stuff of legend.

To KOPRI, the crew of the *RV Araon* and the research team under Chief Scientist Min Kyoung Lee on the 2017 Bellingshausen Sea cruise – thank you for taking me to Antarctica!

To my university teachers, particularly Brent Alloway, Cliff Atkins, Colin Wilson, James Crampton, Gavin Dunbar, James Renwick, John Townend, Julie Vry, Kevin Norton, Lionel Carter, Martha Savage, Mike Hannah, Monica Handler, Rewi Newnham, Simon Lamb, Tim Little, Tim Stern and Warren Dickinson – thank you for unfolding the geological world to me. To my fellow geology students, too many to name, but especially Aidan, Ben, Gav, Hannah, Matt, Patrick, Rex, Sebastian and Tara – thanks for including me, and helping me to see.

To my loving family, Sarah, Hana and John, without whom none of this would have been possible – words are not enough.

Icebergs in pack ice, Southern Ocean, 18 March 2017

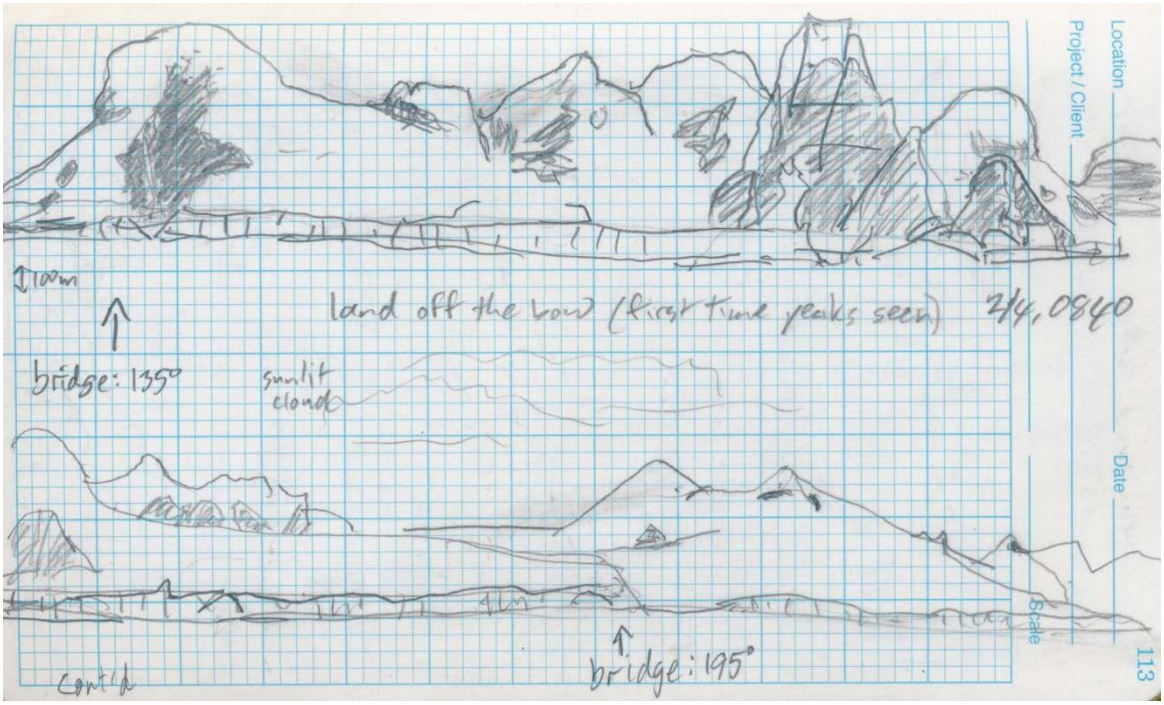

Crystal Sound: view from the Compass Deck, *RV Araon*, 2 April 2017

Contents

Table of Figures

Table of Tables

Abbreviations

^{14}C	radiocarbon
A/A/A	Acid/Alkali/Acid (pretreatment method)
AMS	accelerator mass spectrometry
BP	before present ("present" = 1950)
$[CO_2]$	concentration of CO_2 (among gases present)
CRA	Conventional Radiocarbon Age
DC	dead carbon (^{14}C-free)
EA	elemental analysis
$F^{14}C$	Fraction Modern
GC	gravity core
LGM	Last Glacial Maximum
$/N_2$	liquid nitrogen
MC	modern carbon
Ox-I	Oxalic Acid I, $C_2H_2O_4$
RP	ramped pyrolysis
RRL	Rafter Radiocarbon Laboratory
RTS	ratio to standard
SD	standard deviation
ST	sealed tube
TOC	total organic carbon
UHP	ultra high purity
USF	University of South Florida

1 Introduction

1.1 Project summary – objectives

This study aims to establish a ramped pyrolysis (RP) radiocarbon dating capability at Rafter Radiocarbon Laboratory (RRL), GNS Science, New Zealand. This entails designing, building and testing an RP CO_2 collection system, with input and assistance from advisors, experts at GNS Science and collaborator Dr Brad Rosenheim, who currently runs a laboratory dedicated to an RP system at the College of Marine Sciences, University of South Florida.

The steps of this study:

1. Design of RP system – learning about existing systems, potential adaptations and improvements over existing system.

2. Construction and testing of components (gas delivery, furnaces and temperature control, CO_2 detection, vacuum and processing system).

3. Testing of pyrolysis system – identifying problems; CO_2 traces and repeatability.

4. Testing and diagnosis of blanks and contamination – standard processing and measurement.

5. Comparison with USF system – samples run in both laboratories.

Stratigraphic and paleoclimate interpretations are outside the scope of this thesis.

1.2 Context

Future sea level rise is a pressing concern in today's warming world (e.g. IPCC, 2014). Under high emissions scenarios (Representative Concentration Pathway 8.5), global mean sea level is projected to rise by 0.52m to 0.98m relative to sea level in the period 1986–2005 (IPCC, 2014). The largest uncertainties in future sea level projections are related to warming and meltwater contributions from the Antarctic Ice Sheet (AIS), which are not well understood,

due to complex ice sheet dynamics and the slow equilibrium-response of ice sheets to surface warming compared to that of the atmosphere or ocean (Golledge et al., 2015).

A key analogue for understanding the future behaviour of the AIS is assessing its past behaviour during past shifts in climate, including the warming since the Last Glacial Maximum (LGM, ~20,000 years BP (before present)) (Bentley et al., 2014). Since the LGM, the terminii of marine-based ice sheets around Antarctica have retreated from locations close to the continental shelf break to their present locations on the innermost shelf (Bentley et al., 2014). The timing of ice-sheet retreat can be established by dating key facies successions of diamicts, muds and diatom ooze in Antarctic marine cores, interpreted as showing the transition from grounded ice sheet to ice shelf and open marine settings, respectively (e.g. Licht et al., 1996; Domack et al., 1999; Licht and Andrews, 2002; Salvi et al., 2006; Mosola and Anderson, 2006; McKay et al., 2008, 2016; Bentley et al., 2014).

Accurate dating of layers in Antarctic sediment cores is problematic, however (Andrews et al., 1999; Anderson et al., 2014). Suitable target fossils are often lacking, due to their scarcity and poor preservation (Andrews et al., 1999). Radiocarbon dating of the carbonate in bulk sediment typically produces spuriously old radiocarbon ages due to the presence of reworked organic material in the sediments (Andrews et al., 1999). What is needed is a more sensitive method of dating key sedimentary layers which provide evidence of ice-sheet retreat around the margins of Antarctica. Datable remains in these layers are organic in origin, and the timeframe of interest is post-LGM (<20,000 years BP). For these reasons, a radiocarbon dating method would be optimal.

1.3 Radiocarbon dating

1.3.1 Radioactive decay and radiocarbon dating

Radiocarbon dating is based on decay of the radioactive carbon isotope ^{14}C. The stable carbon isotopes ^{12}C and ^{13}C are vastly more abundant than ^{14}C (Rosman and Taylor, 1998). ^{14}C is predominantly produced when cosmic rays bombard the stratosphere and cause individual ^{14}N atoms to eject a proton, resulting in the formation of a ^{14}C nucleus (Libby, 1946). ^{14}C is rapidly converted to CO_2 and enters the troposphere, atmosphere, earth,

oceans and biosphere (Anderson et al., 1947; Libby, 1956). After an organism's death, if isotopic exchange does not occur, the proportion of ^{14}C which remains is solely a function of radioactive decay (Anderson and Libby, 1951). This proportion can be used to calculate the amount of time which has elapsed since the organism died – a technique widely referred to as "radiocarbon dating" (e.g. Arnold and Libby, 1951; Libby, 1956; Taylor, 1987).

Radioactive decay can be represented mathematically as:

$$dN/dt = -\lambda N \quad [1]$$

where N is the number of atoms that disintegrate, t is time, and λ is the decay constant for the radionuclide. The half-life for a radionuclide – half the original number of radioactive atoms (N_0) that remains after time $t_{½}$ – is given by:

$$t_{½} = \ln 2/\lambda. \quad [2]$$

^{14}C decays with a half-life of ~5730 ± 40 years (the Cambridge half-life; Godwin, 1962). Earlier work had been reported using the Libby half-life of 5568 ± 30 years (Figure 1), based on an average of then-known values (Anderson and Libby, 1951). The current accepted value is 5700 ± 30 years, though recent work has found that the actual value could be 2 ± 1% shorter (Roberts and Southon, 2007).

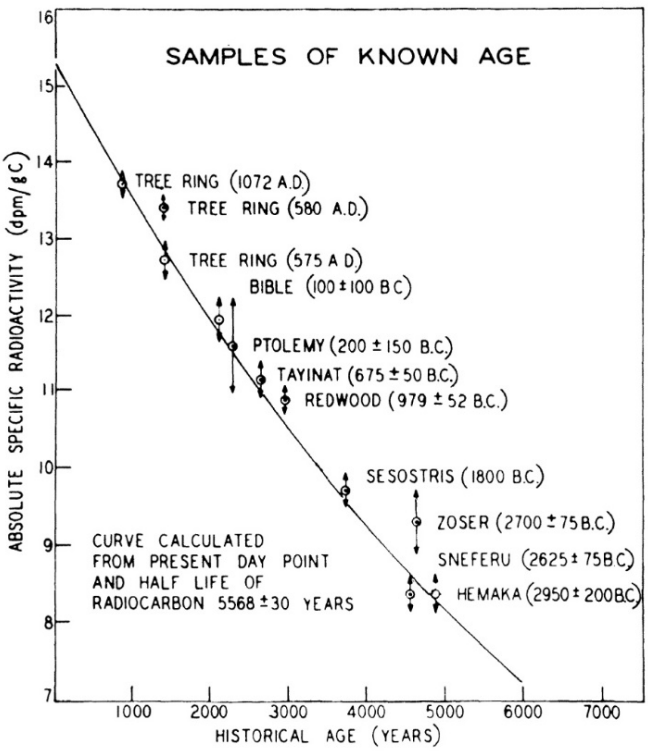

Figure 1.1 Libby's measured results for samples of known age (1956 version). Ages derived from direct counting of ^{14}C decay of samples are compared to their historical ages, known by other means. A decay curve based on the Libby ^{14}C half-life of 5568 ± 30 years shows ages expected from contemporary decay rates. (From Libby, 1956.)

In early radiocarbon dating work, radioactive decay of ^{14}C was directly counted to determine the decay rate per unit mass – the "specific activity" (A), disintegrations per minute per gram C – of the sample, with the age being calculated from this activity compared to "modern" activity (e.g. Libby, 1956; Figure 1.1). In radiocarbon dating, radiocarbon ages are determined by comparing ratios of ^{14}C to ^{12}C in the sample and a standard. A standard is a reference material whose $^{14}C/^{12}C$ proportions are well-known. For radiocarbon dating, the primary standard is Oxalic Acid I or "Ox-I", $C_2H_2O_4$, prepared from a 1955 crop of sugar beets (standard reference material SRM4990B) (Olsson, 1970).

1.3.2 Isotopic fractionation

Isotopic ratios are simpler to measure than absolute abundances of isotopes. Relative differences in isotopic ratios can be expressed in delta values, reported in per mille (‰, parts per thousand), with delta values given by:

$$\delta = [R_{std}/R_{std} - 1] \times 1000 \quad [3]$$

where R is the abundance of the heavy to light isotope as a ratio, s denotes the sample, and std denotes the standard relative to which the sample is measured (Craig, 1957).

A problem when the ^{14}C:^{12}C ratios in the sample tested and the standard are compared is that the materials are typically not the same. The carbon in carbonaceous materials will be composed of ^{12}C, ^{13}C and ^{14}C, but different types of carbonaceous materials have different characteristic relative abundances of these isotopes (Nier and Gulbransen, 1939; Craig, 1953; Figure 1.2, below). The differences are caused by fractionation, the exchange of isotopes due primarily to mass-dependent and kinetic effects. The influence of these effects varies both between reservoirs (e.g. atmosphere and ocean) and between reservoirs and organisms living within them (Hoefs, 2015; Trumbore et al., 2016a). Kinetic isotope effects are seen in fast, incomplete or one-way processes such as evaporation, diffusion and biological reactions (Sharp, 2001). Kinetic processes typically affect reaction rates, for example during photosynthesis in plants, which concentrates ^{12}C in organic matter as lighter ^{12}C reacts and diffuses faster than heavier ^{13}C (Craig, 1954).

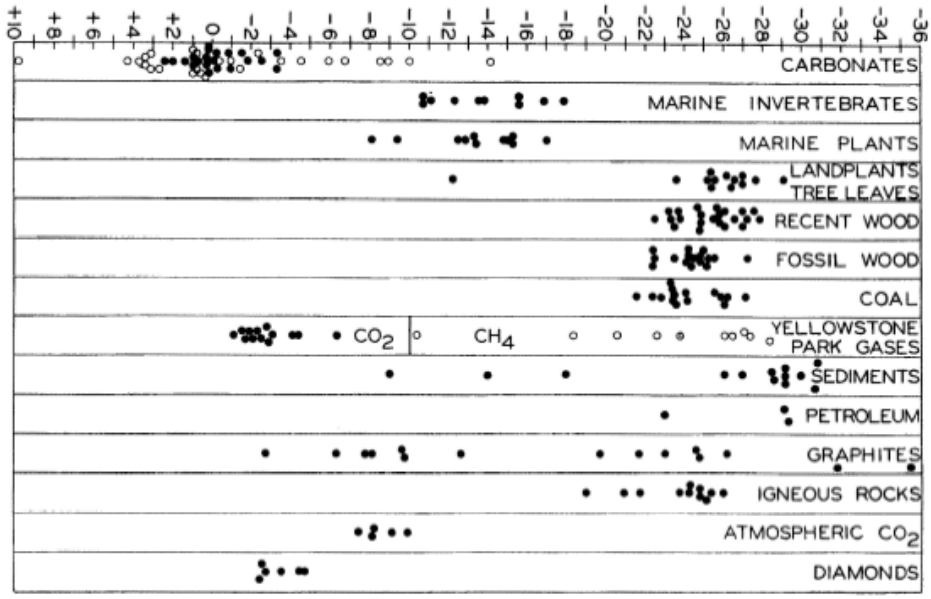

Figure 1.2 The proportions of ^{13}C to ^{12}C for various carbonaceous samples. Values are in parts per thousand (‰). Values for marine carbonates ("carbonates") cluster near zero, as the standard for comparison is itself a marine carbonate, while proportions for terrestrial wood typically cluster around –25‰. (From Craig, 1953.)

The difference in characteristic relative isotopic abundances for different types of materials applies not only to the abundance of ^{13}C relative to ^{12}C (as in Figure 1.2) but also to the abundance of ^{14}C relative to ^{12}C. For this reason, the difference in ^{13}C fractionation between the sample and standard must be accounted for before their ^{14}C:^{12}C ratios can be meaningfully compared (Stuiver and Polach, 1977). ^{13}C values as used in radiocarbon dating are "normalised" (scaled) so that they are expressed relative to terrestrial wood rather than to marine carbonate. The postulated $\delta^{13}C$ mean value of terrestrial wood is –25‰, so for radiocarbon dating purposes, ^{13}C values of samples are effectively re-zeroed with respect to this terrestrial wood value.

A measured ratio of ^{13}C relative to ^{12}C is expressed as $\delta^{13}C$. The original reference standard for isotopic measurements of ^{13}C relative to ^{12}C is Pee Dee Belemnite (PDB) (Urey et al., 1951; Craig, 1957), now exhausted. The current standard is the secondary standard Vienna PDB (VPDB; Coplen, 1994). $\delta^{13}C$ values are conventionally measured relative to one of these standards (Stuiver and Polach, 1977).

Normalised ^{14}C values take into account the differing $\delta^{13}C$ values of different samples. That is, normalised ^{14}C values are calculated on the basis of normalised ^{13}C values. Normalised ^{14}C values are given by:

$$[^{14}C/^{12}C]_{s[-25‰]} = [^{14}C/^{12}C]_{s[\delta‰]} \times [(1 + (-25/1000))/(1 + \delta/1000)]^2 \qquad [4]$$

where δ denotes the ^{13}C value of the sample s (Stuiver and Robinson, 1974).

The exponent 2 in formula [4] reflects the approximately doubled fractionation of ^{14}C compared to ^{13}C, both relative to ^{12}C (Craig, 1954). This is because the fractionation of ^{14}C seen in a sample is approximately twice the fractionation of ^{13}C, as the difference in mass between ^{12}C and ^{14}C is approximately twice the difference in mass between ^{12}C and ^{13}C (Craig, 1954). (Fahrni et al. (2017) find that carbon fractionation ratios for a wide variety of biogeochemical processes is better approximated by the exponent 1.9, but advise against using this exponent so that reporting of ^{14}C dates remains consistent.)

1.3.3 Conventional Radiocarbon Ages

A conventional manner of reporting radiocarbon dates has been adopted by the radiocarbon community. This allows dates which have been determined at different laboratories at different times to be compared. The fundamental radiocarbon age reported is the Conventional Radiocarbon Age (CRA; Stuiver and Polach, 1977). A CRA is based on the adoption of a number of key assumptions. These are:

- Use of the Libby half-life of 5568 years (with its mean life of 8033 years)
- Atmospheric ^{14}C levels have not changed over time
- Isotopic fractionation in all samples is normalised to a base of $\delta^{13}C = -25‰$
- Radiocarbon ages are given in ^{14}C years before 1950 (Before Present (BP))
- The standard for comparison of ^{14}C levels is Ox-I

The second assumption is known to be incorrect. Since the Industrial Revolution, the burning of fossil fuels has introduced ^{14}C-free carbon into the atmosphere (Suess, 1955). So pre-Industrial Revolution ^{14}C levels in the atmosphere differed from those today, and contemporary levels continue to change. Further, artificial ^{14}C was introduced into the atmosphere by atom bomb testing from the 1940s to the 1960s (the "bomb effect"; de Vries, 1958). So ^{14}C levels in the atmosphere are not invariant over time.

Because of the changes in atmospheric ^{14}C levels in the twentieth century, CRAs are calculated on the basis of the specific activity of a wood sample (tree-ring) from 1890 (Stuiver and Polach, 1977). As noted, the primary standard for assessment of a CRA is Ox-I (Olsson, 1970). But Ox-I dates from 1955. To make the Ox-I activity represent the activity of 1890 wood, its value is calibrated to 95% of its 1950 activity (Stuiver and Robinson, 1974; Stuiver and Polach, 1977). As noted above, $\delta^{13}C$ values of samples are by convention normalised to –25‰ (mean terrestrial wood value) with respect to PDB. But the actual $\delta^{13}C$ value of Ox-I with respect to PDB is –19‰. So for CRAs, the Ox-I activity is normalised to –19‰ with respect to PDB (Stuiver and Robinson, 1974).

A CRA is given by:

$$t = -8033 \ln [A_{SN(1950)}/A_{ON(1950)}] \quad [5]$$

where t is the age in ^{14}C years, $A_{SN(1950)}$ is the normalised sample activity and $A_{ON(1950)}$ is the normalised standard (Ox-I) activity (Stuiver and Polach, 1977). As explained above, the normalised activity of the Ox-I standard is 95% of its calculated 1950 activity, with its $\delta^{13}C$ set at –19‰ with respect to PDB (Stuiver and Robinson, 1974; Stuiver and Polach, 1977). The absolute international standard activity is given by

$$A_{abs} = A_{ON}e^{\lambda(y-1950)} \quad [6]$$

where y is the year of measurement and decay constant $\lambda = 1/8267\ yr^{-1}$ (Stuiver and Polach, 1977). 8267 years is the Cambridge mean ^{14}C life (Godwin, 1962). Both the Libby half-life (5568 ± 30 years) and the Cambridge half-life (5730 ± 40 years) are inaccurate. The currently accepted value is 5700 ± 30 years, though this too is imperfect (Roberts and Southon, 2007). A CRA is therefore "untrue", but useful for its comparability.

CRAs are always reported with an associated standard error (Stuiver and Polach, 1977). The standard error accounts for measurement errors, background errors from sample processing and the error in $\delta^{13}C$ determinations (Stuiver and Polach, 1977). The error is reported as ± one standard deviation (1 SD) (Stuiver and Polach, 1977).

1.3.4 Fraction Modern

A CRA is traditionally based on the specific activity of a sample, but decay counting is both laborious and time-consuming. Libby (1956) reports that a single sample measurement would typically take 48 hours, and an important sample, up to 3 months.

Accelerator mass spectrometry (AMS), developed in the 1970s (Litherland, 1980), is quicker and more sensitive. Further, AMS can be performed with smaller-sized samples, a key consideration where datable materials are scarce. In AMS radiocarbon dating, radiocarbon ages are determined by comparing ratios of ^{14}C to ^{12}C in the sample and a standard (see 1.4.3, below).

A simple way of reporting "raw" ^{14}C:^{12}C isotopic ratios as determined by AMS is Fraction Modern ($F^{14}C$) (Donahue et al., 1990). $F^{14}C$ is derived from the fraction of the normalised ^{14}C:^{13}C ratio found in the sample compared to the same normalised ratio found in the standard. $F^{14}C$ is given by

$$F^{14}C = (^{14}C/^{13}C)_{S[-25]}/(^{14}C/^{13}C)_{1950[-25]} \quad [7]$$

where $(^{14}C/^{13}C)_{S[-25]}$ is the ^{14}C:^{13}C ratio found in the sample normalised to a base of $\delta^{13}C$ = –25‰ and $(^{14}C/^{13}C)_{1950[-25]}$ is the ^{14}C:^{13}C ratio found in the standard normalised to the same base $\delta^{13}C$ value, with both ratios being measured in the same year (Donahue et al., 1990). At RRL, both $F^{14}C$ and CRA are reported, with $F^{14}C$ (the primary measurement) being converted to CRA.

1.4 Methods used in radiocarbon dating at RRL

At RRL, radiocarbon dates are determined from AMS measurements. General RRL methods include pretreatment, combustion, graphitisation, AMS measurement, data reduction and corrections for contamination. Methods particularly relevant to sediment samples are also described.

1.4.1 Pretreatment

Pretreatment of samples is required to isolate and purify carbon to be radiocarbon dated (Trumbore et al., 2016b). Pretreatment typically includes physical and chemical pretreatment.

Physical pretreatment at RRL begins with sample identification and cleaning, if appropriate. Samples may be examined under a microscope with extraneous materials being removed. Sediment samples may be sieved to eliminate material below a given size threshold (for example, when sieving for foraminifera). Sediment samples are normally homogenised by grinding, to ensure any small sample is representative of the bulk sample. This will ensure, for example, that any components of different age are uniformly distributed throughout bulk

sediment. In an RP context, homogenising also maximises surface area of particles, which can increase subsequent CO_2 yields.

Chemical pretreatment is performed to eliminate exogenous carbon from the sample material, introduced either while the material was *in situ* or from laboratory handling (e.g. Santos and Ormsby, 2013). A common chemical pretreatment method in radiocarbon laboratories is A/A/A (Acid/Alkali/Acid), a series of weak acid and alkali washes to remove secondary carbonaceous materials such as detrital carbonates (e.g. from limestone) or humic acids (in soils), followed by immersion in an acid bath to remove any CO_2 introduced from the alkali (e.g. Santos and Ormsby, 2013).

At RRL, A/A/A pretreatment typically consists of three washes, each carried out in the same manner. For the first acid wash, a suitable amount of the sample material is transferred to a centrifuge tube and immersed in 0.5M HCl. The tube is placed in a water bath preheated to 80–85^{o}C for 30 minutes. The material is subsequently centrifuged, decanted and rinsed with deionised water, repeated until the supernatant is neutral. The alkali and final acid washes are performed in a similar manner, using 0.1 NaOH and 0.5M HCl respectively. For marine sediments, a single acid bath is appropriate, to remove detrital carbonates while minimising hydrolysis of organic material (Rosenheim et al., 2008).

RP processing at RRL includes use of wood species (kauri) in determining modern carbon contamination (see 1.4.4.1, below). A key pretreatment for wood samples is α-cellulose extraction, performed to remove lignins and other mobile fractions which may translocate carbon atoms within the wood or exchange carbon with the atmosphere, contaminating the sample (Southon and Magana, 2010).

At RRL, α-cellulose extraction includes a 30-minute acid wash (with 0.5M HCl) at 85^{o}C, a 1-hour alkali pulping treatment (with 0.5M NaOH) at 85^{o}C, a 1-hour bleaching treatment (oxidation with 4% H_2O_2) under alkaline conditions (1.5g NaOH/100mL H_2O_2) at 60^{o}C, and a further 30-minute acid wash (with 1.0M HCl) at 85^{o}C (Corran et al., in prep). The pulping and oxidation steps are repeated if required (Corran et al., in prep). The sample is centrifuged and rinsed to neutral with deionised water between treatment steps and at the end, then dried in a 50^{o}C oven (Corran et al., in prep).

1.4.2 Combustion and graphitisation

Carbon isolated by pretreatment may be converted to CO_2 by sealed tube (ST) combustion. At RRL, the ST combustion method of Turnbull et al. (2015) is followed.

Sample material is loaded into a combustion tube (9mm quartz glass tube, sealed at one end) and covered by a quartz wool plug. ~200mg of CuO pellets are added to the tube to provide an oxygen source for combustion. Ag wire is added as an agent to remove sulphides and halogens during combustion (e.g. Gurfinkel, 1987). A further quartz wool plug is added to the top of tube. The tube is connected to a vacuum line by Swagelok Ultra-Torr vacuum fittings ("cajons"), evacuated, then flame-sealed below the top quartz wool plug. The resulting sealed tube is combusted at 900°C for 2 hours. Each tube is then cracked on the RRL Combustion Processing Line, with CO_2 extracted by standard vacuum line techniques – passing the liberated gases through traps immersed in a dry ice/alcohol mix (–78°C) and liquid nitrogen (lN_2, –196°C) to remove H_2O and isolate CO_2 respectively (e.g. Turnbull et al., 2007; Xu et al., 2007).

CO_2 samples are converted to graphite at RRL following the method of Turnbull et al. (2007, 2015). CO_2 is reduced to C (graphite) with H_2 as the reducing agent and iron (Fe(II)) as the catalyst. Briefly, Fe_2O_3 (Sigma Aldrich, 99.999% purity) is pre-baked at 400°C in a Pyrex reactor tube located in a small furnace, to drive off water:

$$Fe_2O_3 + 3H_2 \rightarrow 2Fe^{2+} + 3H_2O$$

The reactor tube is connected to a vacuum line and the water evacuated. Sample CO_2 is frozen into a known-volume Pyrex collection tube by immersing the collection tube in a lN_2 bath. The collection tube is opened to vacuum to remove any remaining non-condensable gases, and the amount of CO_2 present in the tube is calculated from the gas pressure. A stoichiometric amount of hydrogen (with pressure ~2.3 times the CO_2 pressure) is added to produce the net reaction:

$$CO_2 + H_2 \rightarrow H_2O + C \text{ (graphite)}$$

The result is that graphite is formed in an iron matrix. The graphite is stored in a covered vial in a dry environment for no more than a few weeks before AMS measurement.

1.4.3 Accelerator mass spectrometry measurement

Accelerator Mass Spectrometry (AMS) is a technique for measuring the concentrations of rare isotopes. At RRL, amounts of ^{12}C, ^{13}C and ^{14}C in a sample are determined by AMS measurements, following the methods of Baisden et al. (2013) and Zondervan et al. (2015).

All materials for AMS measurement are converted to graphite and loaded onto an AMS wheel. This includes samples (unknowns), standards and blank materials. Standards (typically 6) are included in the wheel so that isotopic ratios found in the unknowns and standards can be compared. It is important that both unknowns and standards experience the same measurement conditions, so must be measured on the same wheel. Further wheel-positions are required to assess contamination that may have been introduced during laboratory processing of the samples. A modern ANU Sucrose sample (reference material IAEA C6 supplied by Australian National University, RRL laboratory number 24779/1; Polach, 1979) and a ^{14}C-free CO_2 sample are included for diagnosing contamination from graphitisation and AMS measurement alone (Baisden et al., 2013; Zondervan et al., 2015).

Graphite positioned on an AMS wheel is bombarded by heated caesium to produce a stream of carbon ions (Zondervan et al., 2015). ^{12}C, ^{13}C and ^{14}C ions are separated by mass in a magnetic field to allow a stream of any one of the ions to be selectively accelerated. Ions which mimic ^{14}C ($^{12}CH^{1-}$ and $^{13}C^{1-}$) are deselected by a bending magnet after passing through an electron stripper (Zondervan et al., 2015). The intensity of ^{12}C and ^{13}C beams is measured in Faraday cups in a vacuum chamber (Zondervan et al., 2015). ^{14}C beams are magnetically filtered before final counting (Zondervan et al., 2015). The relative ^{14}C concentration in the sample can then be compared to the relative ^{14}C concentration in standards measured on the same wheel to derive a radiocarbon age (Zondervan et al., 2015).

1.4.4 Contamination corrections

CO_2 samples of any size can be affected by the introduction of extraneous carbon (Trumbore et al., 2016b). Contaminating carbon may be “modern” (e.g. from an atmosphere leak), or

"dead" (e.g. from the presence of ^{14}C-free carbon in the catalyst used during graphitisation of a CO_2 sample) (Trumbore et al., 2016b). To diagnose contamination, materials sensitive to contamination are processed in the same manner as the sample materials, so that appropriate corrections can be made. Corrections are made after AMS measurements have been completed, when the resulting data is analysed and before a radiocarbon age (e.g. in the form of $F^{14}C$ or CRA) is determined.

1.4.4.1 Contamination in large-sized samples

At RRL, large-sized samples are those that produce 0.3mgC or more at graphitisation. To assess modern carbon contamination in large samples, "blank" material (that is, material nominally containing no ^{14}C) is processed in the same manner as the sample. Any ^{14}C subsequently detected in the blank material can be attributed to contamination introduced during processing (or measurement). No separate correction is needed for dead carbon contamination in large samples, as it is implicit in measurement of the Ox-I standard.

1.4.4.2 Contamination in small-sized samples

Correction for the introduction of contaminating carbon during processing and measurement is more complex with small-sized samples (at RRL, <0.3mgC at graphitisation). In small samples, the mass of contaminating carbon forms a greater proportion of the mass of carbon which is radiocarbon dated, so the influence of contamination on $F^{14}C$ or CRA is correspondingly greater (Santos et al., 2007). The smaller the size of the sample, the greater the effect of contamination is expected to be.

At RRL, correcting for contamination in small-sized samples follows the "modern-dead" method of Santos et al. (2007). Small blanks and standards are processed to quantify the modern and dead carbon contamination introduced by the processing method used across a range of sizes. From these measurements, a size-dependent measure of modern and dead carbon contamination is calculated. Corrections are then applied individually to each small sample processed, depending on the size of the particular sample.

1.4.5 Data reduction

Before ^{14}C:^{12}C ratios can be compared, correction for the $\delta^{13}C$ value of the sample is required. At RRL, this is determined directly from AMS counting of the stable isotopes ^{13}C and ^{12}C in each target (sample, when positioned on an AMS wheel) (Zondervan et al., 2015). ^{14}C atoms produced from each target are also counted, following the methods of Baisden et al. (2013) and Zondervan et al. (2015). From these results, ^{13}C:^{12}C and ^{14}C:^{13}C isotopic ratios are determined. Ratios in samples are measured relative to the ratio in the standard (ratio to standard, RTS).

For the standard, the ratios are calculated as the means of the ratios measured for each appropriately sized Ox-I. RTS errors and a counting error are calculated. Contamination corrections are applied. With adjustment made for the $\delta^{13}C$ values of samples, CRA and $F^{14}C$ are determined following the principles of Stuiver and Polach (1977) and Donahue et al. (1990), respectively. Calculations and determinations are made by RRL laboratory staff using RRL custom software, following the methods of Baisden et al. (2013), Turnbull et al. (2015) and Zondervan et al. (2015).

1.5 Radiocarbon dating of Antarctic sediments

Various Antarctic materials have been radiocarbon dated to give insight into the post-LGM deglacial history of Antarctica. At Terra Nova Bay in the Ross Sea embayment, for example, radiocarbon dates have been obtained for shells, seal skin, penguin bones and guano from raised beaches associated with grounding-line retreat and isostatic rebound (Baroni and Hall, 2004). Despite such a terrestrial setting, however, when materials derive from a marine environment, a marine reservoir correction must be applied (Reimer and Reimer, 2001).

1.5.1 Reservoir effects

When the reservoir a sample comes from has a different ^{14}C value than the atmosphere, an adjustment must be made in determining the radiocarbon age of the sample (Stuiver and Polach, 1977). A reservoir age (or apparent age) R(t) is the difference between the CRAs of samples contemporaneously grown in the atmosphere and the other reservoir (Stuiver et al.,

1986). The global surface ocean age-offset is 200 to 400 years, with a modelled average of 373 years over the past 9000 years (Stuiver et al., 1986). Concentrations of ^{14}C vary in magnitude both between and within different ocean water masses, however, due to the degree of vertical mixing within water masses and the locations of water mass convergence and upwelling, among other factors (Gordon and Harkness, 1992). For Antarctic waters, where upwelling is significant, R(t) is 1200 to 1300 years for the Holocene (Gordon and Harkness, 1992; Berkman and Forman, 1996). For the deep ocean, R(t) is modelled as 1554 years over the past 9000 years (Stuiver et al., 1986).

Regional variations in R(t) are expressed as ΔR (Stuiver et al., 1986). ΔR is the difference between mean R(t) for global surface ocean and the reservoir age for a given region (Stuiver et al., 1986). For the Ross Sea region, for example, ΔR has been calculated as 885 ± 45 years (Stuiver and Braziunas, 1993).

Radiocarbon years are not calendar years (Stuiver and Suess, 1966). The differences between them, empirically determined, are quantified in calibration curves (Stuiver et al., 1986). To calibrate a marine radiocarbon age (that is, convert it to calendar years), the CRA of a sample may be corrected for R(t) then calibrated using an atmospheric calibration curve, or be corrected for ΔR then calibrated using a marine calibration curve (Reimer and Reimer, 2001). The most recent marine calibration curve is Marine13 (Reimer et al., 2013). Where marine sediments are concerned, however, reservoir ages are not the only factor which must be accounted for in radiocarbon dating. There is also the issue of reworking.

1.5.2 Reworking

Where marine sediments rather than intact remains are radiocarbon dated, reworking is a significant issue. For laminated muds indicative of ice grounding line retreat, sedimentation rates are typically low (e.g. 1–5cm/kyr; McKay et al., 2008), and the carbon deposited contemporaneously with the sediment is mixed with “contaminating” pre-LGM carbon eroded from the Antarctic continent (Ohkouchi et al., 2003). This old carbon could be sourced from melting ice, from seafloor sediment winnowed and remobilised by bottom currents, from iceberg scour or from slope instability following ice sheet retreat and isostatic rebound (Domack et al., 1999; McKay et al., 2008; Subt et al., 2016, 2017). As a result, both

aged and fresh carbon co-exist in Antarctic marine sediments. When radiocarbon dates are obtained from such sediments, then, they do not reflect the sediment's age of deposition, but rather a mix of younger and older ages.

1.6 Approaches to radiocarbon dating of Antarctic sediments

Different approaches have been taken to deconstruct such unreliable ages. These include direct radiocarbon dating of fossils, compound-specific radiocarbon dating, and dating of bulk sediments.

1.6.1 Direct dating of foraminifera and marine macrofossils

A key approach to dating post-LGM geological sediment samples is by radiocarbon-dating the organic remains of fossil material contained within sediment. Reliable assessments of the potential for reworking of carbonate organisms can be made through analysis of sedimentary structures and the habitats of the fossil specimens being dated (McKay et al., 2016). But intact calcareous foraminifera are generally absent or rare in Antarctic diatom ooze and muds, due to the actions of corrosive waters (Andrews et al., 1999; Licht and Andrews, 2002). Disintegration and dissolution during long-term storage may also be a contributing factor to the scarcity of preserved foraminifera in Antarctic sediments (Jennings et al., 1995). Therefore direct dating of calcareous fossil material is usually not feasible with Antarctic sediments.

1.6.2 Compound specific dating

Compounds such as C14, C16, and C18 short-chain fatty acids are present in marine sediments, derived from various organisms (Ohkouchi et al., 2003). Compared to long-chain fatty acids, these compounds decompose rapidly, so are not representative of relict organic matter (Ohkouchi et al., 2003). Radiocarbon dating of such compounds, extracted from sediments – compound-specific ^{14}C dating (Eglington et al., 1996, 1997) – can therefore provide dates which are unaffected by the presence of reworked organic matter in sediments. This is particularly useful in an Antarctic context (Ohkouchi et al., 2003, 2008). However, the method is complex, and results in very small samples where any contamination is problematic (Eglington et al., 1996). While compound-specific dating has proved useful

with diatom oozes indicative of open ocean conditions (Yamane et al., 2014; Yokoyama et al., 2016), diatoms are sparse in sandy, muddy and silty units associated with grounding-line retreat (McKay et al., 2008), and compound-specific dating is difficult with these lithologies.

1.6.3 Bulk sediment dating

Where direct radiocarbon dating of fossil material in sediments is not possible, and sediments have low total organic carbon (TOC), a common alternative approach is to date bulk sediment material. To remove any detrital carbonate – typically originating from limestone, so not representative of the time of deposition of the sediment – the sediment is acid-treated. The remaining material is termed acid insoluble organic matter (AIOM).

The method includes immersing dried sediment sample material in acid, decanting and rinsing till the supernatant approaches neutral, extracting CO_2 from the remaining material, converting the CO_2 to graphite, and using AMS techniques to obtain radiocarbon dates from the graphite (e.g. Licht et al., 1996; Domack et al., 1999; Licht and Andrews, 2002; McKay et al., 2008). However, radiocarbon dates significantly older than the reservoir age have been obtained for Antarctic marine AIOM. For example, AIOM from Ross Sea core-top material has been found to have ages ranging from 2000 to 7000 ^{14}C years B.P. (Andrews et al., 1999).

Subtracting core-top ages from stratigraphically-lower ages obtained from horizons further down-core can provide stratigraphically ordered chronologies of key facies transitions (e.g. Andrews et al., 1999; McKay et al., 2008). An assumption in this subtraction method is that the downcore proportions of fresh and aged carbon remain consistent. However, Holocene diatom oozes are typified by high productivity and high sediment accumulation rates (Andrews et al., 1999), while with laminated muds indicative of ice grounding line retreat, a lack of primary production leads to higher proportions of reworked carbon in AIOM (Domack et al., 1999; McKay et al., 2008). Even among facies other than diatom oozes, sedimentary processes relating to the degree of reworking are likely to vary as environment and depositional conditions change (e.g. proximity to ice sheet grounding lines, bottom current strengths, iceberg abundance) (Subt et al., 2016, 2017). Ratios of fresh to aged carbon are therefore also likely to vary at different stratigraphic levels and between different facies (Subt et al., 2016, 2017).

1.6.4 Ramped pyrolysis

A new approach to dating low-TOC Antarctic marine sediments has been developed by Brad Rosenheim and colleagues, working with ideas developed by John Hayes since the 1960s (Rosenheim, personal communication). The underlying principle is that the younger component of AIOM has lower thermochemical stability than the older, diagenetically altered component. Chemical bonds in the fresh-carbon fraction break down at lower temperatures than do bonds in the more resistant forms of carbon in the older, more degraded AIOM fraction (Rosenheim et al., 2008, 2013a, 2013b). Rosenheim's method exploits this behaviour by pyrolysing AIOM through steadily increasing temperatures, so that compounds with differing thermochemical stabilities are released at differing times (Rosenheim et al., 2008, 2013a, 2013b). A temperature ramp of 5^{o}C/minute is used to pyrolyse the AIOM, with the gaseous pyrolysis products being subsequently oxidised to convert released carbon to CO_2, which is trapped cryogenically in a vacuum line in separate aliquots (Rosenheim et al., 2008, 2013a, 2013b). Each CO_2 aliquot can be individually radiocarbon dated using standard AMS techniques. This results in a suite of individual radiocarbon dates from a single AIOM sample, including ages both younger and older than a single radiocarbon date for a bulk sample. The ages for the lowest-temperature fractions have been shown to approach the ages for foraminifera at nearby stratigraphic levels, providing a more reliable estimate of the date of deposition of the sediment than ages for bulk material (Rosenheim et al., 2008, 2013a). An example of results obtained is shown in Figure 1.3.

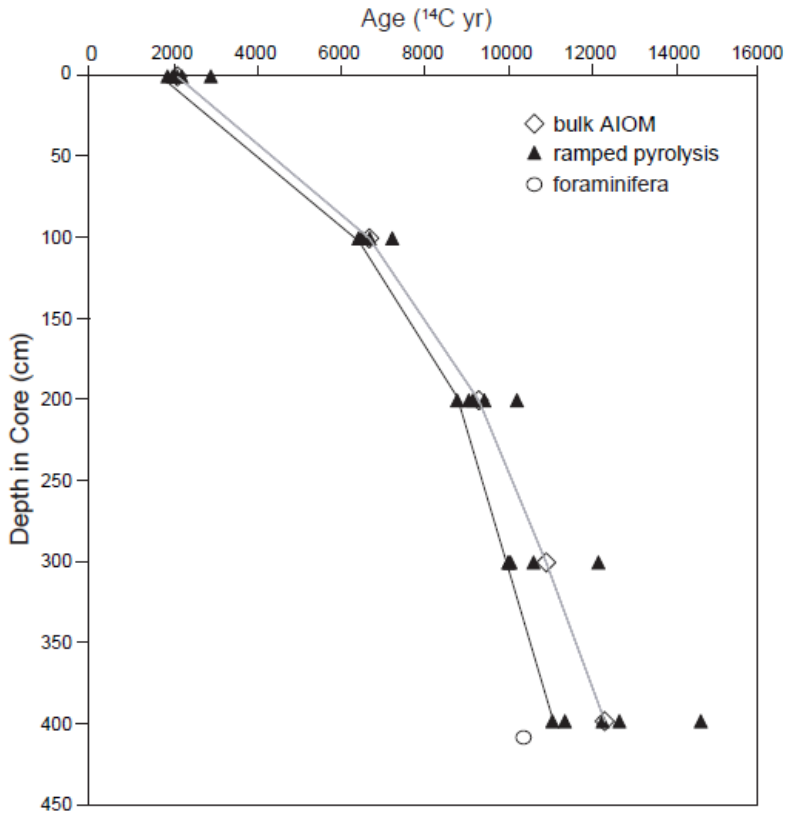

Figure 1.3 CRAs for individual CO_2 aliquots from RP processing of AIOM samples. The samples are from a marine sediment core from Hugo Island Trough, Antarctic Peninsula. The ^{14}C ages for the lowest-temperature CO_2 aliquots are consistently younger than the bulk sediment ages, while the higher-temperature aliquot ages are consistently older. The spread of RP ages for each horizon increases downcore, reflecting increased proportions of "old" reworked carbon downcore. At the deepest horizon, the youngest RP age approaches the age of a stratigraphically-nearby foraminifera. (From Rosenheim et al., 2013a.)

In addition to providing marginal marine and sub-ice shelf sediment chronologies (Rosenheim et al., 2008, 2013a; Subt et al., 2016, 2017), the RP technique has been used to investigate radiocarbon ages for different fractions of soil organic matter (Plante et al., 2013; Williams et al., 2014), to distinguish biologic and geologic carbon fractions in suspended river sediments and tundra-proximal deltaic sediments (Rosenheim and Galy, 2012; Rosenheim et al., 2013b; Schreiner et al., 2014) and to quantify contamination of shore sediments from oil spills (Prendergraft et al., 2013; Prendergraft and Rosenheim, 2014). Other applications such as radiocarbon dating of lake varves are also plausible.

2 The USF ramped pyrolysis system

The essential elements for a ramped pyrolysis system are: a vessel to hold a sample in close proximity to furnace heat while facilitating a through-flow of gases; a means for adding oxygen to the pyrolysis gases so both can be heated by a second furnace, where volatilised carbon is combusted to produce CO_2; and a means of capturing the CO_2 that results. In addition, the temperature of the pyrolysis furnace needs to be controlled so that it steadily increases. If multiple CO_2 aliquots are to taken from a single AIOM sample, then a way of determining when aliquots should be taken is also needed. Moreover, carbon is to be continuously driven off the sample as it is pyrolysed, so CO_2 will be continuously produced. The capacity is needed to interrupt the stream of gases containing the CO_2 so that an aliquot can be taken, while at the same time the gases generated continue to be captured.

To meet these requirements, the RP system constructed by Rosenheim and colleagues (Rosenheim et al., 2008) incorporates four sub-systems: a gas delivery system, a furnace system, a CO_2 detection system, and a vacuum line system.

The gas delivery system provides flow control to deliver both a flow of carrier gas (helium) at 35mL/min and a flow of oxygen combined with helium (4mL/min O_2 in 7mL/min He) (Rosenheim et al., 2008, 2013a).

The furnace system includes a first hollow furnace enclosing quartz glassware which holds the sample and allows a central through-flow of helium, the furnace providing heat to the sample along a temperature ramp to drive off volatiles as the sample partially decomposes, and a second hollow furnace enclosing a quartz glass oxidation chamber where oxygen is introduced to the flow of gases to oxidise any carbon released from the sample, producing CO_2 (Rosenheim et al., 2008).

The CO_2 detection system detects and records the amount of CO_2 flowing from the oxidation chamber, providing a basis for determining when aliquots of CO_2 should be taken (Rosenheim, personal communication).

The vacuum line system allows CO_2 to be separated from the flow of gases, which includes non-carbon-containing gases produced by the pyrolysis, such as water vapour and the driving flow of noncondensible helium. Each separated CO_2 aliquot is sealed in a Pyrex tube for later conversion into graphite, to allow radiocarbon dating (Rosenheim et al., 2008).

A more detailed description of each sub-system follows.

2.1 Gas delivery system

The gas delivery system (shown in schematic form in Figure 2.1) includes cylinders of UHP He and UHP O_2, plus a cylinder of laboratory-grade O_2 used for flame-sealing collection tubes, ⅛" outer diameter (OD) stainless steel tubing to deliver the gases to the furnace system and sealing torch, respectively, and three mass flow controllers to provide the required flow rates of helium and oxygen. The UHP He flow enters a T-junction to be divided into two flows, whose rates are independently controlled by first and second mass flow controllers downstream of the junction. From these mass flow controllers, the 35mL/min carrier flow is delivered to the glassware housing the sample, and the 7mL/min secondary flow continues to a second T-junction. The UHP O_2 flow is controlled by a third mass flow controller. Exiting the controller at 4mL/min, the UHP O_2 flow continues to the second T-junction, where it is combined with the 7mL/min UHP He flow to be delivered to the oxidation chamber.

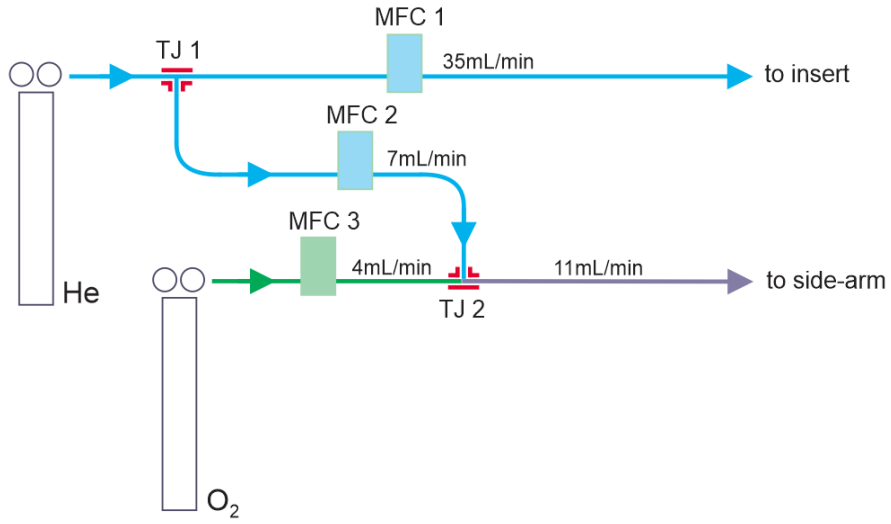

Figure 2.1 Schematic diagram of the USF RP gas delivery system. TJ designates T-junction, MFC designates mass flow controller.

2.2 Furnace system

The USF furnace system (shown in schematic form in Figure 2.2) includes glassware, cylindrical furnaces and temperature controllers. The glassware includes an outer cylindrical shell (the "reactor") and an open-ended inner cylindrical sample-container (the "insert"), with the insert secured to the reactor by a series of cajons. Helium flows continuously through the insert, in which the sample is held between plugs of quartz wool, with oxygen being introduced into the annular space between the reactor and insert tubes via a side-arm. The reactor is enclosed within the first, pyrolysis furnace, which provides heat to pyrolyse the sample at a steadily increasing temperature. At the downstream end of the insert, the reactor tapers to a thin cylindrical tube (the "oxidation chamber") in which volatiles driven off the sample and the oxygen forced through the annular space combine. Nickle, copper and platinum catalyst wires are threaded through the oxidation chamber. With consistent 800°C heating provided by the second, combustion furnace, the carbon contained in the stream of gases is combusted, and thereby oxidised to carbon dioxide.

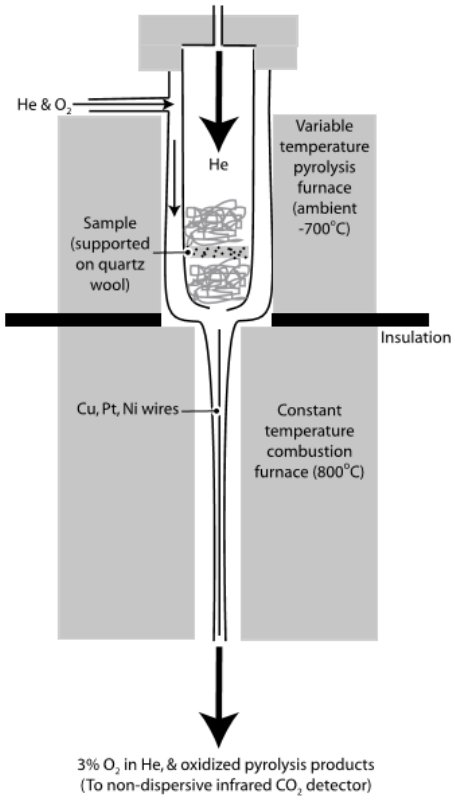

Figure 2.2 Schematic diagram of the USF RP system furnaces and glassware. Gas inputs and outputs are noted. (From Rosenheim et al., 2008.)

Cajons are used to attach gas delivery tubing to the insert, sidearm and oxidation chamber. The furnaces are ceramic fibre cylinders with internal heating wires. The cylinder bores are suitably sized to house the glassware. The furnaces are separated from each other by a barrier of insulating material (quartz welder's blanket). A copper plate is arranged at either side of the blanket to draw away heat, so as to minimise the effect of either of the furnaces on the other. The furnaces are not insulated but are located away from the vacuum line.

Furnace temperatures are controlled by temperature controllers, reliant on input from thermocouples. In the case of the upper (pyrolysis) furnace, thermocouple wires from two separate thermocouples are wound together and pushed between the reactor and the furnace bore to locate the ends of the wires as close as possible to the sample heating zone. One of the thermocouples is electrically connected to the temperature controller, while the other provides input to the computer from which the RP system is run. This allows the same continuous temperature data seen by the temperature controller to be recorded in the computer.

2.3 CO_2 detection system

Pyrolysis and combustion gases exiting the oxidation chamber are carried by ⅛" OD copper tubing to a Sable Systems Ca-10 infrared (photometric) gas analyser calibrated to measure

CO_2 (Rosenheim et al., 2013a), which provides continuous data on the concentration of CO_2 evolved in the oxidation chamber and present in the gases flowing through the analyzer to the computer. The gases are then carried by similar tubing to the vacuum line system.

2.4 Vacuum line system

The use of vacuum lines for collecting CO_2 for the purpose of radiocarbon dating is well established, and exploits the different freezing temperatures of gases such as CO_2, O_2 and H_2O (e.g. Turnbull et al., 2007; Xu et al., 2007). Water, with a high freezing temperature, can be cryongenically extracted from a gas stream by being passed through a trap immersed in a

mixture of dry ice and alcohol ("slush bath," –78°C) (e.g. Turnbull et al., 2007; Xu et al., 2007). CO_2 will not freeze at this temperature, so can pass through and be frozen downstream by passing through a trap immersed in liquid nitrogen (/N_2, –196°C) (e.g. Turnbull et al., 2007; Xu et al., 2007). At the low pressures seen in a vacuum line, gases such as O_2 and N_2 do not freeze, and can be pumped away (e.g. Turnbull et al., 2007; Xu et al., 2007).

The USF RP system vacuum line system begins with an automated six-valve two-trap assembly (shown schematically in Figure 2.3, and with photograph in Figure 2.4). The assembly is used to capture gases which freeze below the temperature of /N_2 from the stream of gases evolved from pyrolysis together with the flow of helium and combustion gases. At the same time, the assembly allows gases which are noncondensible at this temperature, including the carrier helium gas itself, to be vented to atmosphere.

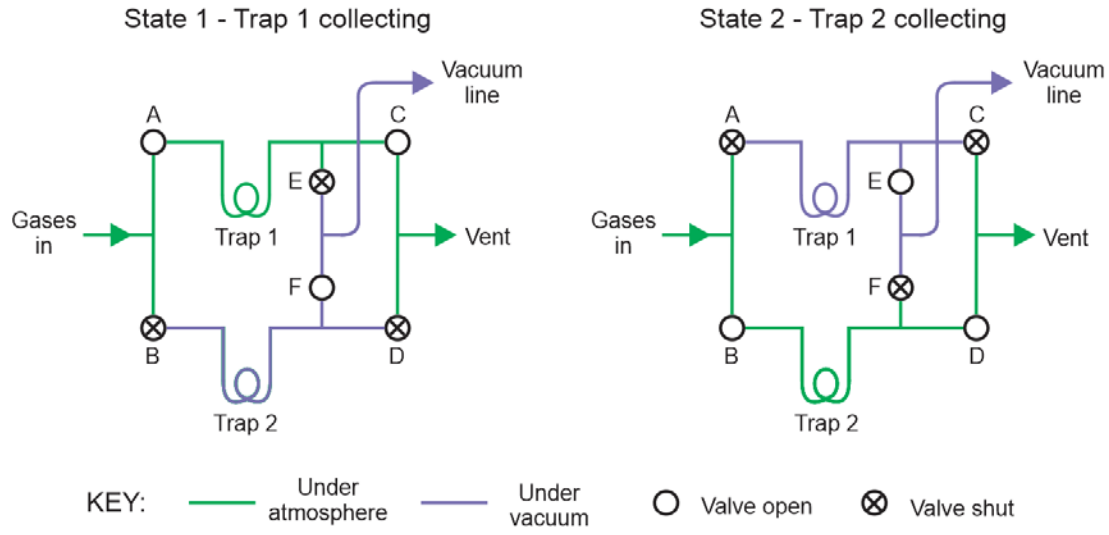

Figure 2.3 Schematic diagram of the USF RP six-valve two-trap assembly. The assembly is for collecting and transferring CO_2 produced from pyrolysis of a sample. A to F designate valves. The CO_2-collecting trap is under atmosphere (pale green); non-trapped gases (primarily the carrier gas) pass through to the vent. In the other branch of the line (purple), previously collected CO_2 is transferred to the vacuum line.

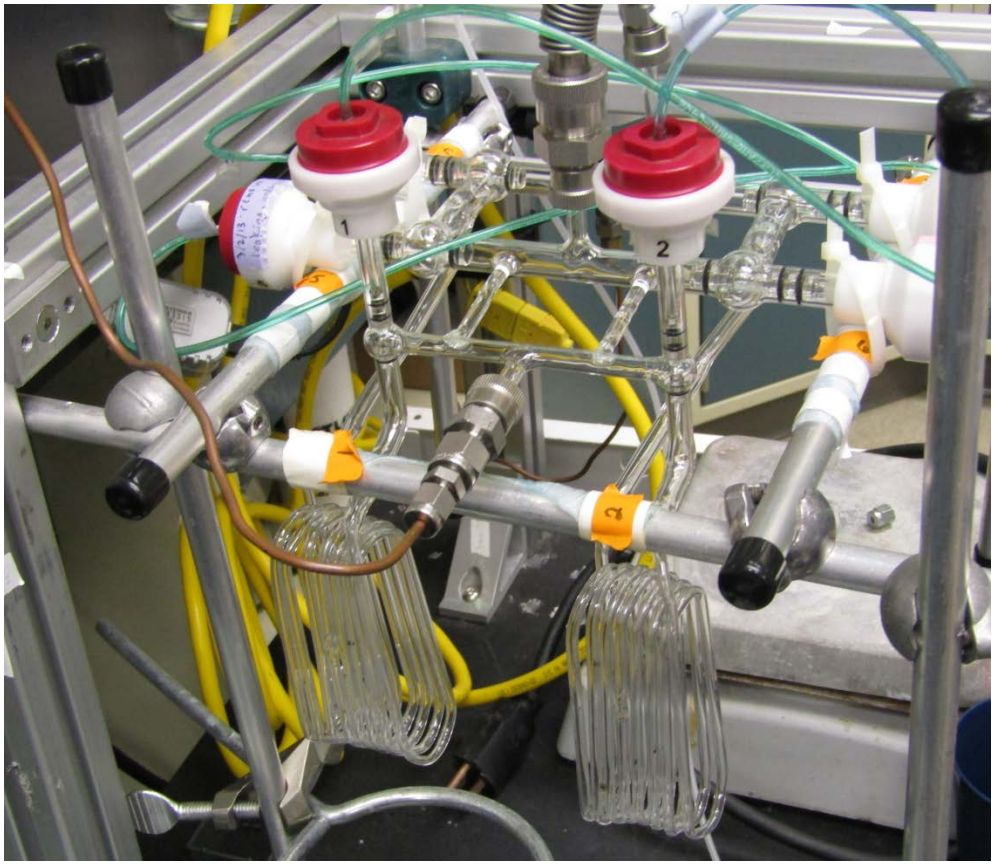

Figure 2.4 Photograph of the USF RP six-valve two-trap assembly. The assembly includes fine-bore 8-loop CO_2 traps at the front, labelled 1 and 2. Input gases arrive through copper tubing from CO_2 detector, with entry into traps 1 and 2 controlled by red-capped valves 1 and 2, respectively. Removal of trapped gases to vacuum line is by the stainless steel hose seen connected to the central glass cross-tube, and is controlled by horizontally-oriented valves 5 and 6. At the rear is a cajon connection to the vent to atmosphere, access to the vent being allowed by valves 3 and 4 (obscured). The fineness of the CO_2 trap bore ensures the interior volume of the trap is small, so that the pressure disturbance when swapping trap-states is minimised.

The assembly includes two CO_2 traps, each made of eight loops of ⅛" OD Pyrex tube with computer-operated valves. The assembly is designed to operate with one trap at atmospheric pressure while the other sees vacuum from the vacuum line, with operation switchable between traps when the valve-state is toggled. Toggling is controlled by a computer switch. Entry of atmospheric gases into the line during the change of trap-states is prevented by 1) precise control of the sequence and timing of the opening and closing of the six valves, and 2) the internal volume of the vent line (a coiled tube, ~6m long). The vent line volume is greater than the valve and trap assembly volume, so any back-flow of room air during a state-switch will not displace gases in the vent line as far back as the assembly.

The prime function of the six-valve two-trap assembly is to trap CO_2 and separates it from the other gases. At the same time, it serves as the interface between the parts of the system operating under atmospheric pressure and the parts operating under vacuum. The small trap-volume minimises pressure disturbances when the valve state is changed.

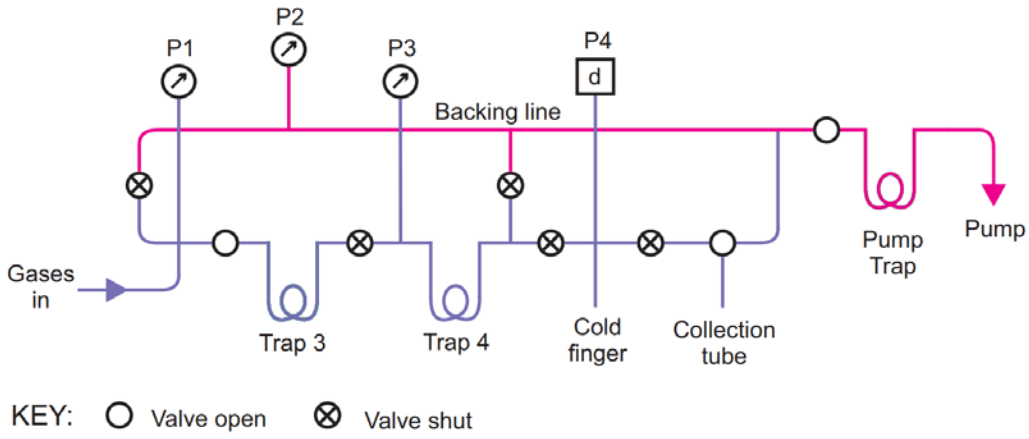

Figure 2.5 Schematic diagram of the USF RP vacuum line. P1 to P4 are pressure gauges.

A connecting line delivers CO_2 and noncondensible gases from the six-valve two-trap assembly to the vacuum line proper (shown schematically in Figure 2.5), which includes two three-loop water traps (trap 3 and trap 4), a manometric trap (a "cold finger" of known volume), a replaceable Pyrex collection tube ("break-seal"), and a pump trap. A backing line allows individual evacuation of the connecting line, the water traps, collection tube and pump trap. Analogue pressure meters are arranged to display pressure inside the connection hose or the connection hose and first water trap (first meter), the backing line (second meter), and the second water trap (third meter), with the pressure in the manometric trap shown on a digital display. Valves between traps along the primary line allow the traps to be isolated from each other so that CO_2 can be moved from trap to trap.

2.5 Operation of the USF RP system

Operation of the USF RP system is now described. Where details are unreferenced, they derive from personal observation during a visit to USF in May 2018 (see Table 8.1 for a summary of USF RP runs and maintenance undertaken in this period).

AIOM is prepared as noted above (1.6.3). For processing, a target mass of the sample is calculated with reference to its %TOC, typically determined beforehand, and a desired amount of CO_2 – normally 100µmol, to yield sufficient CO_2 overall to allow 5 splits to be independently radiocarbon-dated – using the relation:

Target mass (mg) = amount CO_2 (µmol) x 1mmol/1000µmol x 12mgC/1mmol CO_2 x 100/%TOC. [8]

The USF RP system can process a maximum of 400mg of sample, as greater masses have been shown not to pyrolyse consistently or completely, due to insufficient/inconsistent penetration of heat through the sample, or "thermal inertia" (Rosenheim, personal communication). Where the target mass is calculated to be >400mg, only 400mg is used.

The sample is weighed out and enclosed between quartz wool plugs in a clean insert, both the wool and inserts having been pre-combusted in air for 2 hours at 525°C (Rosenheim et al., 2008, 2013a). The insert containing the sample is placed in the reactor and both the reactor–insert and the insert–gas delivery tube connection secured by tightening the connecting cajons.

Running a sample through the system is managed by computer, with key parameters being recorded by hand on a run sheet. The computer displays flow rates from the mass flow controllers, the temperatures of the pyrolysis and combustion furnaces, based on thermocouple readings, the concentration of CO_2 ([CO_2], ppm) in the flow of gases from the oxidation chamber, as recorded by the CO_2 analyser, and the valve state of the six-valve two-trap assembly. The computer displays plots of the combustion furnace temperature with time and [CO_2] with time, and a numeric estimate of the accumulated amount of CO_2 (in µmol) since the counter was last zeroed.

Gases are started several minutes before a run is begun to allow [CO_2] to settle at a background level. With /N_2 raised onto the first CO_2 trap, the oxidation furnace is turned on. Collection begins immediately, as heat from the oxidation furnace may initiate the pyrolysis reaction (depending on the type of sample). The pyrolysis furnace is turned on and the

cumulative CO_2 recorder re-set to zero when the oxidation furnace temperature reaches 800°C.

For an expected yield of 100µmol CO_2, the aim is normally to take splits of the following sizes:

- Split 1: 10–12µmol CO_2
- Split 2: 15–20µmol CO_2
- Split 3: 20µmol CO_2
- Split 4: 25µmol CO_2
- Split 5: 25–30µmol CO_2

The rationale is to capture enough CO_2 to provide a reliable radiocarbon age for the first split, with splits 2 to 4 being larger, as the pyrolysis reaction will typically be proceeding faster at this stage (so taking small splits is more difficult). The final split may be larger as precision is generally less important with the high-temperature-fraction age.

The timing for splits is determined from the numeric cumulative CO_2 estimate. When a split is taken, the cumulative CO_2 counter is re-set to zero and the valve-state for the six-valve two-trap assembly is switched. Non-condensable gases are released before the trapped CO_2 is moved to the vacuum line. In the vacuum line, the CO_2 is moved by shifting lN_2 from trap to trap. Residual H_2O is captured at each move by replacing the lN_2 with slush before the CO_2 is transferred to the next trap.

When the CO_2 has reached the known-volume cold finger, the quantity of CO_2 present in the split can be calculated from the Universal Gas Law,

$$PV = nRT \qquad [9]$$

where P is pressure in pascals, V is volume in cubic meters, n is number of moles of the gas, R is the universal gas constant (8.31436 J (mole K)$^{-1}$), and T is absolute temperature (in kelvins).

This “manometric” calculation of the amount of CO_2 collected in a split is generally more reliable than the “photometric” numeric estimate. The photometric amount is recorded before the assembly valves are toggled, so the amount of CO_2 trapped is greater than the

amount recorded. It is also possible for other gases in the gas-stream to mask the presence of CO_2 in the CO_2 analyser, so the displayed values may under-represent the actual amount of CO_2 present.

After measurement, the CO_2 is transferred from the cold finger to the Pyrex collection tube, which is pre-loaded with ~40mg CuO and a strand of Ag wire. The collection tube is flame-sealed with the CO_2 trapped inside it (the tube being cooled with /N_2) while other gases are evacuated. When cool, the sealed tube is labelled with run and split number. The trapped gases are later combusted at 500^{o}C to eliminate sulphur and halogens which may have been captured together with the CO_2 (Rosenheim et al., 2008), by the method outlined at 1.4.2.

In most runs with sediment samples, the first split accumulates over about an hour from the time the pyrolysis furnace is turned on. Subsequent second, third and fourth splits typically arrive at about ten- to fifteen-minute intervals, while pyrolysis reactions are at their peak, so continuous movement of splits between traps and flame-sealing of CO_2 samples in collection tubes is required. The final split accumulates until the computer-displayed CO_2 level approaches background.

For each run, a "thermograph" showing photometric CO_2 level against pyrolysis furnace temperature is generated from run-data. Different types of samples show different characteristic thermograph shapes. A thermograph for a sediment sample typically climbs gradually from the background level, peaks with a maximum CO_2 output, then falls, usually with a shoulder on at least one of the ascending and descending limbs.

When splits are taken, valve states switch six-valve two-trap assembly (as shown in Figure 2.3). When the switch occurs, the vacuum present in the branch that switches to atmosphere pulls gas rapidly through from upstream, causing pressure to drop at the gas analyser. The optical cell of the analyser requires a stable pressure to produce a consistent estimate of concentration. When the pressure in the optical cell falls, anomalous CO_2 readings are generated. In a thermograph, they appear as abrupt two-way spikes (see Figure 3.23 for an example). These pressure-related anomalies are later removed from the data. An example of a cleaned thermograph is shown in Figure 2.6.

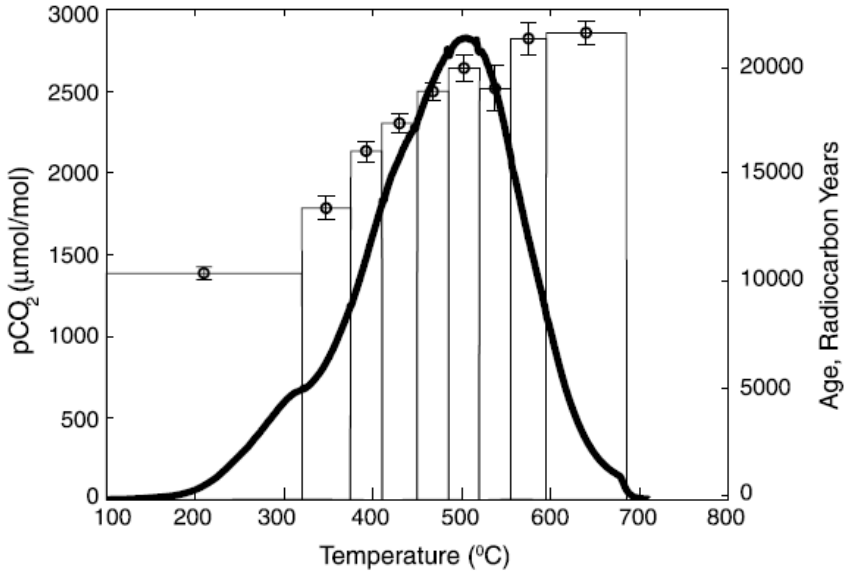

Figure 2.6 Thermograph from RP processing of a marine sediment sample from the Erebus and Terror Gulf, Antarctic Peninsula, showing CO_2 concentration with temperature (dark line). Rectangle widths show the temperature intervals over which splits were taken, while heights show their radiocarbon ages. Age uncertainty is shown as ± 1σ. (From Rosenheim et al., 2008.)

3 Development of RRL RP System

The RRL RP system is composed of 4 major sub-systems: a gas delivery system, a furnace system, a CO_2 detection system and a CO_2 collection system, as shown schematically in Figure 3.1.

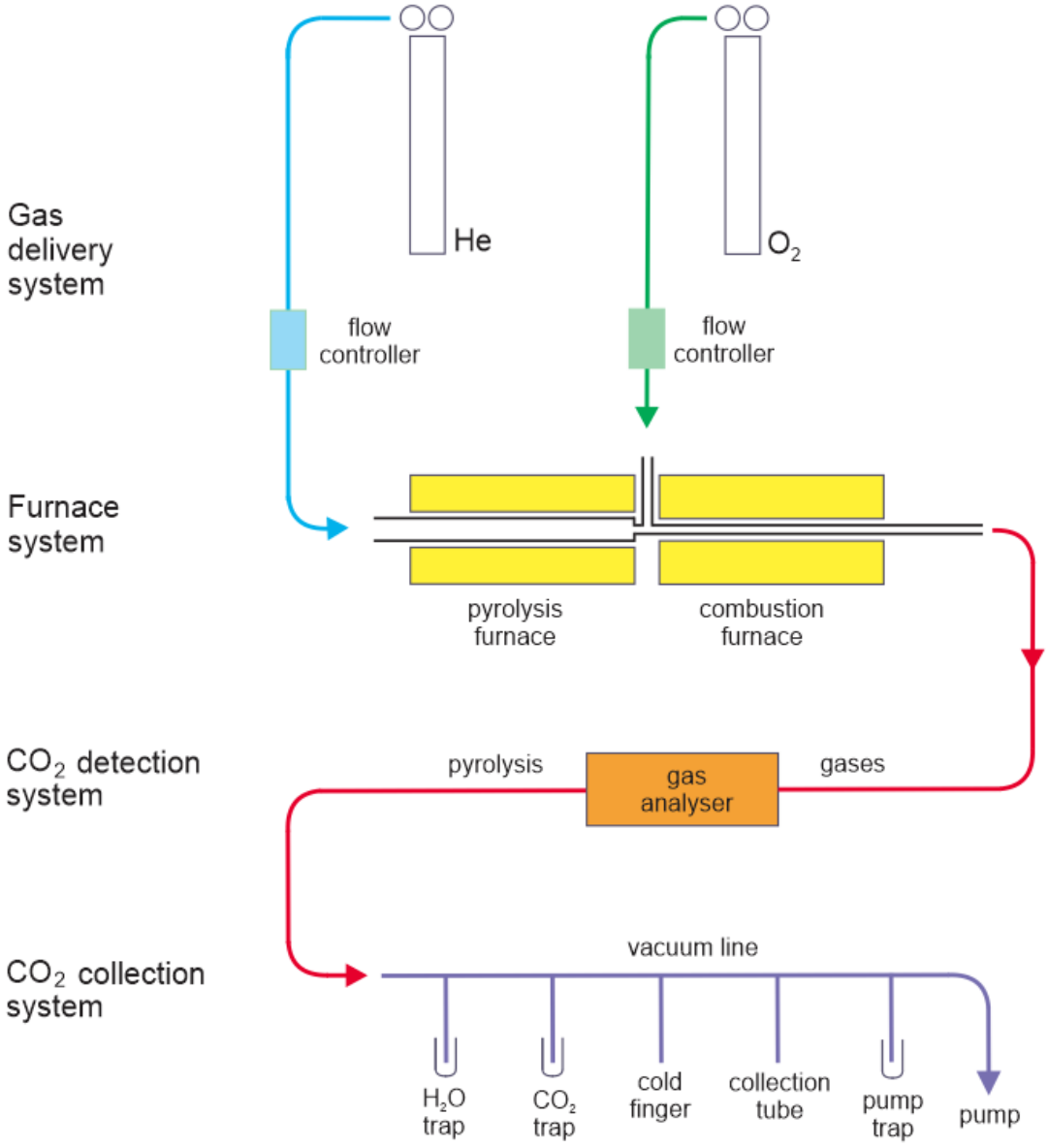

Figure 3.1 The major sub-systems of the RRL RP system. The sub-systems are a gas delivery system, a furnace system, a CO_2 detection system and a CO_2 collection system.

3.1 Differences between USF and RRL RP systems

The key components of each sub-system are outlined in Table 3.1 below. Each sub-system is then discussed in detail.

Table 3.1: The sub-systems and major components of the RRL RP system.

RRL RP system			
Sub-system	Major components	Purpose	Comparison to USF system
Gas delivery	UHP He and O_2 tanks	Supply of carrier and combustion gases	Same
	Flashback arrestor	To prevent explosion in O_2 cylinder	Not present in USF system
	Cleaned ⅛" stainless steel tubing	Delivery of gases without contamination	Similar
	Porter regulators	Flow control for carrier and combustion gases	Different
Furnaces	Pyrolysis furnace	Ramped-temperature pyrolysis of sample material	Same components, different orientation
	Combustion furnace	Combusting released carbo n to CO_2	
	Housing	To insulate furnaces from nearby vacuum and electrical equipment	Not present in USF system
Furnace glassware	Quartz reactor	To house insert while allowing gas flow around it	Same components, different orientation
	Quartz insert	To locate sample and allow through-flow of gases	
	Oxidation chamber	To oxidise carbon from pyrolysis	Same
	Catalyst wires	To promote combustion in oxidation chamber	Same
	Clean-up materials	To remove sulphur and halides from pyrolysis/combustion	Not present in USF system
CO_2 detector	CO_2 analyser	To detect proportion of CO_2 within total gas-flow	Similar
Vacuum line	H_2O trap	To remove water vapour from gas-flow before trapping CO_2	Different
	CO_2 traps	To isolate CO_2 from gas-flow	Different
	Vents	To allow carrier gas to escape after CO_2 trapped	Similar
	Known volume cold finger	To allow quantification of CO_2 obtained	Same
	Collection tube manifold	To allow CO_2 splits to be collected in separate tubes	Different
	Vacuum pump	To induce vacuum in the line	Same

3.2 Gas delivery system

In the RRL RP system, the sample is located in a pyrolysis furnace. A constant flow of inert carrier gas carries the pyrolysis products into a combustion furnace where the gases are combined with oxygen in the presence of a catalyst to convert C to CO_2. The gas delivery system needs to provide a flow of carrier gas upstream of the sample site and a flow of oxygen downstream of the sample site. The oxygen is itself combined with a secondary flow of inert gas for safe delivery into the furnace-space. The simplest method is to provide a single flow of carrier gas which is then divided into a major part for the bulk carrier flow and a minor part for combining with the O_2. Both the carrier gas and the oxygen need to be ultra-high purity (UHP) grade, so as not to introduce any contaminants. Equally, the delivery system itself needs to be as clean as possible, to minimise contamination.

These principles are followed in both the USP and RRL RP systems. Both utilise tanks of UHP He and UHP O_2, use ⅛" tubing for gas delivery, and flow controllers. Where gas flow in the USF system is controlled by mass flow controllers, the RRL system uses high precision Porter regulators (Model 8311, Parker Hannifin, Cleveland, Ohio, USA) (Figure 3.2). Mass flow controllers, once programmed, are simple to operate and provide generally reliable flows, but are also relatively expensive. The RRL system employs Porter regulators to limit the already small flows provided from cylinders with low-pressure dual stage regulators, balanced against other sources of resistance introduced downstream. To divide and combine flows, Swagelok T-junctions are used in both systems.

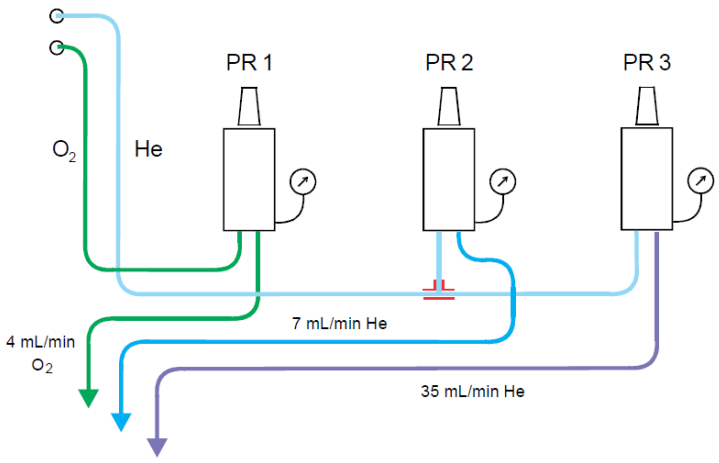

(a)

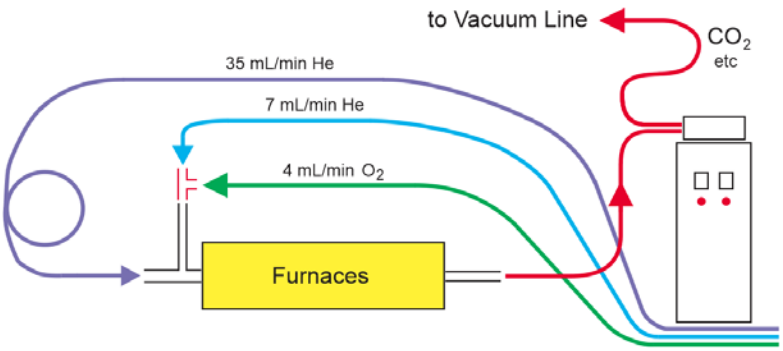

(b)

Figure 3.2 Schematic diagrams of the RRL gas delivery system. Flow control is shown in (a). Porter regulator 1 controls UHP oxygen flow. UHP helium flow is divided via a T junction, with 7mL/min flow controlled by Porter regulator 2 and 7mL/min flow controlled by Porter regulator 3. Gas delivery is shown in (b). 4mL/min oxygen flow and 7mL/min helium flow are combined in the T-junction above the reactor side-arm. The loop in the 35mL/min line allows sufficient flexibility in the tubing to enable simple connection and disconnection of the tubing to the insert via cajons.

In practice, flow control proved challenging. After several experiments involving crimping the ⅛" tubing to provide enough resistance for the low flows required to be governable by Porter regulators (flows around 300mL/min were produced), a solution was found: introducing lengths of 1/16" tubing downstream of the regulators. For the 35mL/minute flow, a 50cm length of 0.02" wall-thickness 1/16" tubing with a crimp applied produced sufficient resistance so that Porter regulator 3 could be set to a reproducible pressure (between 0 and 1 bar). For the 7mL/minute and 4mL/minute flows, smaller-bore tubing was required: introducing 10cm of 0.01" inner diameter 1/16" tubing proved effective for achieving the 7mL/minute flow, and use of 20cm of the same tubing was effective for the 4mL/minute flow (Figure 3.3). The net result was that each Porter regulator could be set to a reproducible pressure and would provide the correct flow.

Figure 3.3 Porter regulators to provide flow control for RRL RP gas delivery system. Different resistances are introduced downstream of each regulator so the appropriate flow can be delivered. With gas flow opened via in-line valves (green for oxygen, blue for helium), the black bonnet on each regulator is turned until the required pressure is shown on the gauge. A gauge of the dual stage regulator for the helium cylinder is visible through the window.

To minimise contamination of the UHP gases, clean materials were used: stainless steel dual stage regulators for use with the cylinders; and to convey the gases, ultrasonically cleaned ⅛" stainless steel tubing. Cleaning was to remove any potentially contaminating oils and greases. Cajons connect the tubing to the regulators. A locally-available brass flashback arrestor was provided to the oxygen cylinder dual stage regulator, to prevent any possible heat/flame propagating backwards from the furnace system and causing explosive ignition of oxygen in the cylinder. The arrestor includes elastomer seals which may absorb/desorb CO_2 and other gases, so poses a contamination risk. Possible contamination from this source has not been investigated at this time.

3.3 Furnace system

An RP system requires two furnaces: one in which sample material is pyrolysed, and one in which pyrolysis gases are combusted to produce CO_2. The sample material needs to be contained in a vessel within the first furnace, and the pyrolysis gases need to be entrained to pass through the second furnace. The essential components are shown schematically in Figure 2.2, above, with the vertical orientation reflecting the physical orientation of the USF

system. The bench on which the USF RP system is located has the vacuum line on one side and the furnaces on the opposite side, physically removed from the vacuum line and from the operator working the system.

The RRL furnace system includes the same key elements, but is arranged horizontally, to sit on a benchtop within the same space occupied by the vacuum line (Figure 3.4). Given the proximity of both the vacuum line and another processing line on the opposite side of the bench and the presence of nearby electric cables and electrically-powered components such as heat guns and gauges, the RRL furnaces are contained within an insulating housing. The housing is a box-like arrangement of easily workable but temperature-resistant ceramic fibre board, 2.5cm thick, to insulate the furnaces from the immediate environment. The board is also used to separate the furnaces, to minimise heat from one affecting the temperature in the other. The board is held together by high temperature-resistant shrink wrap and braided strapping.

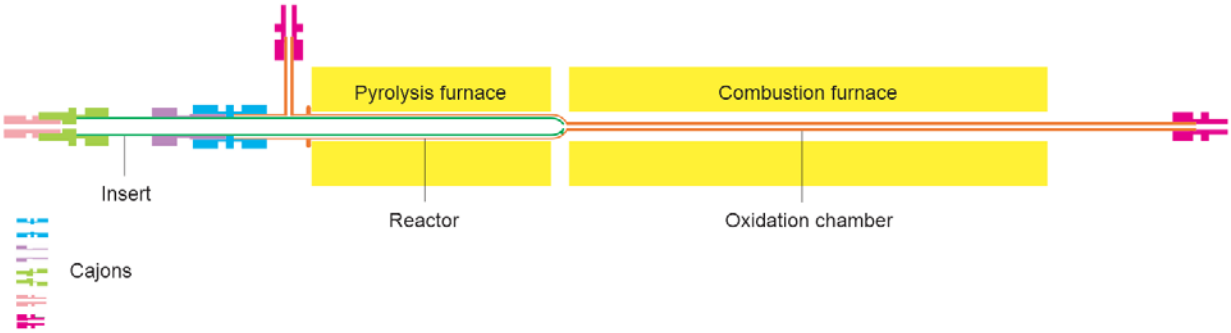

Figure 3.4 Schematic diagram of the RRL furnace system, including glassware and connecting cajons.

The change in physical layout affects the way heat travels in the respective systems. In the USF system, with the combustion furnace arranged below the pyrolysis furnace, heat rises through the furnace system once the combustion furnace is turned on and affects the temperature in the pyrolysis zone before pyrolysis begins. Copper plates at either side of the insulating blanket separating the furnaces to draw heat away from the system core, to minimise this effect. In the RRL system, the heat-rising phenomenon is absent, but heat does spread from the combustion furnace, once turned on. While the insulating housing lessens heat spreading out to affect nearby systems, it also contains furnace heat in proximity to the furnaces, so that the combustion furnace heat affects the temperature in the pyrolysis zone

in analogous fashion to the rising heat in the USF system. It also increases the cool-down time for the RRL system relative to the USF system, where the furnaces are uninsulated.

The RRL furnace system includes serially arranged hollow cylindrical Watlow ceramic furnaces (VC400N06A and VC400N012A, Watlow, St. Louis, Missouri, USA) within which are nested a quartz-glass reactor and a quartz-glass insert of the same design as the USF glassware. Beyond the location of the insert, the reactor narrows to an oxidation chamber which contains Cu, Pt and Ni catalyst wires which, in the presence of oxygen, promote combustion and the oxidation of C to CO_2. As in the USF system, the reactor and insert are located relative to each other by cajons, with similar fittings being used to connect gas lines to the insert, side-arm and oxidation chamber exit. The RRL combustion furnace and oxidation chamber are double the length of the same components in the USF system to allow enough space for effective performance of sulphur clean-up chemicals in the oxidation chamber (see 3.11, below).

3.4 Furnace temperature control

Temperatures in the RRL RP system furnaces are controlled by programmed CAL temperature controllers (CAL 9500P; CAL Controls Inc, Libertyville, IL, USA). The same type of temperature controller is used to control furnace temperatures in the USF system.

3.4.1 Furnace system testing

Early testing of the pyrolysis furnace showed that the temperature ramp was not smooth, but overprinted by an approximate sine-wave (Figure 3.5). The ramp improved iteratively in subsequent testing, with a significant gain when the proportional cycle time in the temperature controller was reduced from 4 seconds to 05. seconds.

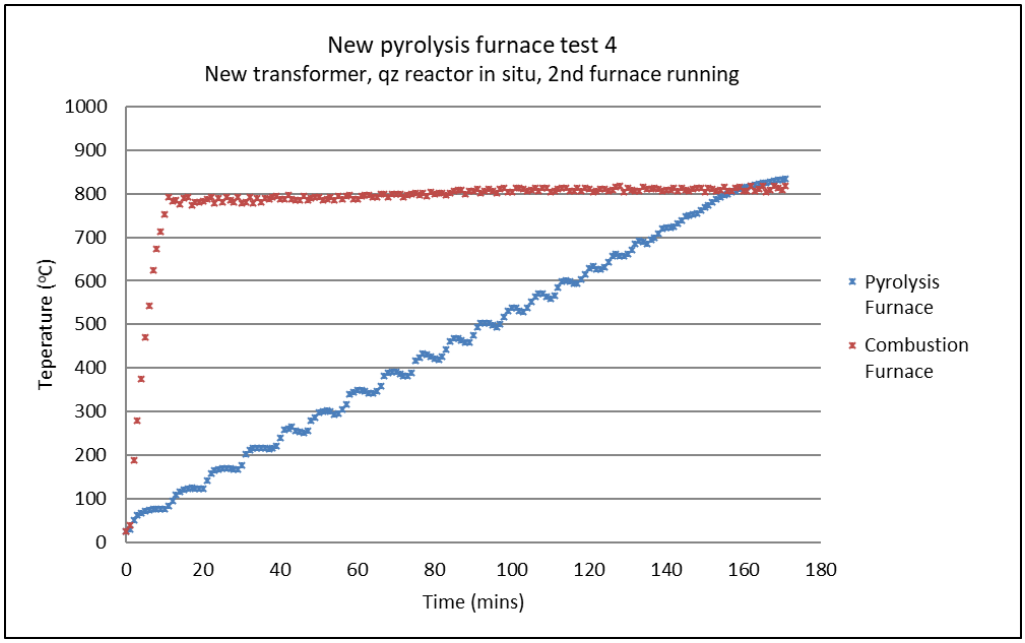

Figure 3.5 Testing of RRL RP furnace temperatures, both furnaces running. The traces show temperature controller readings at one-minute intervals. The blue trace shows oscillations approximating a sine wave superimposed on the pyrolysis furnace temperature ramp. The red trace shows the combustion furnace temperature, which climbs from a little below 800°C (e.g. 785°C) to a value above 800°C (e.g. 820°C) as the temperature in the pyrolysis furnace exceeds ~400°C.

Good temperature control depends on positioning of the pyrolysis furnace thermocouple. Profiling of temperatures seen along the reactor and oxidation chamber during component testing indicated differences in temperature depending on location. Detailed profiling followed. This profiling showed that the temperature at the sample location was approximated reasonably well by the temperature at the factory thermocouple location, midway along the furnace (Figure 3.6(a)). Along the oxidation chamber, the hottest zone occurs between 10 and 20cm along the chamber, relative to its join to the reactor glass (Figure 3.6(b)). However, when the integrated RP system was tested (Figure 3.7), this time with the thermocouple jammed between the reactor and the furnace bore (as located at USF), a significant divergence between the temperatures recorded at the sample and factory locations was found: a mean difference of ~54°C over the duration of the test, with a maximum difference of 66°C. With this difference, the temperature at the sample location is significantly hotter than shown by the temperature controller with the thermocouple positioned at the factory location, with implications for the speed of the pyrolysis reaction –

namely, that it will have advanced further than expected on the basis of the displayed temperature.

(a)

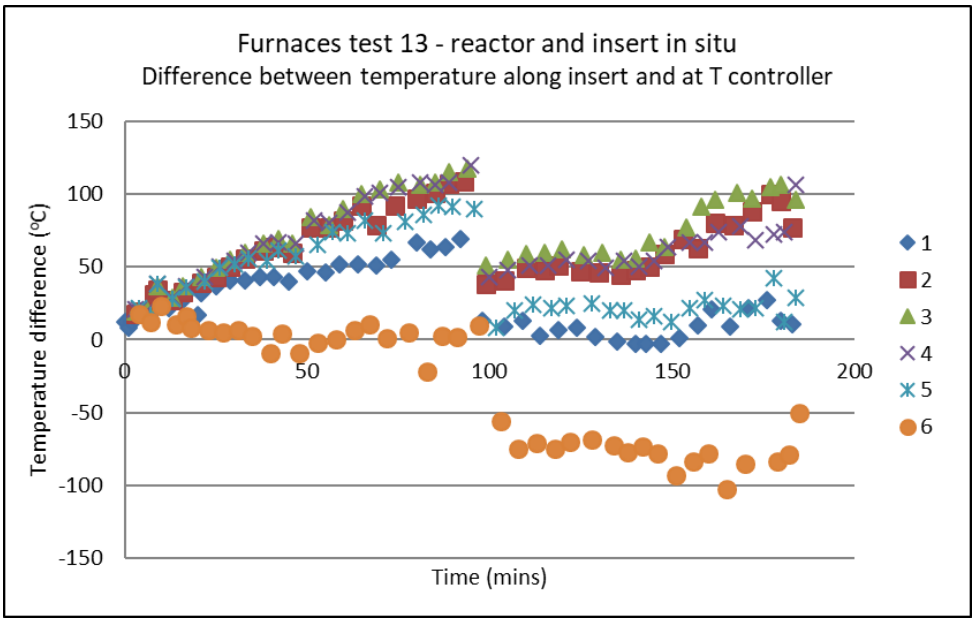

(b)

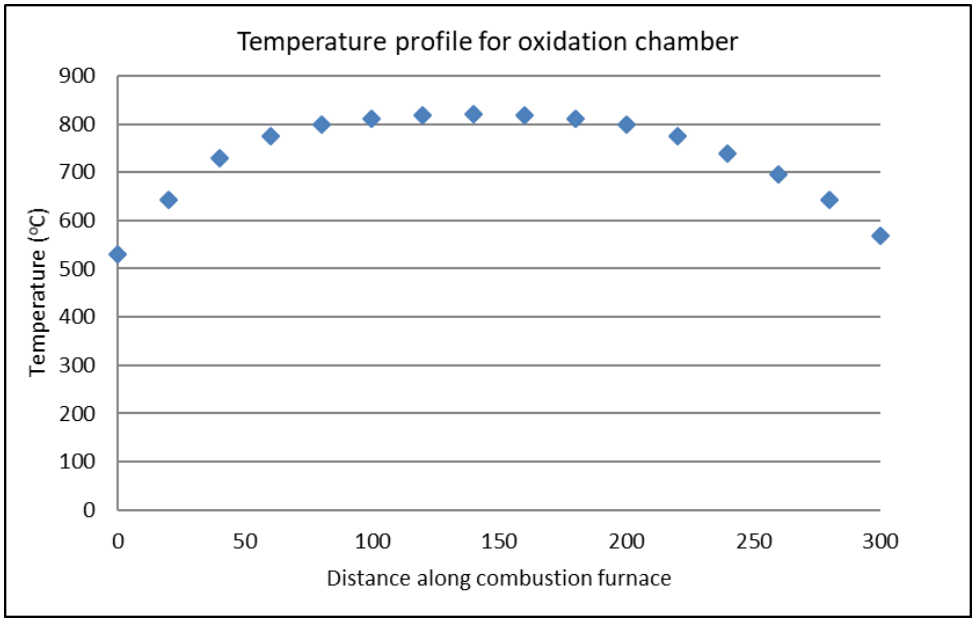

Figure 3.6 Detailed temperature profiling along the RRL pyrolysis and combustion furnaces. For the pyrolysis furnace (a), points tested are at 2cm intervals along the furnace length, tested by thermocouple probe positioned within the quartz insert. Location 1 approximates the sample location; location 6 is near where the reactor is first enclosed within the furnace. At 98 minutes, the factory-location thermocouple was found 1cm from the reactor glass, producing a divergence between the temperatures seen by this thermocouple and the probe; when the thermocouple was re-positioned, temperatures re-converged. For the combustion furnace (b), points tested are at 2cm intervals along the furnace length from the junction with the reactor, with testing by thermocouple probe positioned within the oxidation chamber. The temperature points shown are averaged from over the duration of a temperature ramp taken

up to 850°C. (In practice, the temperatures along the combustion furnace trend hotter as the pyrolysis furnace temperature ramps up, as can be seen in Figure 3.5.)

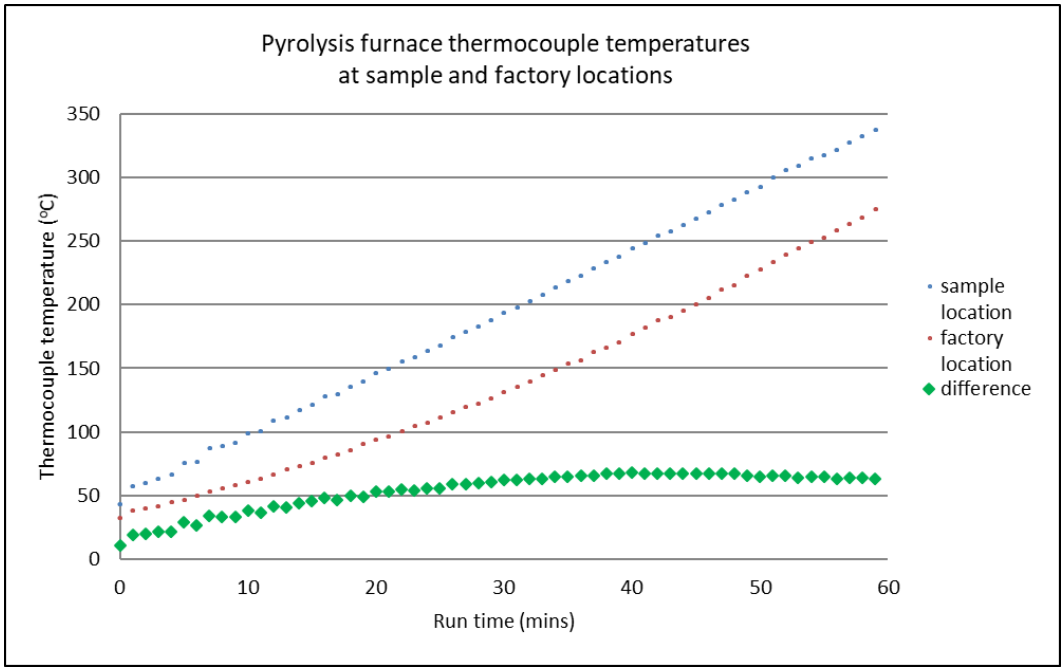

Figure 3.7 Effect of re-positioning the thermocouple between the reactor glass and pyrolysis furnace bore. (Given the earlier furnace failure, use of this arrangement had previously been eschewed in the RRL system.) The sample location is close to the inner end of the pyrolysis furnace, adjacent the combustion furnace, so the temperature seen at this location is not produced solely by the pyrolysis furnace but is affected by heating from the combustion furnace also. A second thermocouple was placed in the factory location, with its temperature being monitored via a portable multi-meter. The mean difference between the temperatures recorded at the sample and factory locations over the duration of the test is ~54°C.

An implication of the differences in temperature found in the reactor in different tests is that temperatures seen in the reactor may vary not only due to thermocouple placement, but also from run to run. One issue is that precise replication of thermocouple placement from run to run is difficult, as the reactor is jostled when a fresh insert is loaded (as happens with every run). (At USF, the vertical orientation of the furnaces makes movement of the reactor less likely.) This is significant where repeatability of thermographs from run to run is concerned (discussed at 3.10).

Following an early failure of a furnace during testing, it was decided that a thermocouple temperature of 900°C should not be exceeded in the pyrolysis furnace during a run. It also meant that positioning of the thermocouple between the reactor glass and the furnace bore, close to the furnace heating wires (which were partially visible), was initially avoided.

3.5 CO_2 detection system

A CO_2 detector is useful in an RP system to monitor the levels of CO_2 being produced during the pyrolysis reaction, so as to best determine the characteristics of a given reaction – when it begins and ends, what CO_2 levels are generated, when CO_2 production peaks, what changes in rate of CO_2 production occur over time. Based on such information, when to take splits for an untested sample so that each split is suitably sized for ^{14}C dating can be decided. The RRL CO_2 detection system is essentially similar to the USF CO_2 detection system: both use off-the-shelf CO_2 analysers. The RRL detector is a Li-Cor CO_2 gas analyser (LI-820, Li-Cor Biosciences, Lincoln, Nebraska, USA). Like the USF analyser, the LI-820 is an optical analyser, absorbing infrared energy from gases passing along a fixed-length optical path, with a filter channel corresponding to the absorption band for CO_2 (LI-820 CO_2 Analyzer Instruction Manual, 2002).

As supplied, the LI-820 includes lengths of plastic tubing connecting the inlet to the optical bench and the optical bench to the outlet; however, such plastic contains carbon, so would be a potential contamination source for CO_2 passing through the analyser. With the supplied bench connections changed for connections compatible with Swagelok fittings, the plastic tubing was replaced with suitably bent stainless steel tubing (Figure 3.8).

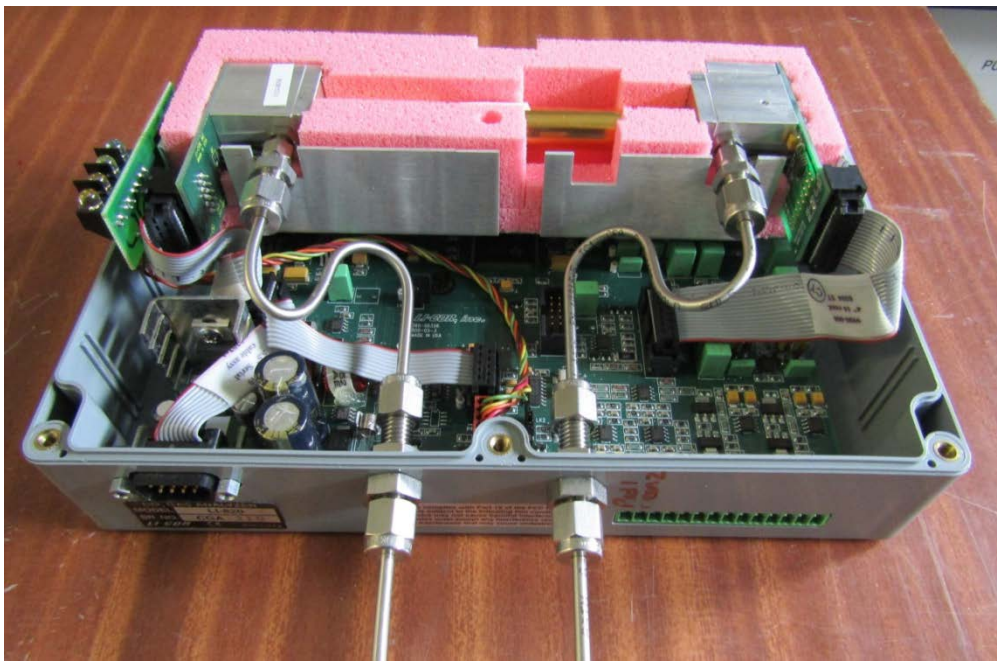

Figure 3.8 Li-Cor CO_2 gas analyser with tubing modified for the RRL RP system. The optical pathway extends through gold tube between the silver inlet and outlet housings (left and right, respectively). The optical bench is encased in protective foam. Bored-through bulkhead fittings at front of unit allow uninterrupted stainless steel tubing to attach directly to oxidation chamber and vacuum line via Swagelok Ultra-Torr vacuum fittings.

The CO_2 detector is computer-run, with CO_2 concentrations displayed in ppm on a computer chart in numeric and graphic form, so that changes in CO_2 concentrations during a run can be seen. CO_2 concentrations show significant drift over time, up to 10ppm in the course of a day. The analyser can be calibrated, but the key utility of the CO_2 detector is to show the shape of a run's CO_2 profile, rather than its magnitude. In operation, a background CO_2 concentration is determined before a run is begun, with this amount being subtracted from CO_2 readings during the run. Even if some drift occurs during a run, the resulting run shape can be used to characterise the reaction profile and determine where splits should optimally be taken.

3.6 Vacuum line system

The key function of a vacuum line in an RP system is to isolate and capture CO_2 produced from combustion of pyrolysis products. During an RP run, pyrolysis products are continuously generated as a sample is pyrolysed, so a suitable vacuum line needs to be able to switch between collecting and processing modes. This means at least a part of the line needs to consist of two lines where either or preferably both of these functions can be carried out.

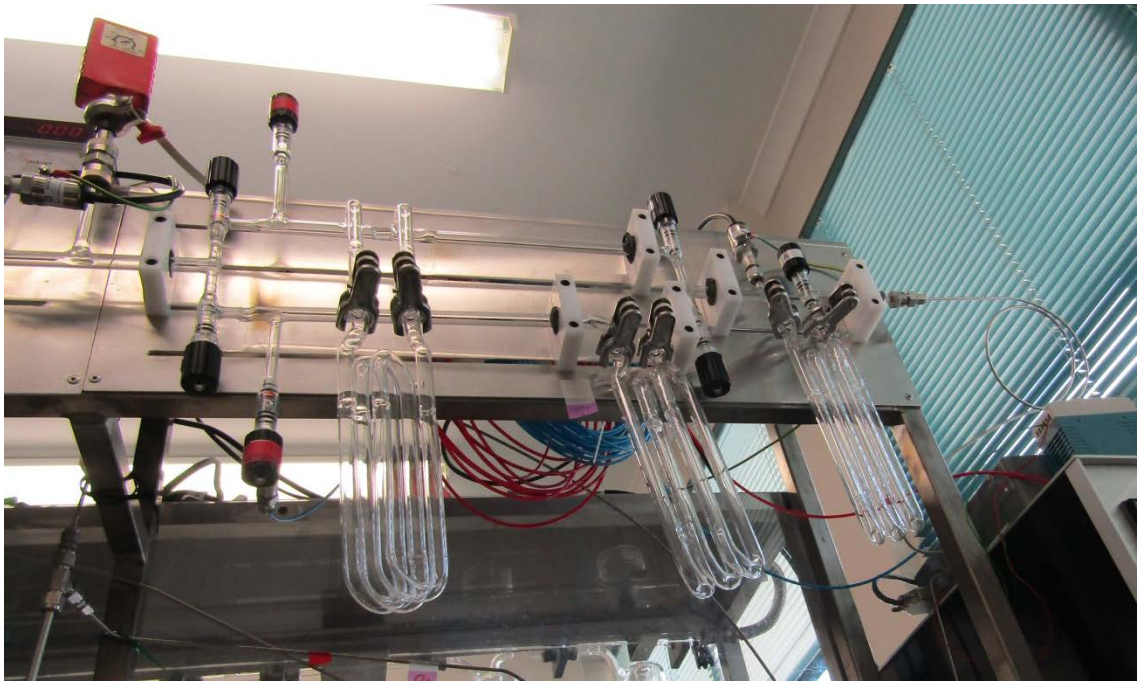

Figure 3.9 Upstream end of RRL RP vacuum line. The vacuum line connects to outlet tubing from the CO_2 detector, at right. The water trap is closest to the CO_2 detector. After the water trap, the line diverges to upper and lower collection branches, with a CO_2 trap extending from each. The traps are interchangeable, in case of breakage. Valves have black knobs and are manually operated. Vents (with red-tagged knobs) attach to the line before the branches re-converge, and connect to coiled blue and red tubing (exiting the lower and upper limbs, respectively). The valve upstream of the water trap allows the line to be tested under vacuum for leaks from the water trap to the pump trap. White clamps for securing glassware are located in slots in the front panel. Slots are equally spaced so that the same clamps can be used anywhere along the line.

Both the USF and RRL vacuum lines include a section where the line diverges into two separate collection lines which subsequently re-converge, but the way in which these sections are designed differs. The RRL vacuum line is designed along classical vacuum line principles (e.g. Turnbull et al., 2007; Xu et al., 2007), with a water trap cooled by a bath of dry ice in alcohol (–78°C) located upstream of CO_2 traps cooled by $/N_2$ (–196°C), so that the majority of any water vapour present in gases passed through the line is trapped before CO_2 is isolated (Figure 3.9). The USF vacuum line begins with the six-valve two-trap assembly described above, including CO_2 traps cooled by $/N_2$, which capture not only CO_2 from the stream of pyrolysed gases but also any water vapour present. Two further traps follow in the USF vacuum line proper, for successive removal of water vapour. Also, in the RRL system, switching between CO_2-collecting branches is by manual valve-operation, while at USF, switching is computer-controlled. The way the CO_2-collecting section swaps between

collecting and processing states in the RRL system is shown schematically in Figure 3.10. Whether water vapour is trapped before or after CO_2 is perhaps unimportant, but there is a significant corollary in terms of the way the USF and RRL lines operate.

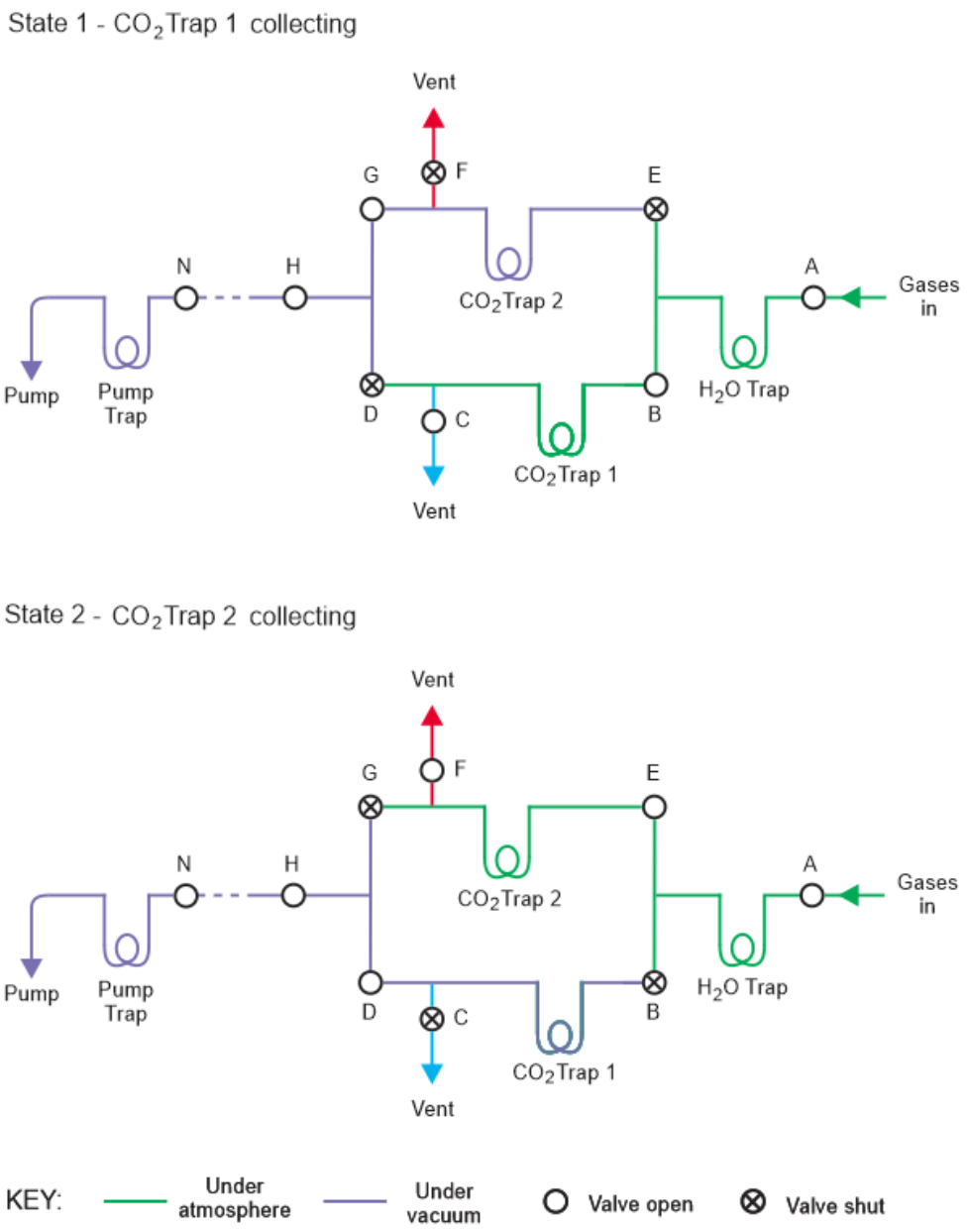

Figure 3.10 Schematic diagram of trap states for collecting and transferring gases in the RRL RP vacuum line. The diagram is oriented in same direction as is the physical system (Figure 3.9). When collecting in CO_2 trap 1 (State 1), valves A, B and C are open. Valve C is not opened until the pressure in the branch is above atmospheric pressure, to prevent room gases being drawn in through the vent. Once valve C is opened, untrapped gases – primarily the helium carrier gas – pass out of the system through the vent. Valve G is opened to transfer CO_2 from CO_2 trap 2 to the known-volume cold finger, at H. When collecting in CO_2 trap 2 (State 2), valves A, E and F are open.

While in diagrammatic form, the system looks similar to the USF equivalent shown in Figure 6, the difference in physical structure (Figure 2.4 and Figure 3.9) is telling. In particular, the USF system has a CO_2 trapping system made of fine-bore glass and having a small internal volume. When the inlet to the trap previously under vacuum is opened in the USF system, both traps are restored to atmospheric pressure after ~5 seconds. Then the other trap is opened to vacuum. In the RRL system the branch volumes are considerably larger, and the time from opening the inlet valve (E or B) to the branch previously under vacuum until the incoming gases establish atmospheric pressure and the branch vent can be opened is 5 to 7 minutes. So the time for pressure equilibration in the RRL system is considerably longer than the equivalent time in the USF system.

While pressure equilibrates in an RP system, the [CO_2] data is unreliable, appearing as spikes in thermographs. Compared to the near-instantaneous pressure spikes seen in USF thermographs (an example can be seen in Figure 3.23), the pressure-spikes in RRL thermographs extend over much longer intervals (see Figure 3.11). But these are artefacts of pressure disturbances. CO_2 production and collection continues, but the pressure levels in the optical bench are either too low or too high for CO_2 concentrations to be effectively recorded.

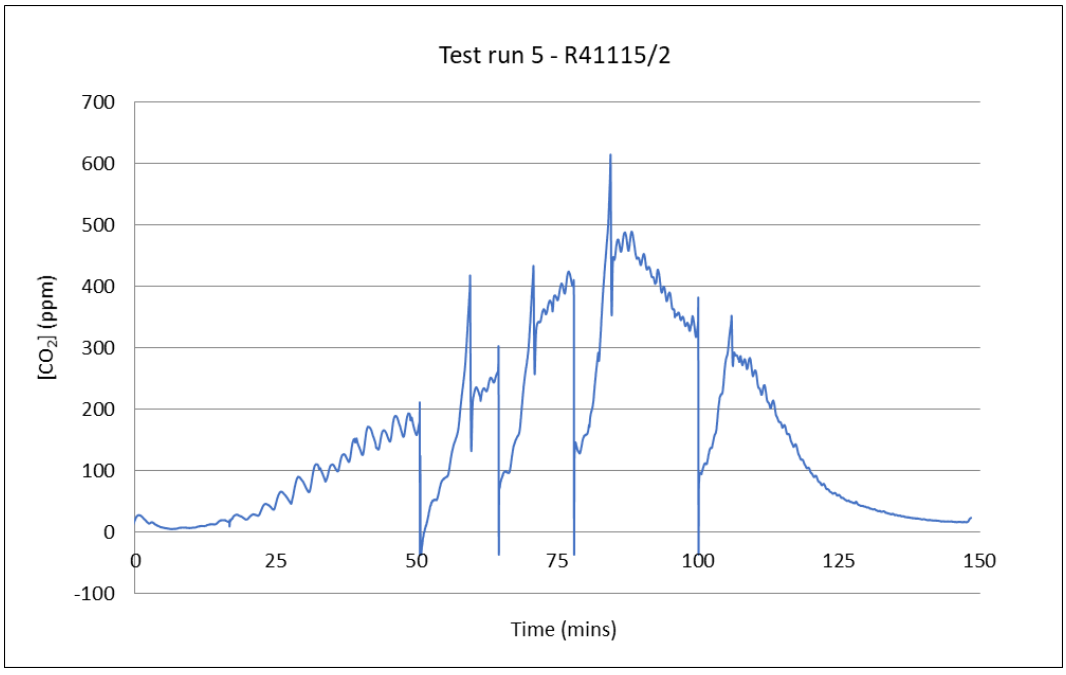

Figure 3.11 Thermograph for the first RRL RP test run with Antarctic sediment. Splits were

taken at 286°C, 350°C, 417°C, 532°C and 771°C – the same temperatures at which splits were taken in the USF run with the same material. The pressure disturbances where splits are taken result in considerable gaps in [CO_2] data, but do not imply a loss of CO_2. The oscillations in [CO_2] superimposed on the underlying thermograph shape indicate that the temperature ramp was not well-controlled. Changing the proportional cycle time in the temperature controller from 4 seconds to 0.5 seconds improved ramp regularity.

It is possible, however, that lowered pressure in the insert affects the pyrolysis reaction itself. A lower-pressure environment is less thermally conductive (molecules in a less-occupied space are expected to have longer free paths, interacting less frequently with other molecules/surfaces), so the sample could be heated to a lower temperature than it was previously experiencing. If so, there may be a lag in CO_2 production while the sample passes through a part of the temperature ramp it has already reacted through, so that CO_2 evolution is diminished while the temperature rises (with pressure) back to the point where the valve-state was switched, after which CO_2 evolution can continue through the temperature ramp. However, the furnace temperature will have continued to climb in this interval, so it could be that the final amount of CO_2 produced is unaffected, regardless of intervening pressure changes. It could be merely that CO_2 is produced at different rates during different intervals. Such possible phenomena have not been investigated at this time.

The orientation of the furnaces is also potentially significant. In the USF system, the furnaces are oriented vertically, as seen schematically in Figure 2.2. The combustion furnace heats first, with the heat rising towards the pyrolysis furnace and the sample location. Although the USF furnace system uses insulating and heat-diverting materials between its furnaces, it is possible that heat from the combustion furnace penetrates regardless, due to heat rising through the oxidation chamber and into the reactor, and that the temperature the sample sees differs from the thermocouple temperature shown by the temperature controller.

3.7 Operation of the RRL RP system

The RRL RP system was tested, with operating protocols being developed and refined, over a period of 5 months, between November 2018 and April 2019 (see Table 8.2 for a summary of RRL RP runs and maintenance undertaken in this period). As a result of testing and refinement of procedures, the RP operational protocols arrived at during this study were:

- Thermocouple for pyrolysis furnace is located between inner surface of tubular pyrolysis furnace and outer surface of quartz glass reactor at sample location
- Proportional cycle time in the temperature controller is set at 0.5 seconds
- For runs with blank material and sediment samples, collection of pyrolysis gases is from 105^{o}C, to avoid any handling contamination
- During collection of pyrolysis gases, /N_2 on the CO_2 trap is topped up and the dewar fractionally raised at regular intervals (e.g. every 7 minutes) to ensure any CO_2 frozen is not exposed above the /N_2 level (due to /N_2 evaporation) so does not sublime
- When collecting branch changed or splits taken, branch inlet valve opened metering-style (valve opened by very small increments, with valve not opened further until pressure has equilibrated) – takes approximately 4 minutes to fully open valve
- During transfer of CO_2 samples:
    - When carrier gases released to vacuum while sample held in CO_2 trap under /N_2 (with branch inlet valve and branch vent closed), branch exit valve opened metering-style (over ~4 mins) – during this time, /N_2 regularly topped up and/or dewar incrementally raised
    - After release of carrier gases (with branch inlet and exit valves and vent closed), /N_2 dewar is dropped from trap and trap heated with heat-gun until all traces of frosting and condensation gone (all trapped gases volatilised), then slush-bath raised for 5 minutes to ensure all water vapour re-freezes – only then are gases transferred to cold finger
    - It is important to keep the water trap at –80°C or below to ensure all water vapour is removed
- A thermograph for an RRL RP run is constructed from [CO_2] measurements every second and the temperature for the same second, calculated from discrete recordings of temperatures and times (e.g. at 50^{o}C intervals)
- Zero-and-span of CO_2 analyser is performed periodically rather than routinely to minimise system disturbance; [CO_2] readings for runs are adjusted for background [CO_2] level

- UHP He and UHP O_2 gas flows checked periodically rather than routinely, to minimise system disturbance, with Porter regulator pressures being adjusted as required to produce correct flows.

3.8 Quartz wool contamination

Thermographs from RRL Runs 14 to 17 with Renton Road Kauri material (discussed at 3.10.4) collectively showed apparent contamination peaks at around 100°C, with a suggestion of further contamination inputs around the first half of the saddle between the peaks (see Figure 3.12). Potential contamination sources were investigated. To simulate background conditions for a normal RRL RP run, a run was undertaken with a clean reactor loaded with quartz wool. If no contamination was present, no CO_2 should be collected, and a near flat-line thermograph produced. However, an appreciable amount of CO_2 was collected from the run (from pressure in the cold finger, ~0.1mgC), and the thermograph showed several peaks, the most prominent at about 140°C, with others around 235°C and 325°C (Figure 3.12). The location of the two highest peaks showed a broad correspondence with the location of possible contamination peaks or shoulders in the early kauri runs.

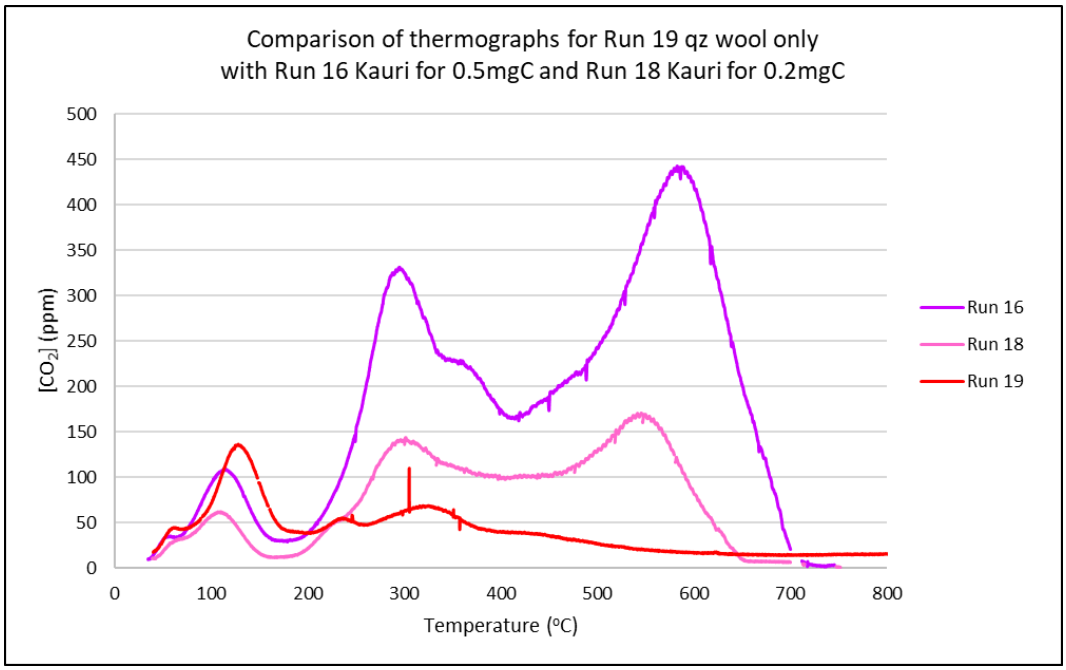

Figure 3.12 Comparison of thermographs from early kauri runs and Run 19 with an insert loaded with quartz wool only. The Run 19 thermograph is not flat, but shows peaks located close to possible contamination peaks or shoulders in the kauri runs.

It was clear from the Run 19 thermograph that carbon was entering or present in the system somewhere. It is possible that the source was a leak. To show up on the thermograph, such a leak would need to be upstream of the CO_2 analyser, so could not be due to backflow from the carrier gas vent, for instance, or absorption after the gases were turned off. (While a leak downstream of the CO_2 analyser is also possible, it would not be evident from the thermograph). A gas would be unlikely to join either of the tank gases at source, as both are supplied under positive pressure, so an external gas would need to overcome that pressure to enter the gas-stream. This could occur while the gases are turned off, but the system is always flushed with the UHP He and UHP O_2 before use, so any residual modern atmosphere gases would be vented before a run begins. Moreover, if a gas other than UHP He or UHP O_2 was entering the system, a constant trace of such ingress would be expected. The fact that the trace displays peaks suggests that the CO_2 is not from a constant trickle-type source but is evolving from combustion, so the source is likely to be found within the normal system set-up. Possible set-up sources include the quartz wool used to locate the sample, and the glassware itself – in particular the insert, as a fresh insert is used with every run, whereas the in-place reactor and oxidation chamber are baked with every run.

To investigate these possibilities, Run 20 was conducted with an insert only, pre-baked at 900^{o}C and stored in the normal way. Clean gloves were worn while the insert was installed in the reactor, with the insert only handled by the part of the outer wall which sees room-air during a run. From this run, slight contamination only could be seen, with [CO_2] barely above background levels. The run shape shows an early peak at around 50^{o}C, with small humps at ~300^{o}C and ~400^{o}C (Figure 3.13). From the pressure detected in the cold finger (1, at 24.0^{o}C room temperature), approximately 0.005mgC was evolved during the run.

For Run 21, an insert pre-loaded with quartz wool was baked overnight at 900^{o}C. The Run 21 thermograph showed a CO_2 profile highly similar to that for Run 20, but more subdued (Figure 3.13). Pressure in the cold finger was zero. From this experiment, the major cause of the contamination was clear: the quartz wool as normally handled. When the quartz wool in an insert was used directly after baking, no contamination was found during an RP run.

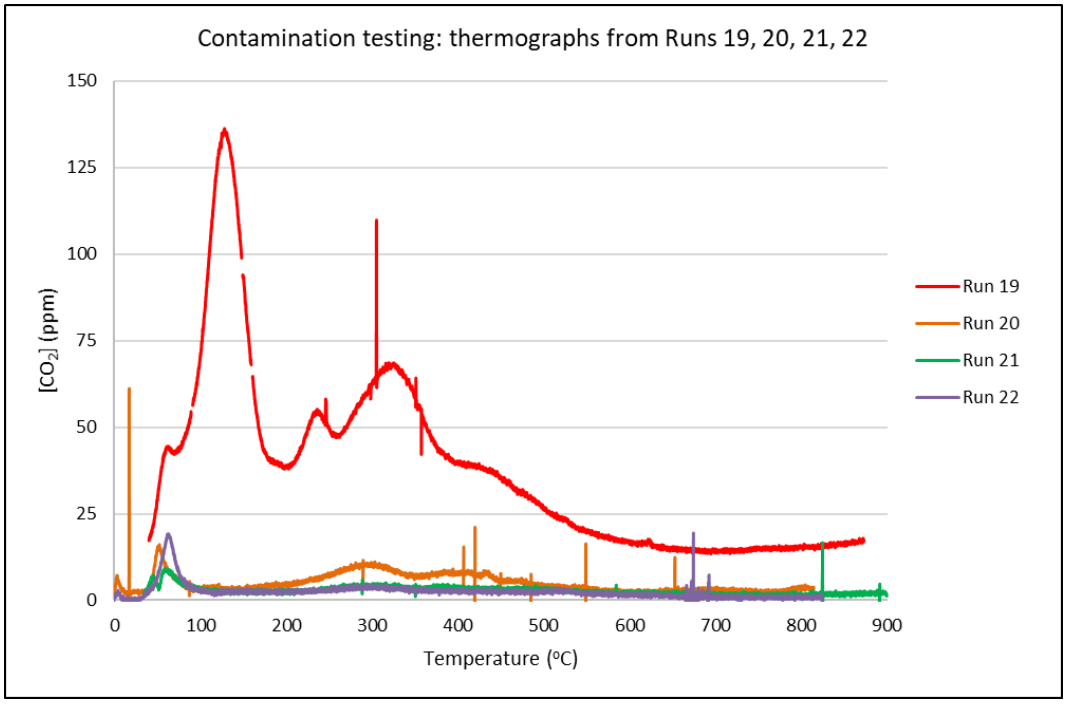

Figure 3.13 Thermographs from runs to investigate contamination in the RRL RP system. The Run 19, with quartz wool only, shows that the wool is a source of contamination. The minor humps in the Run 20 thermograph show that storage in plastic is also potentially contaminating.

The quartz wool normally used to locate samples in an insert had been pre-baked at 900°C then stored in a plastic bag in the RRL preparation laboratory. It is possible that the quartz wool stored in this way had absorbed contaminants from the plastic. Diethyl phthalate, commonly used as a plasticizer to improve the flexibility and durability of plastics, is readily absorbed by quartz wool, and has a boiling point of 295°C (Jo et al., 2016; the authors used a quartz wool sorbent tube to sample phthalates in air). Diethyl phthalate is seen as a pyrolysis product at least over the temperature range 200°C to 300°C (Chen et al., 2018). If the quartz wool had absorbed contaminants such as diethyl phthalate from the plastic in which it was stored, those contaminants could then be released during pyrolysis and oxidised to CO_2 during combustion to produce the CO_2 profile seen in Run 19. As diethyl phthalate is a common component of plastics and is a known pyrolysis product in the temperature range in which the contamination is shown in the Run 19 thermograph, our working hypothesis is that contamination is related to storage of quartz wool in plastic, and that diethyl phthalate is a likely major contributor to the contamination seen.

As a consequence, a new storage protocol for quartz wool was introduced. A quantity of quartz wool is baked in a ceramic tube at 900°C overnight, removed from the tube with clean tweezers, wrapped in tin foil pre-baked at 500°C with an opening left at the top of the resulting package. The package is placed in a clean beaker, with the package opening and the beaker being separately covered with pre-baked tin foil. Small amounts of the wool can then be removed from the package with clean tweezers after the beaker cover and package cover have been removed, also with clean tweezers. Periodic tests using the quartz wool prepared and stored in this way have been conducted subsequently, after storage periods of two weeks, one month and two months, to check whether any contamination of the quartz wool is seen over time. None of the tests resulted in any CO_2 being collected, so we conclude that the new quartz wool storage protocol is effective.

With these new clean-handling protocols in place, it was expected that the CO_2 contamination profile for future RRL RP runs should more closely resemble the profile for Run 21 than for Run 20. This was borne out with the run immediately following, Run 22, using a clean insert loaded with clean quartz wool only, with both the insert and wool prepared and handled according to the new protocols, where a close correspondence between the shapes for Runs 21 and 22 is apparent (Figure 3.13).

A significant corollary of the discovery that contaminating quartz wool was being used in the RRL RP system was that none of the first 18 RRL RP runs could be used for radiocarbon dating purposes. The potential influence of contamination on thermograph shapes cannot be discounted either, so the early RRL RP runs were disregarded for thermograph comparison also.

3.9 Clean handling

Following Run 20 (discussed above), all inserts were baked at 900°C for 2 hours. After baking, the inserts were handled with clean gloves and using clean tweezers. The major length of each insert was wrapped in tin foil which had been pre-baked at 500°C for 2 hours, and the ends of insert were separately wrapped in pre-baked foil to allow access to either end while the major length remained covered in clean foil.

To load a sample, clean tweezers are used to introduce a plug of clean quartz wool into a pre-baked insert, stood upright in a clean beaker and handled (with gloves) by its foil wrapping. The sample material is weighed out into a clean small petri dish then transferred to the insert (on top of the quartz wool) via a clean funnel. A second plug of clean quartz wool is loaded on top of the sample material. The insert is covered with clean foil until loaded into the reactor. For loading the insert is handled by its major-length wrapping, which is progressively removed as the insert is fed into the reactor. The cajons are tightened and the tightness checked. Gloves are removed only when insert is securely in place inside the reactor.

3.10 Sulphur clean up

A drawback of the USF RP system is that the CO_2 collected from the pyrolysis reaction is sealed in a Pyrex tube containing copper oxide pellets and silver wire (Rosenheim et al., 2008). This is in preparation for subsequent combustion to eliminate any sulphur and chlorides present in the pyrolysis gases, as these can poison graphite reactions and prevent conversion of CO_2 to graphite. In the RRL RP system, the same clean-up materials – Ag wire and CuO pellets – are incorporated directly into the oxidation chamber downstream of the Cu, Pt and Ni catalyst wires, so as to remove these contaminants before the CO_2 is collected. To allow enough space in the combustion chamber to achieve this, the RRL combustion furnace is double the length of its USF counterpart.

In the RRL furnace system, a braid of catalyst Cu, Pt and Ni wires is inserted in the oxidation chamber. The clean-up materials comprise two silver wire plugs inserted downstream of the catalyst wires. CuO pellets are located between the plugs to provide an oxygen source (Figure 3.14). To ensure effective clean-up, the materials were positioned on the basis of oxidation chamber temperature profiling (Figure 3.6(b)) so that they were located in the relatively hot part of the chamber. After several test runs, however, it was found that the materials had worked their way along the chamber, gradually propelled by the gas flow, so that they were visible beyond the furnace. A brace of Ni wire was constructed with a plug positioned at the end of the chamber, where movement is limited by the connecting cajons, to ensure the clean-up materials maintained their intended position (Figure 3.14).

Figure 3.14 Initial set-up for clean-up chemicals in the RRL combustion chamber. The measuring tape shows the approximate location of the materials within the combustion furnace. CuO pellets are located between plugs of Ag wire in the quartz-glass combustion chamber. The tail of the braided Pt, Ni and Cu catalyst wires can be seen prior to the 200mm mark. The Ni bracing wire is visible beyond the second Ag wire plug, beginning at 250mm.

At the end of Run 31, with Antarctic marine sediment, it was noted that the gas collected in the breakseal appeared yellow. It was concluded that the clean-up chemicals had failed. A fresh reactor was prepared, with its combustion chamber being loaded with new catalyst wires. New clean-up chemicals in the form of Ag plugs to either side of CuO pellets were positioned downstream of the catalyst wires, with the downstream Ag plug made three times as long as in the previous arrangement. A length of twisted Ni wire was again used to brace the clean-up chemicals in position (Figure 3.15).

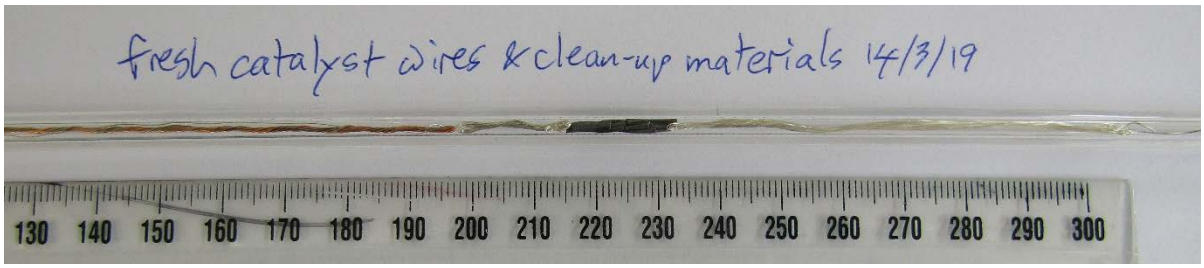

Figure 3.15 RRL clean-up chemicals set-up following Run 31. The upstream end of the Ni wire brace can be seen to the right of the longer Ag plug, just beyond the 300mm mark.

To cleanse the CuO of any carbon adsorbed from room air (despite its having been pre-baked at 900^{o}C), a conditioning run followed (Run 32), using an insert loaded with quartz wool only. 0.22mgC was collected. A second conditioning run was conducted to ensure that no further

CO_2 was collected. None was. Runs 34 to 36 were with kauri blank material, with colourless gases collected in each case, but for Run 37, with Antarctic marine sediment, the gas collected in the cold finger and breakseal appeared pale yellow once more. It was concluded that at least for runs with sediments, with their more heterogenous chemical sources, the new clean-up chemicals were not effectively removing sulphur compounds. On inspection of the combustion chamber, it was apparent that the Ag wire plugs did not entirely fill the combustion chamber bore, so it was possible gases were passing through without making contact wire the Ag wires. The combustion chamber was therefore re-loaded with new wires and clean-up chemicals, this time the Ag plugs being more densely packed (each new plug being made from a 90cm rather than 60cm length of Ag wire), and with three separate, similar-sized Ag plugs being loaded downstream of the CuO pellets (Figure 3.16).

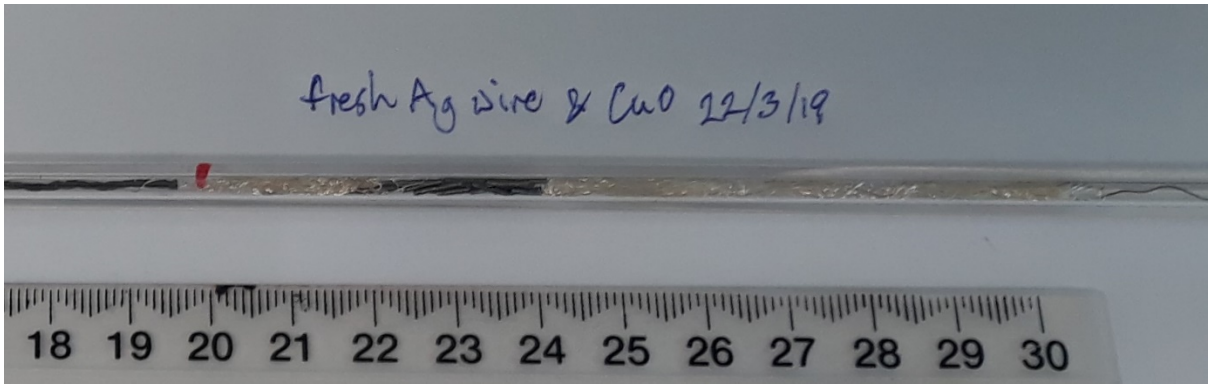

Figure 3.16 Clean-up chemicals set-up following RRL Run 37. The Ag wire is now configured as four separate plugs, one upstream and three downstream of the CuO pellets.

A single conditioning run followed, as it had now been demonstrated that one run was sufficient to clean the CuO of CO_2-producing carbon. Run 39, with sediment, again produced yellow-tinged gas. It was concluded that with failure of the initial clean-up chemicals, the RRL RP system had become contaminated with sulphur downstream of the sample location, either in the combustion chamber, in the stainless steel tubing between the combustion chamber and vacuum line, in the CO_2 analyser optical bench or in the vacuum line itself. The issue could not be resolved within the timeframe of the present study.

The failure of the clean-up chemicals in the RRL RP system and the apparent contamination of the system with sulphur meant that for all runs after and including Run 31, when the failure was first discovered, CO_2 had to be transferred into or collected in clean Pyrex tubes

containing CuO strands and Ag wire and subsequently recombusted at 500°C overnight to ensure sulphur compounds were removed before graphitisation. This further exposure to CuO becomes a potential source of additional contamination.

3.11 Differences in thermograph shape and likely causes

For RP radiocarbon dating, both sample and control materials need to be processed through the RP system in a consistent manner. One measure of consistency that was looked for was repeatability in thermograph shape, as thermograph shape is itself a reflection of progress in the pyrolysis reaction. When consistency in thermograph shape is looked for, then, an underlying question is: with RP processing, is the pyrolysis reaction for a given material itself consistent from run to run?

The following possible influences on thermograph disparities were identified:

- Pyrolysis furnace temperature ramp: if notably different from 5°C/min, run-shape can be skewed, reflecting an accelerated/retarded reaction rate. Thermocouple position is critical to ramp characteristics.
- Initial thermal conditions: affect initiation of pyrolysis reaction in Ox-I runs, as Ox-I reaction begins at a low temperature.
- Change in flow rate: a likely influence on run-shape.

Thermographs from repeat runs with the same materials processed through the same RP system were compared. Observations are also made on processing of the same materials through different RP systems. However, not all RRL RP runs are considered.

3.11.1 RRL runs excluded from final dataset

A complete schedule of RRL RP runs conducted for this study is shown in Table 8.2. Among these runs, the following are excluded from the final dataset, for the reasons noted:

- Runs 1 to 19 – affected by quartz wool contamination
- Runs 20–22, 30, 32, 33, 38, 43 – runs to test contamination or to bake clean oxidation chamber CuO (new clean-up chemicals)

- Run 23 – an inspection of the UHP He and UHP O_2 tanks was conducted during this Ox-I run, whose thermograph showed 3 distinct peaks, likely due to disturbance of gas flows
- Run 25 – gases lost during sealing
- Run 27 – kauri run with collection from ambient, not from 105^{o}C (as with later kauri runs, to avoid the early contamination peak)
- Run 35 – gases comprised during sealing
- Run 41 – failed at graphite (S contamination)
- Runs 46–51 – gases collected into tubes pre-loaded with CuO strands and Ag wire, but CuO potentially contaminated by exposure to atmosphere (see 4.4.1).

Run 23 is useful for thermograph comparison, however.

3.11.2 USF Ox-I runs

For both the USF and RRL RP systems, the standard used is Ox-I (Olsson, 1970). Ox-I has been regularly processed in the USF RP system, so is known to fully decompose at <150°C (Fernandez et al., 2014). Because its decomposition reaction begins at <100^{o}C, RP runs with this material are sensitive to the initial temperature settings of the combustion furnace (Fernandez et al., 2014).

Three Ox-I runs were conducted during the USF visit for this study (Figure 3.17). From the thermographs, DB-1770 has a [CO_2] peak of 1773ppm at 133^{o}C, DB-1774 has a [CO_2] peak of 1475ppm at 134^{o}C, and DB-1775 has a [CO_2] peak of 1734ppm at 129^{o}C. The initial mass of Ox-I material was lower for DB-1774 (1.108mg, compared to 1.336mg for DB-1770 and 1.333mg for DB-1775), so it is expected that DB-1774 will produce a smaller amount of CO_2 than the other two runs. Given this difference, the Ox-I thermographs appear consistent.

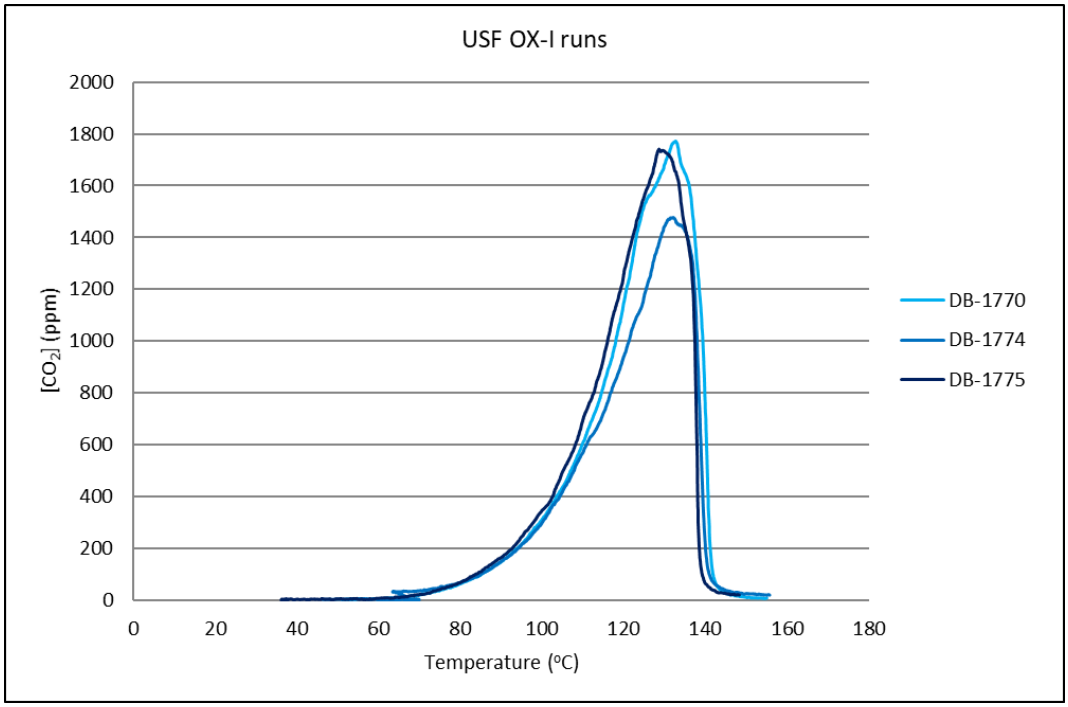

Figure 3.17 Thermographs for USF Ox-I runs. The lower peak for the DB-1774 run reflects the lower initial mass of Ox-I material for this run compared to the other two.

3.11.3 RRL Ox-I runs

Ox-I material was processed in the RRL RP system after the clean-handling protocols described at 3.8 and 3.9 above were introduced. It was expected that repeat runs on the RRL RP system with clean-handled same-material samples would produce thermographs with consistent shapes, but this did not prove the case. Thermographs for runs with Ox-I samples showed many shape variations. While all the RRL RP Ox-I run-shapes are broadly similar, no two are matching (Figure 3.18).

Thermograph shapes for RRL RP Ox-I Runs 24, 25 and 28 are generally similar, showing a rapid rise to a single major peak and a steep fall afterwards. As noted above, Run 23 is anomalous, due to gas flow disturbance during the run. It shows three sub-peaks rather than the single peak shown for Run 24, sized for the same amount of CO_2. The pyrolysis reaction also finishes later than it does for Run 24. The reaction in Run 26 initiates later and finishes later than for other RRL RP Ox-I runs. It also shows two sub-peaks. There is a suggestion here that Run 26 was also subject to gas flow disturbances, though this cannot be proven (see discussion at 3.11.8).

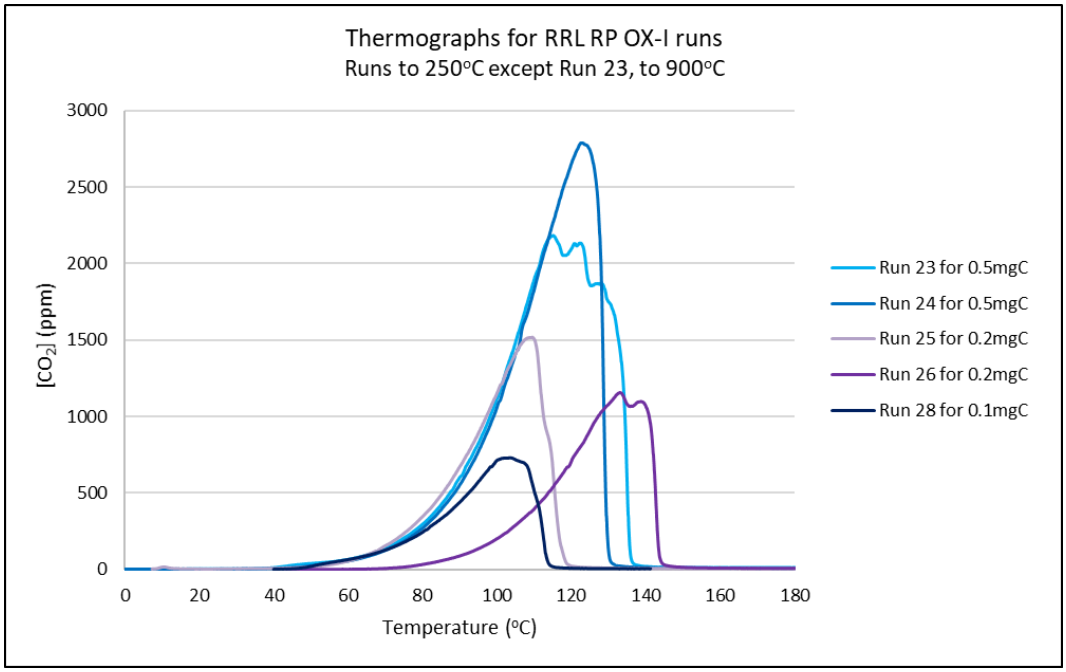

Figure 3.18 Thermographs for RRL RP Ox-I runs. Runs 24, 25 and 28 show expected thermograph shapes. Run 23 was likely subject to gas-flow disturbance. Its thermograph shows three sub-peaks and a delayed reaction-completion. The double peak and late completion in the Run 26 thermograph suggest this run may also have seen gas-flow disturbance.

The ascending limb slopes for Runs 24, 25 and 28 (and also for Run 23) are highly similar. Peaks for the "normal" 0.1mgC, 0.2mgC and 0.5mgC runs (28, 25 and 24) occur at successively higher temperatures (103, 110 and 123°C respectively). Their reaction finishing times also increase with sample size (~115°C for the 0.1mgC run, ~120°C for the 0.2mgC run and ~130°C for the 0.5mgC run). From this it appears that sample size is the major control on the duration of the pyrolysis reaction for Ox-I RP runs, at least in the RRL system. (The effect is not apparent in the USF runs, where the differences in sample size are smaller.)

It is notable that the in RRL Ox-I runs, the pyrolysis reaction for Ox-I initiates by ~50°C (see Figure 3.18), ~10°C earlier than in USF Ox-I runs (Figure 3.17). It is likely, though, that the Ox-I material is itself thermally decomposing in the same manner and at the same actual temperatures inside the respective systems. The 50°C temperature indicated in the RRL set-up and the 60°C indicated in the USF set-up likely relate to the same temperature within the insert. What is different is the thermal set-up in the two systems. The differences may well extend to the way heat is subsequently conducted, so apparent reaction rates in the two systems may also differ, as equivalent temperatures seen by the sample occur at different

run-times in the two systems. The apparent temperatures at which Ox-I reactions initiate in the two systems provides evidence that the vertical furnace orientation at USF and the horizontal furnace orientation at RRL do indeed contribute to different initial thermal set-ups.

3.11.4 USF blank runs: graphite

In the USF RP system, the material for determining the modern carbon contamination in RP processing is ^{14}C-free high-purity (99.9999%) powdered synthetic graphite (Alfa Aesar, stock number 14734; Fernandez et al., 2014). Thermographs from USF graphite runs conducted for this study are shown in Figure 3.19.

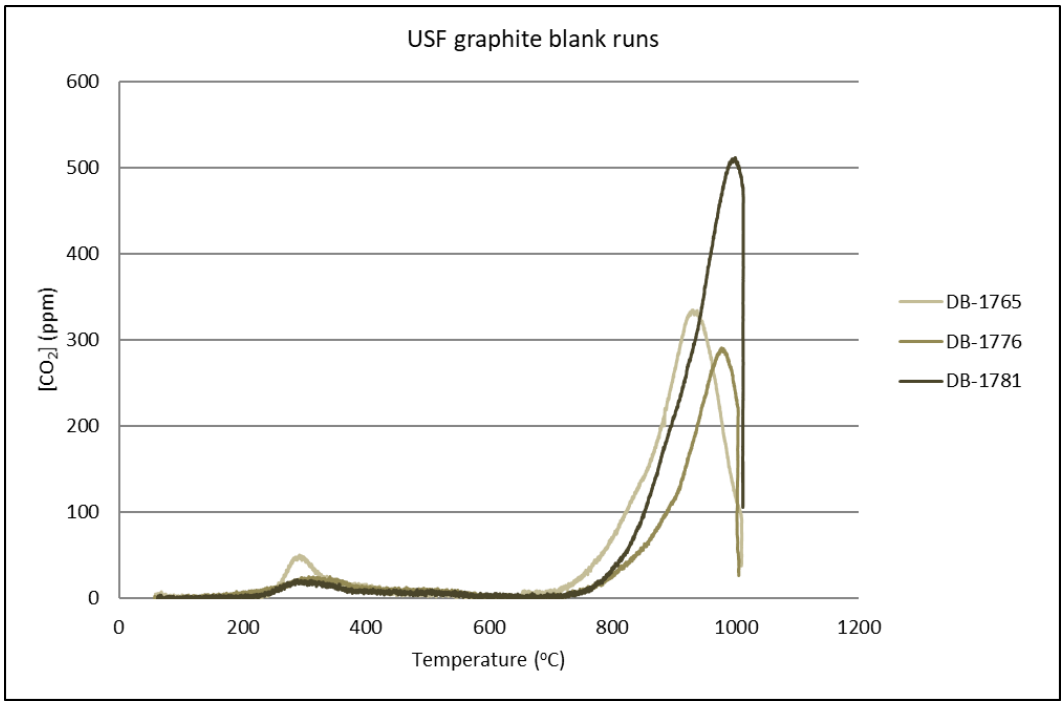

Figure 3.19 Thermographs for USF graphite runs. The higher peak for DB-1781 reflects a markedly greater yield, following replacement of the reactor, with fresh catalyst wires being loaded in the oxidation chamber.

Among the USF graphite runs, DB-1765 has a [CO_2] peak of 335ppm at 929°C, DB-1776 has a [CO_2] peak of 290ppm at 980°C, and DB-1781 has a [CO_2] peak of 512ppm at 999°C. The earlier reaction-initiation temperature and peak [CO_2] value occurrence in the DB-1765 run suggests a significant difference in the pyrolysis reaction rate for this run. The differences between the graphite runs also appear to be more pronounced than the differences between the USF Ox-I runs. It is probable that the temperature seen by a sample from run to run is

variable even in the same system, and that the effect is enhanced at higher temperatures, where the graphite reaction occurs.

The DB-1781 run follows replacement of the pyrolysis furnace and reactor, with the oxidation chamber being loaded with fresh combustion catalyst wires (see Table 8.1). This run produced a significantly higher CO_2 yield (as determined from pressure in the known-volume cold finger, during RP processing) than expected from initial weight. The result is confirmed by the significantly greater mass of carbon being produced at graphitisation at RRL (Table 3.2). (The only completed sediment run after replacement of these parts was DB-1782, with a yield of 133% (Table 5.3 and 3.11.6).)

Table 3.2: Initial mass of graphite and CO_2 yields (based on manometric pressure) for USF graphite runs for this study.

USF Run	Initial mass graphite (mg)	CO_2 expected (μmol)	CO_2 obtained (μmol)	Yield (from μmol CO_2)	Mass C at graphitisation (mg)	Yield (mass at graphitisation vs initial mass)
DB-1765	0.364	30.33	19.91	62.96%	0.198	54.40%
DB-1776	0.310	25.83	14.35	55.57%	0.150	48.39%
DB-1781	0.313	26.08	27.62	105.9%	0.297	94.89%

This finding raises the possibility that C released from pyrolysis is incompletely oxidised to CO_2 during combustion when the catalyst wires are "tired". This could be an issue where the amounts of CO_2 generated and available for conversion to graphite are small. With small sample sizes, contamination is a greater problem and uncertainties for radiocarbon ages increase. When samples are sufficiently large incomplete conversion to CO_2 may not be an issue, provided there is sufficient CO_2 to enable reliable radiocarbon dating.

From a maintenance standpoint, the finding suggests that the catalyst wires should be replaced regularly, rather than only being replaced when a fresh reactor is installed. How often this should be done is a question for further study.

3.11.5 RRL blank runs: kauri

In the RRL RP system, the ^{14}C-free blank material processed is Renton Road Kauri (Marra et al., 2006; Lorrey et al., 2018; RRL laboratory number 40142/7). Renton Road Kauri is a

subfossil tree toppled by a pre-eruptive event then buried by volcanic ashfall at Manukau Harbour, Auckland (Lorrey et al., 2018), with a CRA of >55,000 ^{14}C years BP (Marra et al., 2006; Lorrey et al., 2018). From stratigraphic and other considerations, Renton Road Kauri is at least MIS5 in age (Marine Isotope Stage 5, last interglacial, ~130,000–80,000 years BP, based on benthic δ^{18}O records; Lisiecki and Raymo, 2005) (Lorrey et al., 2018).

While ideally blank material should be similar to the material typically processed in the system, no large source of Antarctic marine sedimentary material devoid of ^{14}C could be readily found. Antarctic marine sedimentary material is precious, and moreover cannot be guaranteed to be free of reworked carbon of younger age, so cannot be known to be ^{14}C "dead". Renton Road Kauri is used routinely as a blank material at RRL, for ST and EA combustion, making it a suitable candidate for RP processing. The ^{14}C-free graphite routinely processed in the USF RP system to quantify modern carbon contamination was not considered ideal due to the high temperatures required for processing (700°C to 1000°C, see Figure 3.19), particularly following a furnace failure during testing, after which it was decided to set 900°C as the RRL RP maximum pyrolysis furnace temperature.

Kauri is a softwood, and softwoods are typically composed of 39 to 48% cellulose, 18 to 29% hemicellulose, and 24 to 36% lignin (Wang et al., 2017). During pyrolysis, cellulose, hemicellulose, and lignin thermally decompose in several stages, by competitive and/or consecutive reactions (Popescu et al., 2011).

Renton Road Kauri is pre-treated by α-cellulose extraction as outlined at 1.4.1 to remove lignins and other mobile wood fractions. With lignins removed, RP processing of Renton Road Kauri is expected to largely reflect the combined effects of cellulose and hemicellulose decomposition under pyrolysis and combustion. Consistent with other studies of wood decomposition under pyrolysis (Williams and Besler, 1996; Yang et al., 2007; Zhao et al., 2017), Gao et al. (2013) find that under pyrolysis at a heating rate of 10°C/min, pine sawdust decomposes with a main weight loss occurring between 200 and 405°C, associated with hemicellulose decomposition, and a maximum weight loss at 361°C associated with the maximum decomposition rate of cellulose. They further find that under combustion decomposition occurs over two major ranges, 226–329°C and 349–486°C, with a second peak at 466°C (Gao et al., 2013). Analysing the gases evolved through these processes, in

pyrolysis peak CO production occurs at ~360°C and ~700°C, with peak CO_2 production at ~360°C (Gao et al., 2013; Figure 3.17(a)), while during combustion peaks in CO_2 production are seen at ~340°C and 468°C (Gao et al., 2013; Figure 3.17(b)).

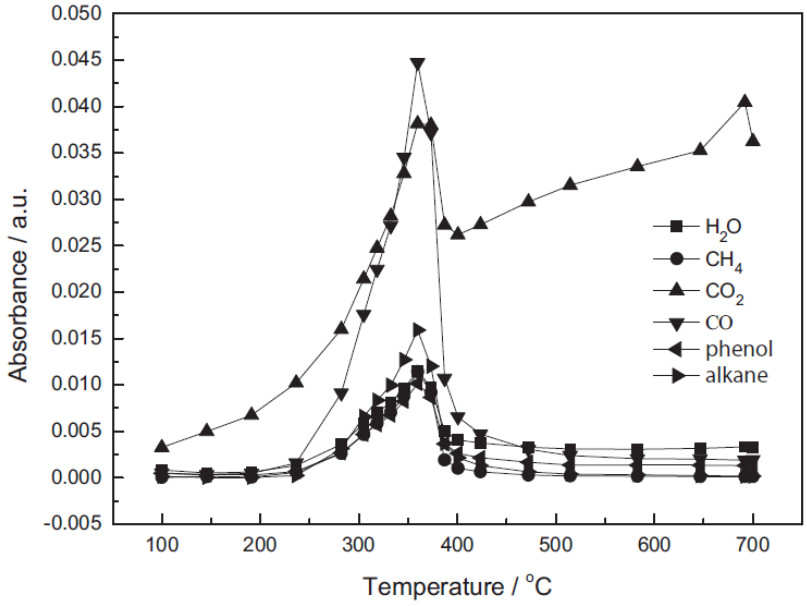

a)

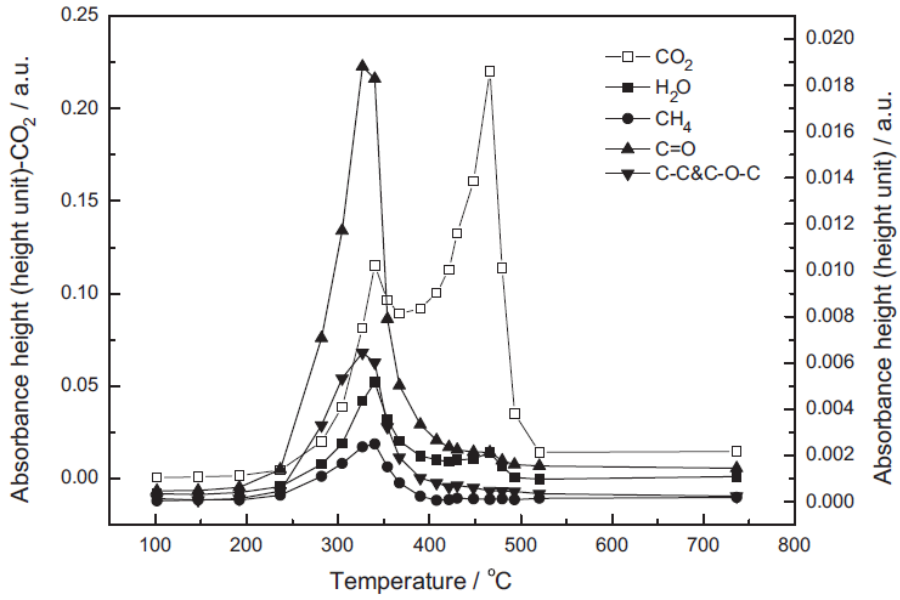

b)

Figure 3.20 Evolution of gaseous products during (a) pyrolysis and (b) combustion of pine sawdust. Temperature is increasing at 10°C/min. Absorbance height is proportional to gas concentration (note separate scale for CO_2 absorbance in (b)). Under both pyrolysis and combustion, there are two distinct peaks in CO_2 generation. (From Gao et al., 2013.)

During ramped pyrolysis, Fernandez et al. (2014) find that IAEA-C3 cellulose reference material (distributed by the International Atomic Energy Agency; Fernandez et al., 2014) has

a decomposition reaction that is so predictable that it is used to verify reproducibility in the USF RP reactor set up. No details of any pre-treatment of the IAEA-C3 material is noted by Fernandez et al. (2014) (they are for other materials), so it is assumed that the IAEA-C3 material was RP processed in its as-supplied state. During pyrolysis in the USF RP system, cellulose undergoes thermal decomposition with peaks at 361 ± 10^{o}C and 535 ± 10^{o}C (Fernandez et al., 2014; Figure 3.21, below). The first of the IAEA-C3 cellulose thermal decomposition peaks noted by Fernandez et al. (2014) is identical to the maximum weight loss of pine sawdust under pyrolysis found by Gao et al. (2013). Moreover, two distinct CO_2 peaks are shown both from the separate pyrolysis and combustion of pine sawdust by Gao et al. (2013) and from the RP processing of pure cellulose (Fernandez et al., 2014; Figure 3.18).

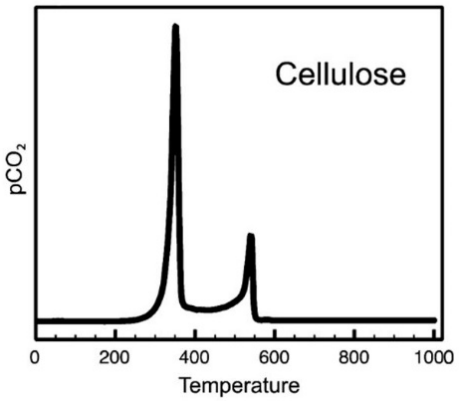

Figure 3.21 Exemplary thermograph from USF IAEA-C3 run (from Fernandez et al, 2014.)

Gao et al. (2013) and earlier workers show that various hydrocarbons are produced from pyrolysis of pine (Williams and Besler (1996) show the production of methane and ethane). During RP processing, gases evolved from pyrolysis are subsequently combusted and the carbon present thereby oxidised, so any hydrocarbons driven off during pyrolysis will contribute to the CO_2 produced, provided they break down in the conditions provided in the combustion chamber. For example, methane has been found to have a minimum auto-ignition temperature in air of 600^{o}C (Robinson and Smith, 1984). Methane produced from pyrolysis in RP processing would therefore be expected to be oxidised to CO_2 when exposed to O_2 at 800^{o}C. Such effects are likely to be reflected in both RP processing of pure cellulose in the USF RP system, as shown by Fernandez et al. (2014), and of pre-treated kauri in the RRL RP system.

Thirteen runs with Renton Road Kauri blank material were completed in the RRL RP system with clean-handling procedures in place (see Table 8.2). However, Runs 27 and Runs 46 to 51 were eliminated, as noted above. Run 29 was with original clean-up materials, while Runs 34 to 36, 42 and 45 were with replacement clean-up materials (see 3.10). The thermograph shapes of the viable runs are broadly similar, showing two major peaks, with the second peak higher than the first, and a lower "saddle" in between (Figure 3.22). The peak-heights broadly reflect sample size. Run 29 is a clear outlier.

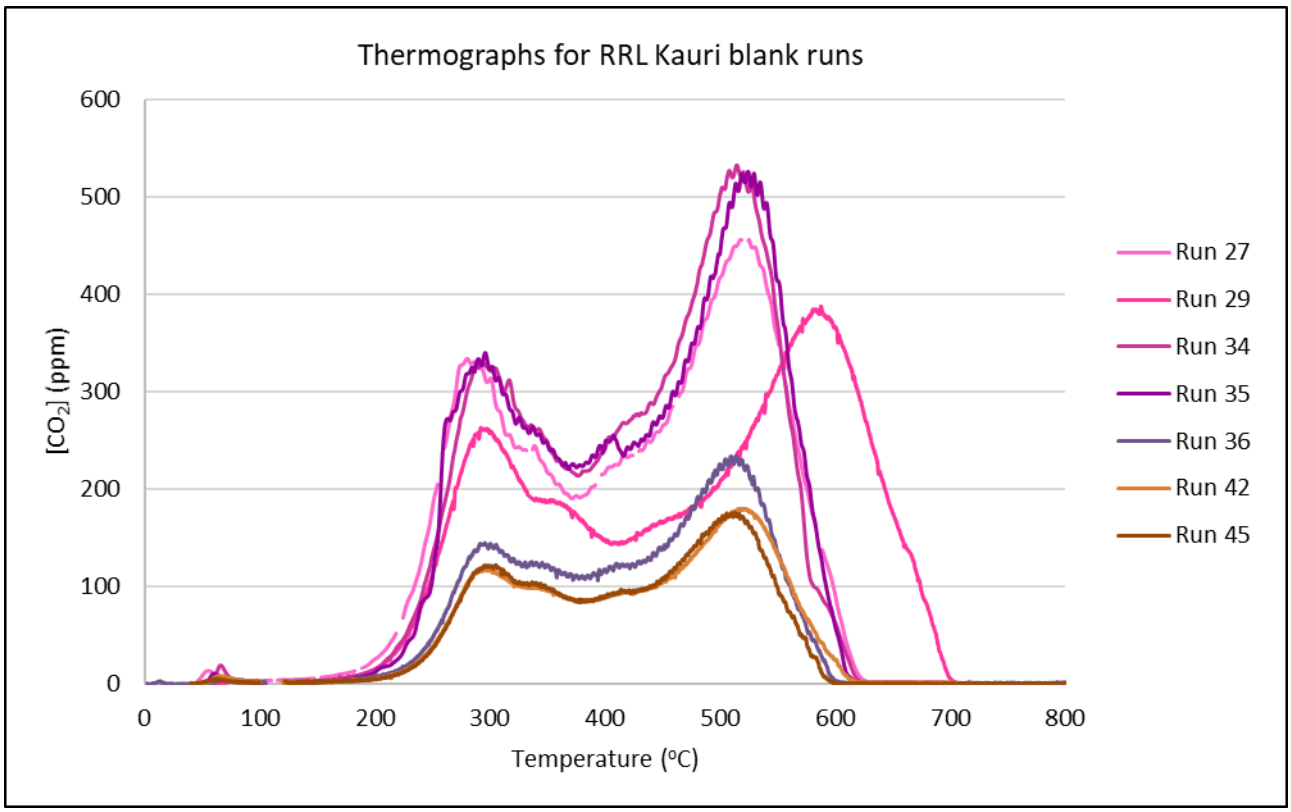

Figure 3.22 Thermographs for viable RRL RP Renton Road Kauri runs. The 0.5mgC runs are in pink/purple shades, the 0.2mgC run is in blue and the 0.1mgC runs are in brown shades. In terms of thermograph shape, Run 29 is a clear outlier.

First peak values vary from around 285°C (Run 34) to 300°C (Run 45). Other than for Run 29, second peak values vary from around 515°C (Runs 34, 36 and 45) to 530°C (Run 35). The first peak temperatures are lower than the first IAEA-C3 cellulose thermal decomposition peak noted by Fernandez et al. (2014), but within the 250–350°C hemicellulose decomposition range observed by Williams and Besler (1996). Most of the second peak temperatures are near or within the second IAEA-C3 cellulose thermal decomposition peak range of 525–545°C noted by Fernandez et al. (2014).

Among the runs for 0.5mgC, the thermographs for Runs 27, 34 and 35 are broadly similar. The second peaks fall within the range 515°C (Run 34) to 530°C (Run 27), with end-reaction temperatures from 610°C (Run 35) to 630°C (Run 27). Run 29 shows a lower first peak, a protracted fall in the saddle region, a delayed and stunted second peak at 590°C and a significantly higher end-reaction temperature of 705°C. The reaction rate for Run 29 clearly differs from the others. An unusually high initial pyrolysis furnace temperature, 59°C, was observed for Run 29 (Run 29 was the second attempt at the run on the same day, with the pyrolysis furnace not having completely cooled from the first attempt). But conditions at the start of the run would not be expected to exert much influence on the pyrolysis reaction late in a run, unless those initial conditions affect the way the reaction evolves as a whole. Two possible explanations for the generally retarded reaction rate for Run 29 are anomalous thermocouple placement, and a flow control issue.

Thermographs for 0.2mgC (Run 36) and 0.1mgC (Runs 42 and 45) are generally similar to each other, scaled to their relative sizes, though the first peak for the 0.2mgC run seems a little low. First peaks occur at ~300°C and second peaks at ~515°C (Runs 36 and 45) or 520°C (Run 42).

3.11.6 USF runs with Antarctic marine sediment

Most Crystal Sound sediment samples were processed only once in the USF RP system, so in most cases comparisons between different runs with the same material cannot be made. With R41115/4 sediment, however, two runs failed (DB-1777 and DB-1778), but in each case not before three splits were taken, with a third run then being completed (DB-1782). This resulted in three partially-overlapping thermographs which can be compared (Figure 3.23).

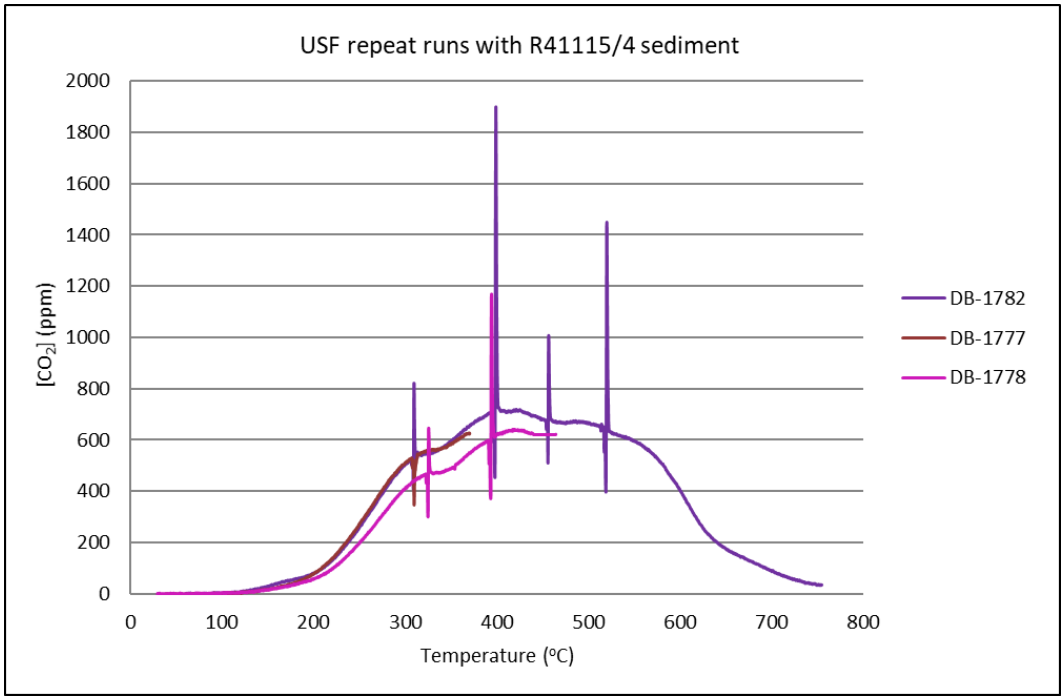

Figure 3.23 Thermographs for repeat USF runs with R41115/4 material. To allow comparison the thermographs are plotted from raw data, so include the [CO_2] artefacts associated with pressure spikes when splits are taken. The thermograph shapes appear similar, showing only subtle variability.

Compared to the DB-1777 and DB-1782 runs, the DB-1778 run shows a subtle shift of the ascending limb to higher temperatures, so climbing a little later, with the [CO_2] peak appearing slightly later and also being more clearly defined than the corresponding DB-1782 peak. The minor difference in peak heights is likely to reflect drift in the CO_2 analyser. However, the differences seem trivial. On the available evidence, repeat USF RP runs with the same sedimentary material produce largely similar thermograph shapes.

3.11.7 RRL runs with Antarctic marine sediment

Thermographs for RRL RP runs with R41115/2 Antarctic marine sediment included four runs for a single split taken at 900ºC (Runs 31, 37, 39 and 40) and one run for 5 splits (Run 44). The thermographs show variability in underlying reaction rate, with peaks and descending limbs appearing earlier in some runs than in others, but shapes that are broadly similar (Figure 3.24).

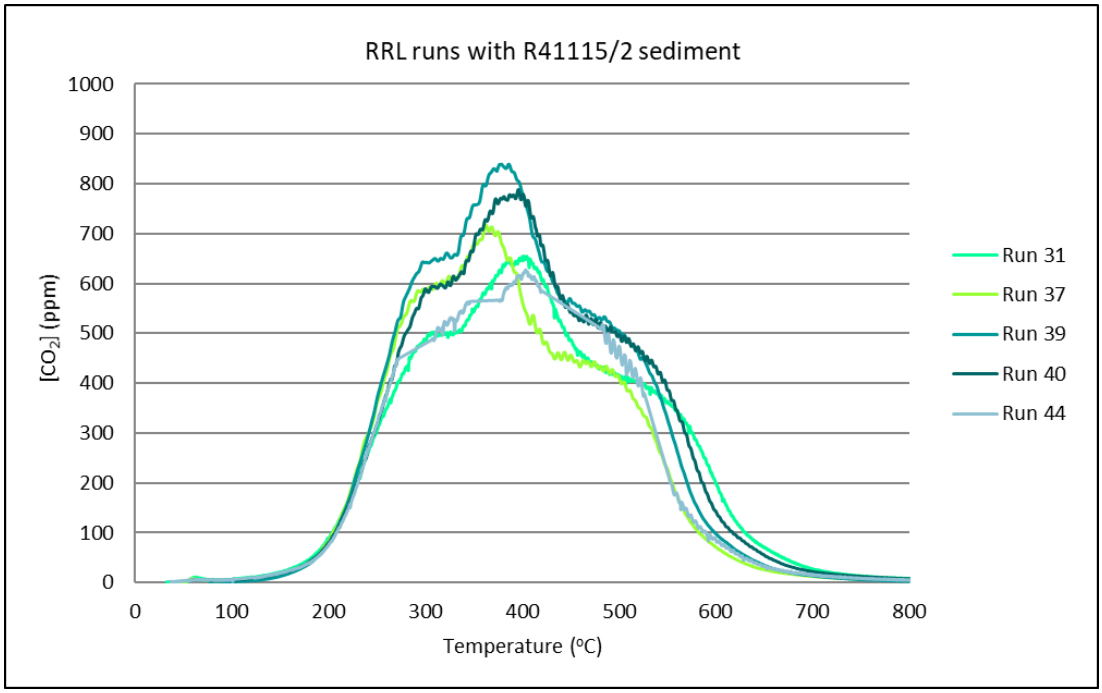

Figure 3.24 Thermographs for clean-handled RRL runs with R41115/2 material. Apparent variations in peak height are largely the result of drift in the gas analyser. Shapes show broad similarity, though peaks and descending limbs appear up to 30°C sooner in some runs than in others.

All runs show the same reaction initiation, with ascending limbs all initially coincident. The range for peak [CO_2] values is ~30°C, from Run 37 at ~375°C to Runs 31 and 44 at ~405°C. The runs showing early peaks also show early descending limbs, with the descent from the shoulder in some runs occurring ~25°C (5 minutes) sooner than in others. Visually, the Run 31 and 37 thermographs are compressed and offset versions of those for Runs 39 and 40.

Given the different thermal set-ups of the USF and RRL RP systems, it is not expected that a direct comparison of the 5-split runs with the same Antarctic sedimentary material on each system will produce very similar thermographs. In fact, the early stages are highly similar, with deviation occurring only when the first split is taken (Figure 3.25). After the first split, the ascending limb shoulder of the RRL run drops significantly below the corresponding USF run shoulder, and after the second split, the peak is even more subdued. Peak [CO_2] values do occur at similar temperatures, at 401°C for the USF run and at 407°C for RRL Run 44. The stepped appearance of the RRL thermograph contrasts the USF case, however, where the underlying thermograph shape continues uninterrupted after a split is taken. Also, the RRL

pyrolysis reaction appears to finish sooner (by ~50°C, between the 200ppm and 100ppm [CO_2] levels).

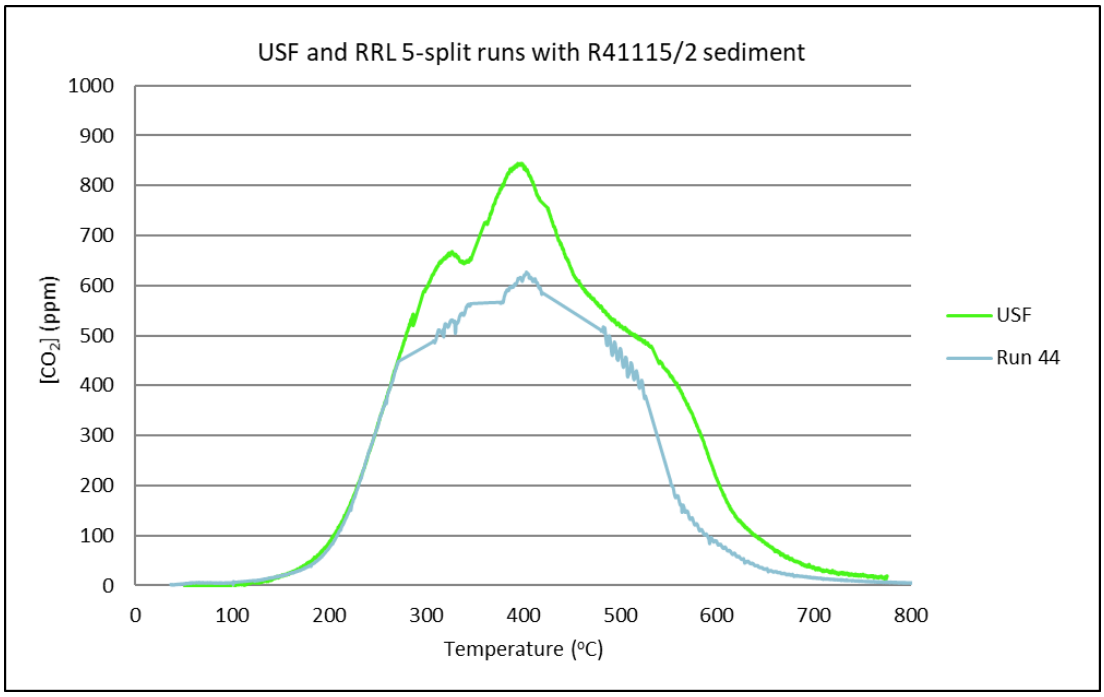

Figure 3.25 Thermographs for USF and RRL 5-split runs with R41115/2 material. The shapes deviate where splits are taken. Straight-line sections in the Run 44 plot are where splits have been taken, and artefacts related to pressure disturbance removed. The length of the straight-line sections indicate the time taken for pressure equilibration, and do not indicate loss of CO_2.

It is possible that the pressure changes at the pyrolysis location affect the pyrolysis reaction itself. If the reaction proceeds faster under reduced pressure, or if it slows due to less effective heat transfer in a lowered-pressure environment, or a combination of both, there may be a change in reaction rate. After pressure re-equilibration, the reaction may proceed at its normal rate after an interval of being retarded or accelerated, or both. These possibilities have not been investigated, but it is plausible that pressure changes in the system during split-taking affects reaction rate and, consequentially, the rate of CO_2 production. As the amounts of CO_2 collected are small, small changes in the rate or character of the pyrolysis reaction may affect thermograph shape. It may be that thermograph shape changes are unavoidable under the dynamic conditions of split-taking from run to run, even within the same system.

The progressive dwarfing in the thermograph for the RRL 5-split run compared to the USF equivalent may be largely an artefact of pressure changes. Alternatively, they may indicate changes in the underlying pyrolysis reaction as it proceeds. Thermographs for single-split RRL runs with R41115/2 sediment provide evidence of differing reaction rates from run to run, as well as general similarity. Given the variability across the RRL single-split runs, the variability between 5-split runs on different systems is unsurprising, and is evidence that the systems operate slightly differently, particularly when split-taking is involved.

3.11.8 Thermograph variations: flow rate

In the RRL RP system, individual flow rates for gas delivery cannot be checked during a run. Combined UHP He and UHP O_2 flows can be monitored with a flow meter at the vent outlet, but this is not typically done during a run, as the operator is normally too busy once split-taking has begun. (In the USF system, individual flow rates are continually displayed.)

At the vent outlet, in a non-run situation, O_2 flow can be checked with the He flow turned off, and combined 7mL/min and 35mL/min He flow can be checked from the total vent flow (42mL/min expected), with the O_2 flow turned off. However, for the UHP He 7mL/min flow to be checked separately (with the O_2 flow off), the stainless steel tubing for the 7mL/min He flow must be disconnected from the side arm, a Pyrex stub-tube attached to the stainless steel tubing, and the flow meter connected to the stub-tube. The 35mL/min He flow can be checked from the total vent flow, once the 7mL/min He flow has been checked. With the O_2 flow turned on, the total vent flow of 46mL/min is expected. So it is simple to check O_2 and total He flows, but interference to the system is required to check the 7mL/min He flow independently.

Gas flow in the RRL RP system was checked before the initial test run, then after Runs 2 (small adjustments made to Porter regulator settings), 14 (O_2 flow had fallen to 3.7mL/min, 7mL/min He flow had dropped to 6.3mL/min, and total He flow to 43mL/min; Porter regulators readjusted), and 31 (total He flow 42mL/min, combined He and O_2 flow 46mL/min; no adjustments made).

While no major changes in gas flow rate were detected when tested, and flow rates seemed consistent from Run 14 onwards, it is possible that small changes matter. Pressure fluctuations may occur within or between runs, so that the behaviour of the Porter regulators and hence flow rates changes, even though when sporadically tested on different days flow rates appear highly similar. A reduced or enhanced carrier gas flow rate could affect the way the pyrolysis reaction occurs and the rate at which carbon is given off and CO_2 evolved as a result. This possibility has not been investigated. However, flow rates could be deliberately altered to test the effect on thermograph shape.

3.11.9 Thermograph variations: summary observations

Thermographs from runs with the same material are generally similar, but variations are seen. Primarily, the variations are with Ox-I runs, where the pyrolysis reaction begins at a low temperature.

The temperature reading is taken on the outside of the quartz reactor, while the sample is located within the insert. The initial temperature inside the insert is likely to be lower than the thermocouple temperature, as the thermocouple temperature is taken at the internal furnace surface, two quartz walls and an air gap away from the sample. As the temperature increases, temperature inside the insert will eventually catch up to the measured temperature. Small variations in initial thermal environment from system to system or in thermocouple position from run to run could propagate to differences in reaction rate and thermograph shape, particularly at low temperatures. This would explain the variability in the observed Ox-I pyrolysis initiation temperature.

The runs with kauri and sediment material show generally good repeatability, as evidenced by their thermographs. Variability in thermograph shape when multiple splits are taken is unsurprising, given the dynamic conditions which prevail. The inconsistencies which remain may be characterised as noise it would be good to eliminate, rather than a major issue.

Pyrolysis reactions are likely to be sensitive to changes in thermal conditions from run to run, or within a run itself. The influence of disturbed flow within a run is seen in the Run 23 thermograph, so it seems likely that changes in flow rates of incoming gases within or between runs will produce an effect on reaction rate and thermograph shape. Pressure

instabilities due to split-taking are seen to affect thermograph shape and may also influence flow rate, as gas flows in the RRL system are controlled by pressure-sensitive membranes in high-precision regulators. Whether the underlying pyrolysis reaction is affected is unknown. Thermocouple movement from run to run is a likely contributor to thermograph variability.

The differences in set-up between the RRL and USF RP systems result in different thermal environments, as evidenced by the difference in reaction initiation temperatures with Ox-I runs. As a result, exact replication of thermograph shapes for parallel runs on the two systems cannot be expected.

4 Determination of blank corrections for RP processing

4.1 Methods

Collection and processing of any sample for radiocarbon dating will almost inevitably introduce contamination. Such contamination must be assessed and corrected for if an accurate radiocarbon date is to be provided.

Blank material which nominally contains no ^{14}C is used to assess modern contamination (for example, from an atmosphere leak). The blank material is subjected to the same processing steps that the unknowns whose ^{14}C:^{12}C ratio is to be measured are subjected to. Any ^{14}C which is present after processing can be attributed to the processing itself, so a correction for contamination introduced by processing can be made. In this study, the blank material is Renton Road Kauri (Marra et al., 2006; Lorrey et al., 2018).

Standard reference materials are used to assess dead contamination (for example, from dead carbon present in the iron catalyst that graphite is precipitated onto (Turnbull et al., 2007)). The standard is processed in the same manner as the unknowns. Its measured ^{14}C:^{12}C ratio is compared to the ^{14}C:^{12}C ratio for a portion of the same standard which has not been so processed (other than being graphitised), measured on the same AMS wheel. Any departure from the well-known $F^{14}C$ for the processed standard can be attributed to dead contamination from processing. (While modern contamination may also be introduced, this will have a much smaller effect, as $F^{14}C$ for the standard is already close to 1 (modern).) For this study, the standard used is Ox-I (Olsson, 1970). The non-processed Ox-I material is “flask” Ox-I graphitised in the same manner as unknowns (Turnbull et al., 2007).

4.2 Contamination corrections for large samples

At RRL, large samples are those which produce 0.3mgC or more at graphitisation. For samples of this size, correction is made by direct comparison of measured ^{14}C:^{12}C ratios for the unknowns with the ^{14}C:^{12}C ratios for blanks and standards measured on the same wheel (to ensure all materials are measured under the same conditions).

Correction for contaminating modern carbon (MC) introduced by processing is on the basis of $F^{14}C$ measured for the sample minus $F^{14}C$ measured for the blank (Renton Road Kauri). The blank value is average of large-sized blanks which have been processed and measured in RRL AMS system over the preceding ~6 months.

At RRL, no separate correction is needed for dead carbon (DC) contamination large samples, as it is implicit in measurement of the Ox-I standard which has not been RP-processed.

4.3 Contamination corrections for small samples

4.3.1 Contamination corrections for USF RP-processed small samples

For USF RP processing, each split is collected over a certain length of time while the temperature seen by the sample rises. Before AMS measurement, the sample is ST combusted and graphitised. So an RP-processed sample spends a length of time in the RP system, then undergoes additional processing.

Fernandez et al. (2014) demonstrate that MC contamination accumulates with time spent in the RP system by measuring accumulated amounts of MC in samples of crude oil. The oil is nominally ^{14}C-free and begins to break down at low temperatures. It was found that the longer an oil sample spent in the RP system, the more MC contamination it accumulated (Figure 4.1, below).

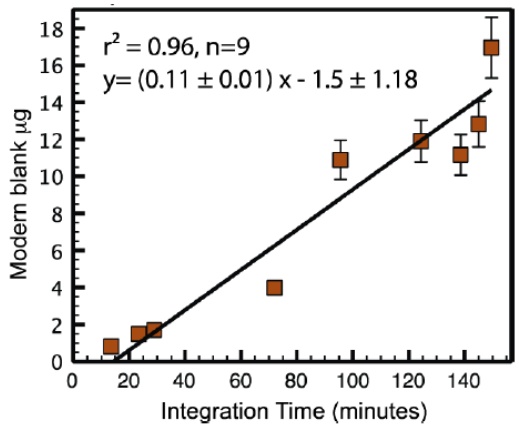

Figure 4.1: Time-dependent modern carbon contamination accumulated in crude oil samples which have spent different amounts of time in the RP system (from Fernandez et al., 2014). MC contamination for a full RP run to 1000°C (195 minutes of RP processing time) was calculated by RP-processing small-sized samples of Alfa Aesar graphite. The graphite is

sensitive to MC inputs as it contains no modern carbon, but unresponsive to dead carbon inputs as its $F^{14}C$ is close to zero (Fernandez et al., 2014).

MC contamination for time zero (25°C, no RP-processing time) was calculated from ST combustion only of the same graphite (Fernandez et al., 2014). This is justified as every RP-processed sample must undergo ST combustion for sulphur clean-up. The time-zero MC contamination was measured as 1.95 ± 0.7 μgC, and the 195-minute MC contamination as 8.8 ± 4.4 μgC (Fernandez et al., 2014). To calculate the time-dependent component, the time-zero value is subtracted from the 195-minute value. The sample is assigned a proportion of this remaining value relative to the fraction of the total time it has spent in the system. The time-zero (time-independent) component is then added back in (Fernandez et al., 2014).

DC contamination was determined from repeated measurements of RP-processed IAEA-C3 (Fernandez et al., 2014). IAEA-C3 is a cellulose standard (Rozanski et al., 1992) distributed by the International Atomic Energy Agency (IAEA). It is post-modern – that is, includes bomb-pulse carbon – with a consensus $F^{14}C$ of 1.2941 ± 0.0006 (Fernandez et al., 2014). The contamination measured for the cellulose includes both DC and MC components. To isolate the DC component, cellulose results are first corrected for MC contamination as determined from graphite measurements. Results showed the mass of contaminating DC to be highly variable from run to run, and in the range of 4.2 ± 5.5μg per run.

It was further found that when separate splits were taken for each of the two CO_2 peaks produced in a cellulose RP run (see 3.11.5 and Figure 3.21, above), each split showed a mass of contaminating DC similar to that shown by a single split from a complete cellulose run (Fernandez et al., 2014). Therefore the full DC blank was assigned to each split taken, regardless of how much RP-processing time was involved in split-collection. It was concluded that the DC blank accumulated in RP processing does not result primarily from processing in the RP system itself. Rather, it is likely due to the reagents used in ST combustion (Fernandez et al., 2014).

The full contaminating blank for USF RP processing, then, is found to be a composite of time-dependent and time-independent masses of contaminating MC and a substantially time-independent mass of contaminating DC (Fernandez et al., 2014).

4.3.2 Blank corrections for USF RP-processed samples combusted and graphitised at RRL

Three Alfa Aesar graphite samples and three Ox-I standards were RP-processed at USF for this study (discussed at 3.11.2 and 3.11.4). The CO_2 collected from these USF RP runs was ST combusted at RRL by laboratory staff as outlined at 1.4.2 and the combusted CO_2 cryogenically extracted on the RRL combustion processing line as outlined at 1.4.2. The extracted CO_2 was graphitised at RRL by laboratory staff as outlined at 1.4.2. The CO_2 from the DB-1770 Ox-I run was lost during cryogenic extraction. This left three USF RP-processed graphite samples and two USF RP-processed Ox-I standards for determination of the modern and dead carbon contamination for USF RP processing.

The long-term RRL estimate of MC contamination from ST combustion and graphitisation is 0.00083mgMC (determined from ST-combusted ^{14}C-free kauri samples). This was used as an estimate of the time-independent component of MC contamination for USF RP-processed samples for this study. It is appropriate as the time-independent component of MC contamination determined by Fernandez et al. (2014) was on the basis of ST combustion and graphitisation, and ST combustion and graphitisation for this study was performed at RRL. The time-dependent mass of contaminating MC was calculated from the three USF RP-processed graphite samples as 1.3615×10^{-5}mgMC/min, following the method of Fernandez et al. (2014). However, this value was not considered robust, as it was based on so few samples. Instead, the long-term USF time-dependent mass of 9.74359×10^{-6}mgMC/min (Rosenheim, personal communication) was adopted. This is suitable as it was the USF RP system that the Crystal Sound samples were processed on, and this is the value used for other samples RP-processed at USF around the same time.

The mass of contaminating DC was calculated from the two USF RP-processed Ox-I standards as 0.0024mgDC, following the method of Fernandez et al. (2014). However, this value was based on only two samples, so again was not considered robust. Instead, the long-term USF estimate of the DC mass of 0.0015mg (Rosenheim, personal communication) was adopted. This is a compromise, as the USF estimate includes an MC correction with the time-independent component based on ST combustion of graphite, whereas we use the RRL long-term value based on ST combustion of kauri. Rather than sub-dividing the USF MC correction

on the basis of USF and RRL determined-components and applying this to a USF-determined total (of both MC and DC components) to isolate the DC component, it was considered simplest to adopt the USF estimate as a whole (though imperfect).

4.3.3 Small-sized samples: RRL RP modern carbon contamination corrections

To assess the modern carbon contamination for RP-processed samples of small size, a range of small-sized and large-sized samples of Renton Road Kauri were RP-processed. After AMS processing and data reduction, a graph was constructed plotting the ratio to standard (RTS, as determined from AMS measurements) against 1/M, where M is the mass of carbon as determined from graphitisation, with the slope forced through the origin, following the method of Santos et al. (2007). Only Runs 29, 34, 36, 42 and 45 were considered reliable (see Table 8.2 and 3.11.1), so a plot was constructed using values from these runs (Figure 4.2). Runs 29 (0.5mgC-size) and 42 (0.1mgC-size) were to 705°C, while Runs 34 (0.5mgC-size), 36 (0.2mgC-size) and 45 (0.1mgC-size) were to 905°C. The effect of contaminating modern carbon on RTS is greater in smaller-sized samples (seen to the right in the plot) due to its higher proportion relative to sample mass. The slope "m" of each line gives the mass of contaminating modern carbon accumulated during the run-time – 0.0035mgC for runs to 905°C and 0.0024mgC for runs to 705°C.

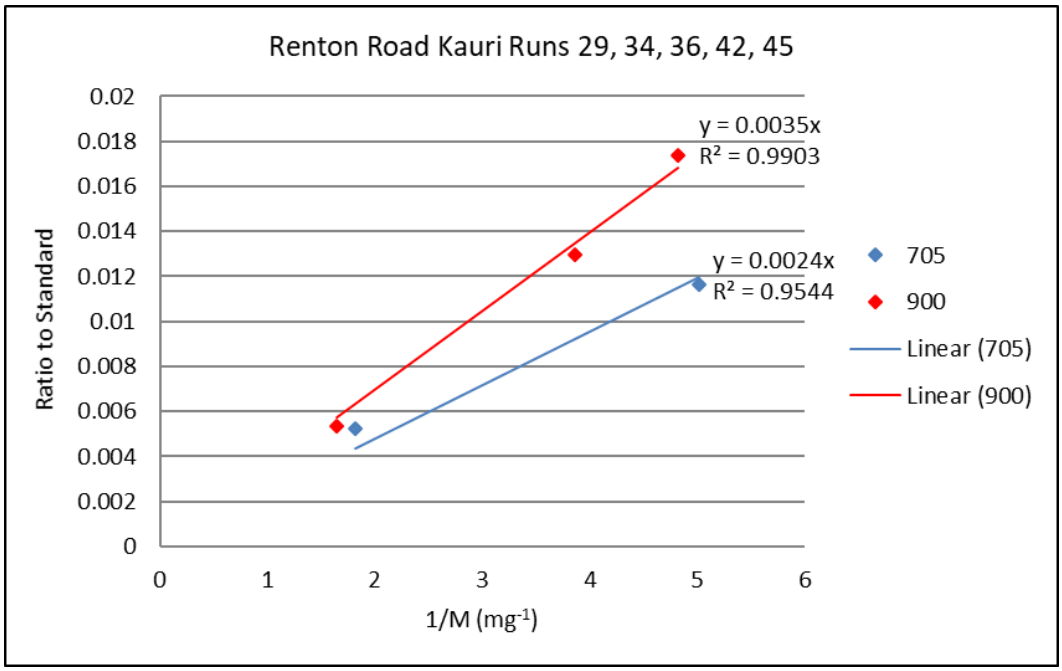

Figure 4.2 Graph of RTS against 1/M for RRL RP Runs 29, 34, 36, 42 and 45 with Renton Road Kauri blank material. The slope of each line gives the mass of contaminating modern carbon accumulated during the run-time (Santos et al., 2007). While only a small number of data points are available from this study, the difference in m between the runs to 705°C and the runs to 900°C suggest that modern carbon contamination from RRL RP processing includes a time-dependent component.

The method of Fernandez et al. (2014) was followed to determine MC and DC contamination for RRL RP processing. For MC contamination, we assumed that contamination includes both time-dependent and time-independent components. For determining m, we used the RTS against 1/M plot for the 900°C runs only. We have the most data points for runs of this length, and for consistency, runs of the same length were used, as each run then has the same opportunity for time-dependent contamination to be introduced.

For the time-independent MC contamination from RP processing, the long-term RRL estimate of MC contamination from ST combustion and graphitisation of small Renton Road Kauri blanks (0.00083mgC) was adopted. This amount was subtracted from slope m to find the RP-only component of the modern carbon contribution for the 900°C RP runs. The per-minute time-dependent modern carbon contribution for the RP system was found by dividing the RP-only component by the run-time over which this component was accumulated. This gives:

$$m(t\text{-}d) = [m - m(t\text{-}ind)]/\text{RP time} \quad [10]$$

where m(t-d) is the time-dependent component and m(t-ind) the time-independent component of modern carbon contamination (both in mgC), and RP time is the pyrolysis time over which the time-dependent component was accumulated. A typical 900°C RRL RP run takes ~171 minutes total run-time, but the CO_2 fraction produced to 105°C is not collected (as it includes potential handling contamination), so the time to reach 105°C is not included in the RP time (which for a 900°C run is ~160 minutes).

This gives m(t-d) = (0.0035 – 0.0008)/160 = 1.69 x 10^{-5}mgC/min, and m(t-ind) = 0.00083mgC. For a given run, the per-minute RP contribution is multiplied by the time (after 105°C) over which the CO_2 was collected to give the time-dependent component. The accumulated mass of contaminating MC (m) for an RP-processed sample is this time-dependent component plus the time-independent contribution from ST combustion and graphitisation (m(t-ind), previously subtracted). That is,

m = m(t-d)*(RP time) + m(t-ind). [11]

4.3.4 Small-sized samples: RRL RP dead carbon contamination corrections

To determine the DC (^{14}C-free) contamination that processing adds to a sample, a range of small-sized Ox-I standards are processed in the same manner as the unknowns. For this study, Ox-I Runs 24 (0.5mgC-size), 26 (0.2mgC-size) and 28 (0.1mgC-size) were used (see Table 8.2 and 3.11.1). Following the method of Santos et al. (2007), their respective masses (M) and AMS-measured RTS values were used to construct a plot of [1 – RTS] against [1/M – 1/M_S], where M_S is the mean mass of large "flask" and EA Ox-Is measured on the same wheel (Figure 4.3). As the RTS expected for Ox-I is close to 1 (that is, modern), [1 – RTS] gives a value close to zero. The smaller mass M is, the further 1/M deviates from 1/M_S. The slope of the line of best fit forced through the origin gives the mass "d" of contaminating DC. From these runs, d = 0.0043mgC. The small number of data points and the looseness of the fit (as reflected by the low R^2 value) indicate that this estimate is not very robust, but the value itself indicates that dead carbon contamination is significant in RRL RP processing.

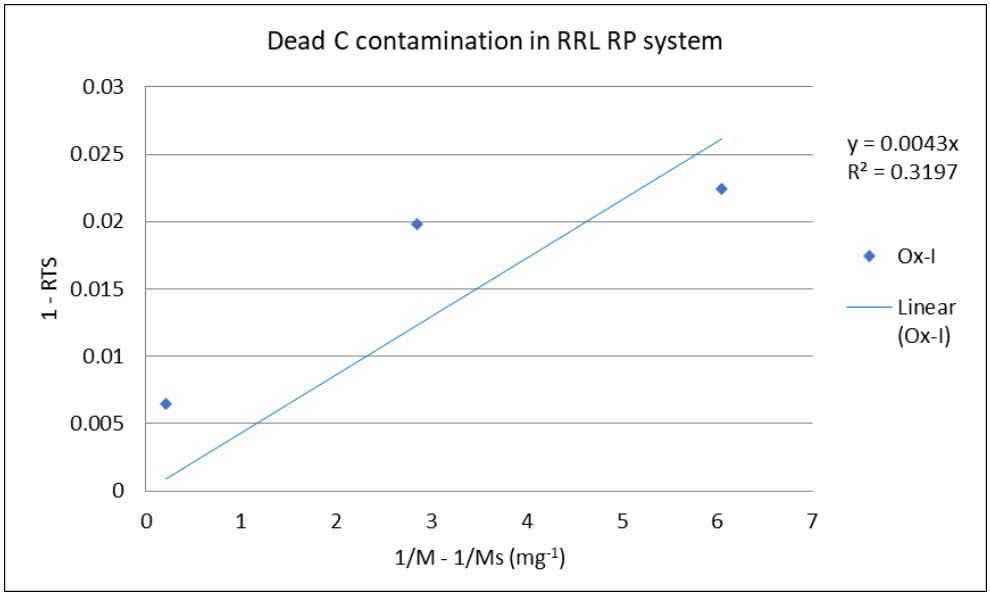

Figure 4.3 Graph of (1 – RTS) against (1/M – 1/Ms) for RRL RP runs with Ox-I material, following the method of Santos et al. (2007). M is the mass of carbon as determined from graphitisation, and Ms denotes the average mass from graphitisation of the larger non-RP processed Ox-I samples. The 0.5mgC value is closest to y-axis, the 0.2mgC value is at the centre and the 0.1mgC value is at the right. The slope of the line of best fit approximates the mass of contaminating dead carbon (0.0043mgC).

The Figure 4.3 plot shows the importance of sample size to the relative contribution of the dead carbon blank. For the small samples, the proportional contribution of the dead carbon blank to the deviation in RTS (from a value of 1) is greater than it is in the case of large samples, as expected.

We follow Fernandez et al. (2014) in assuming that d is a time-independent value. This is consistent with their finding that in RP processing of cellulose, splits collected from an entire run or from part of a run showed a similar mass of contaminating DC. They therefore assigned the full DC blank to each split, regardless of how much RP-processing time was involved (Fernandez et al., 2014). It is assumed that RRL RP processing will be similar to USF RP processing in this respect.

Our d-value is large compare to the typical range of 0.0005–0.0025mgC (average 0.0017mgC over the past 5 years) diagnosed for small samples at RRL, and high compared to the d-value of 0.0015mgC for USF RP processing (Rosenheim, personal communication). However, the USF d-value has been determined over many runs with protocols which are well-established, and is itself three times the upper-end d-value reported by Santos et al. (2007) for small-sample processing at the W.M. Keck Carbon Cycle Accelerator Mass Spectrometer Facility at the University of California, Irvine (0.1–0.5μgC). Even the well-determined d-value for USF RP processing suggests that RP processing is not particularly "clean."

4.3.5 Applying modern and dead carbon contamination corrections to small-sized unknowns

Using the m and d values calculated from plots constructed from RTS and M values from RP processing and subsequent AMS measurements, corrections for contamination in small-sized RP processed samples can be derived following the method of Santos et al. (2007). The modern carbon correction (MCC) and dead carbon correction (DCC) for a particular small sample are calculated by dividing mass m and d (respectively) by the mass of the sample (Santos et al., 2007). The sample mass is as determined at graphitisation. From the measured $F^{14}C$ for the sample, a corrected fraction modern $F^{14}C'$ is calculated by:

$$F^{14}C' = [F^{14}C - MCC]/[1 - DCC - MCC] \quad [12]$$

(Santos et al., 2007).

At RRL, 100% uncertainty is assumed for MCC and DCC values. This is to account for the variability seen from testing small samples of Ox-I and Renton Road Kauri over time. At present we have only a small amount of data from RP processing of these samples, so there is limited certainty around our calculations for m and d. Applying 100% uncertainty to MCC and DCC values obtained for small samples recognizes that our current estimates for m and d are approximations only.

5 Comparison of USF and RRL bulk sediment and RP results

Samples taken from the same Antarctic sediment materials were RP-processed at both USF and RRL. This chapter outlines how the samples were pre-treated and RP-processed, the ages obtained for bulk sediment samples and individual RP splits, how these ages compare to each other and how results from RRL and USF compare.

5.1 Crystal sound sediment sample description

A suite of Antarctic marine sediment samples was prepared at RRL and processed through the USF RP system. The samples were obtained on the KOPRI 2017 Bellingshausen Sea cruise from gravity cores taken from the seafloor in Crystal Sound, at cruise stations 16 (66°37.5350'S, 66°56.6366W, water depth 1442m), 17 (66°38.3951'S, 66°54.6033W, water depth 1451m) and 18 (66°44.2629'S, 66°56.0963W, water depth 1218m). Descriptions and physical pre-treatments of the samples are summarised in Table 5.1.

Table 5.1: Description and physical pre-treatment at RRL of Crystal Sound marine sediment samples. In subsequent discussion, the samples are identified by laboratory number only.

Sample (lab no.)	Core & depth	Description & physical pre-treatment
R41115/1	BS17-GC16 3.18–3.20m	10260mg raw sample received. Light greenish grey mud (Munsell colour Gley 1 10Y 8/1). 4 large irregular chunks (largest dimension ~1.5 to ~2.5cm), with many smaller chunks, flakes and grains. Ground with mortar and pestle. Chemical pre-treatment by acid only. Final weight after pre-treatment 8580mg.
R41115/2	BS17-GC17 3.90–3.92m	10080mg raw sample received. Light greenish grey mud (Munsell colour Gley 1 10Y 8/1). 2 large irregular chunks (largest dimension ~2 to ~2.5cm), with many smaller chunks, flakes and grains. Ground with mortar and pestle. Chemical pre-treatment by acid only. Final weight after pre-treatment 6870mg.
R41115/3	BS17-GC18 6.10–6.12m	12200mg raw sample received. Light greenish grey mud (Munsell colour Gley 1 10Y 7/1). 1 large chunk adhered to conical end of container (largest dimension ~2cm), broken up, with many smaller chunks, flakes and grains, and one angular pebble, largest dimension ~1cm (removed). Ground with mortar and pestle. Chemical pre-treatment by acid only. Final weight after pre-treatment 7440mg.
R41115/4	BS17-GC18 6.61–6.63m	13200mg raw sample received. Light greenish grey mud (Munsell colour Gley 1 10Y 7/1). 1 large chunk adhered to conical end of container (largest dimension ~2cm), broken up, with many smaller angular chunks, flakes and grains. Ground with mortar and pestle. Chemical pre-treatment by acid only. Final weight after pre-treatment 5510mg.

R41115/5	BS17-GC18 7.43–7.45m	23870mg raw sample received. Light greenish grey mud (Munsell colour Gley 1 10Y 7/1), mostly in angular blocks, with many smaller flakes and grains. Ground with mortar and pestle. Chemical pre-treatment by acid only. Final weight after pre-treatment 8240mg.
R41115/6	BS17-GC18 8.78–8.80m	19610mg raw sample received. Light greenish grey mud (Munsell colour Gley 1 10Y 7/1). 2 large angular chunks (largest dimensions ~1.5 and ~3cm), with many smaller flakes and grains. Ground with mortar and pestle. Chemical pre-treatment by acid only. Final weight after pre-treatment 4010mg.

Chemical pre-treatment was by acid only. Each sample was immersed in 2M HCl overnight, rinsed with deionised water, centrifuged and decanted, with rinsing, centrifuging and decanting repeated until pH of the supernatant approached neutral. Sample material was then placed in 50^{o}C oven until dry.

From the final weight after pre-treatment, a portion – approximately 400mg – of each pre-treated sample was used to obtain a CRA for the bulk sediment, to serve as a point of comparison for ages to be obtained for individual splits from RP processing. Of the remaining material, a further ∼2g of material from each sample was taken to USF for RP processing.

For each raw sample received, a portion was kept in untreated state for further investigation, if required (e.g. sieving for foraminifera).

5.2 Radiocarbon measurement of bulk samples

To obtain CRAs for bulk sediment samples, the ∼400mg portions of the pre-treated samples were roughly halved, to provide suitable amounts for processing. With processing by RRL laboratory staff, each sample portion was ST combusted and converted to graphite, as outlined at 1.4.2. %TOC was calculated from the mass of C obtained from combustion relative to the mass of material combusted. The samples were processed for AMS measurement by RRL laboratory staff, as outlined at 1.4.3, with F^{14}C and CRA determinations being made as outlined at 1.4.5. As %TOC was very low for R41115/5 and R41115/6 sediments, CO_2 from two separate combustions of these materials was combined for graphitisation and CRA determinations. Results are shown in Table 5.2

Table 5.2: ST combustion details and bulk sediment Conventional Radiocarbon Ages for Crystal Sound marine sediment samples. The results are presented graphically in Figure 5.1.

Sample (RRL laboratory number)	Weight for combustion (mg)	mgC obtained from combustion	%TOC	Bulk sediment $F^{14}C$	Bulk sediment CRA (^{14}C years BP)	NZA
R41115/1	228.2	0.63	0.28	0.3742 ± 0.0012	7897 ± 26	64973
R41115/2	202.2	1.27	0.63	0.3699 ± 0.0012	7988 ± 26	64974
R41115/3	225.0	0.99	0.47	0.2439 ± 0.0012	11335 ± 38	64975
R41115/4	200.9	0.53	0.26	0.2082 ± 0.0011	12606 ± 44	64976
R41115/5	217.9	0.23	0.11	0.1861 ± 0.0011	13507 ± 49	64977
R1115/5a	202.0	0.19	0.09			
R41115/6	200.5	0.17	0.08	0.1717 ± 0.0012	14155 ± 54	64978
R41115/6a	200.3	0.17	0.08			

5.3 Results of RP splits from USF and RRL

5.3.1 Splits obtained from USF RP processing

Samples were processed through the USF RP system using the procedure outlined at 2.5, above. Runs conducted are summarised in Table 8.1. For each sample, the target mass, based on the pre-determined %TOC, was calculated (from Equation 8, at 2.5) so that 100µmol CO_2 was expected to be obtained. If, based on the %TOC, the mass to produce 100µmol CO_2 was greater than 400mg, then 400mg was taken as the target mass. The actual mass is the amount actually weighed out and loaded in the insert in each case. CO_2 expected is the amount of CO_2 expected on the basis of the actual mass weighed, given its pre-determined %TOC. A standard run is for five splits. Timing for the run is taken from the time the combustion furnace is turned on. For each split, elapsed time and temperature at which the split was taken is recorded. Photometric and manometric measurements of the amount of CO_2 obtained for each split are recorded. Individual split amounts are combined to give photometric and manometric totals, and by comparing the totals obtained to the amount of CO_2 expected, yields are calculated. %TOC is re-calculated from the manometric yield. Results are shown in Table 5.3.

Table 5.3: Splits collected from USF RP runs with R41115/1 to R41115/6 samples.

Sample	%TOC	Target mass	Actual mass	CO_2 expected	Split	Elapsed time	Temp (°C)	Photo (µmol)	Mano (µmol)
R41115/1	0.28	400 mg	392.35 mg	91.55 µmol	1	51 min	270	11.21	12.71
					2	63	330	20.78	27.63
					3	74	386	21.97	28.59
					4	82	427	26.95	36.00
					5	89	461	23.99	32.36
					6	103	535	39.95	64.32
					7	151	773	34.73	51.67
							Total	179.60	253.28
							Yield	196.2%	276.7%
							%TOC recalculated from manometric yield		0.77
R41115/2	0.63	190 mg	190.67 mg	100.10 µmol	1	63 min	286	25.11	11.52
					2	75	350	15.10	19.39
					3	89	417	20.15	31.21
					4	111	532	25.11	37.12
					5	159	771	13.32	16.18
							Total	98.79	115.42
							Yield	98.7%	115.3%
							%TOC recalculated from manometric yield		0.72
R41115/3	0.47	255.3 mg	256.24 mg	100.36 µmol	1	64 min	305	11.29	13.49
					2	83	400	20.43	26.65
					3	96	464	15.05	21.98
					4	111	536	15.52	20.99
					5	161	783	17.53	22.45
							Total	79.82	105.56
							Yield	79.5%	105.2%
							%TOC recalculated from manometric yield		0.49
R41115/4	0.26	400 mg	399.65 mg	86.59 µmol	1	64 min	306	12.27	13.00
					2	82	395	19.90	26.35
					3	94	426	15.50	22.15
					4	106	516	15.32	20.95
					5	153	752	25.61	32.70
							Total	88.60	115.15
							Yield	102.3%	133.0%
							%TOC recalculated from manometric yield		0.35
R41115/5	0.10	400 mg	400.36 mg	33.36 µmol	1	71 min	348	11.20	12.64
					2	85	420	12.05	11.24
							Total	23.25	23.88
							Yield	69.7%	71.6%
R41115/6	0.08	400 mg	401.38 mg	26.76 µmol	1	67 min	315	3.71	5.32
					2	85	405	6.57	9.08
					3	100	479	6.78	9.61
					4	120	580	9.04	11.65
					5	172	838	3.02	4.81
							Total	29.12	40.47
							Yield	108.8%	151.2%
							%TOC recalculated from manometric yield		0.12

For the USF run with R41115/1 material, seven splits were taken. Early splits were taken on the assumption that the run would produce a total of 100µmol CO_2. However, this amount was exceeded before the fifth split was taken, while the reaction was still at its peak. To prevent this split becoming excessively large, further splits were taken, with seven splits collected in total. From the initial ST combustion %TOC estimate of 0.28, %TOC for this material was re-calculated as 0.77. This indicates that the initial ST combustion was only partially successful, leading to a low %TOC estimate. (Why combustion was incomplete is unknown.) Other recalculations of %TOC are also higher than initial estimates, but small differences are to be expected, due to measurement uncertainties. Only two splits were obtained from R41115/5, due to run failure (malfunction of the O_2 mass flow controller, leading to formation of bubbles in the CO_2 trap).

In addition to runs with sediment samples, three runs with graphite and three runs with Ox-I were conducted, to quantify modern and dead carbon contamination from RP processing.

5.3.2 RRL radiocarbon dating of USF-processed RP splits

For the purposes of this study, it was important to obtain suites of radiocarbon ages for at least one of the materials processed at USF, as a basis for parallel processing through the RRL RP system. It was not known at the time which run(s) might be targeted. As many splits were processed for ^{14}C dating as could be accommodated on an AMS wheel. All splits from the runs with R41115/1 to R41115/5 material were processed, and priority was given to low-temperature and larger-sized splits from the R41115/6 run. The CO_2 from each split was ST combusted by laboratory staff as outlined at 1.4.2 to remove sulphur compounds, cracked on the RRL Combustion Processing Line to isolate CO_2, and the CO_2 subsequently graphitised by laboratory staff, as outlined at 1.4.2. AMS measurements were made by laboratory staff, as outlined at 1.4.3. Contamination corrections were applied as outlined at 4.3.2. Results are presented in Table 5.4 and in graph-form in Figure 5.1. The graph also includes bulk sediment ages (Table 5.2).

Table 5.4: $F^{14}Cs$ and CRAs for splits from USF runs with material from R41115/1 to R41115/6. Mass is the amount of carbon as determined at graphitisation at RRL.

Sample	Split	Elapsed time (min)	Temp (°C)	Mass (mgC)	$F^{14}C$	$F^{14}C$ error	CRA (^{14}C yrs BP)	NZA
R41115/1	1	51	270	0.13548	0.39321	0.00782	7498 ± 159	65779
	2	63	330	0.28875	0.39028	0.00323	7558 ± 66	65780
	3	74	386	0.31181	0.38929	0.00303	7578 ± 62	65781
	4	82	427	0.39593	0.36904	0.00239	8007 ± 51	65782
	5	89	461	0.35349	0.37880	0.00267	7798 ± 56	65783
	6	103	535	0.55869	0.34298	0.00188	8596 ± 44	65784
	7	151	773	0.48650	0.29112	0.00242	9912 ± 66	65785
R41115/2	1	63	286	0.12276	0.39663	0.00967	7428 ± 195	65786
	2	75	350	0.21075	0.39806	0.00433	7399 ± 87	65787
	3	89	417	0.35605	0.36864	0.00267	8016 ± 58	65788
	4	111	532	0.28131	0.39649	0.00349	7431 ± 70	65789
	5	159	771	0.17360	0.33992	0.00640	8667 ± 151	65790
R41115/3	1	64	305	0.14570	0.26173	0.00830	10767 ± 254	65791
	2	83	400	0.26777	0.25214	0.00347	11067 ± 110	65792
	3	96	464	0.22072	0.25341	0.00403	11027 ± 127	65793
	4	111	536	0.21874	0.22891	0.00410	11844 ± 143	65794
	5	161	783	0.22404	0.19815	0.00539	13003 ± 218	65795
R41115/4	1	64	306	0.13756	0.23532	0.00908	11622 ± 310	65796
	2	82	395	0.28868	0.22871	0.00323	11850 ± 113	65797
	3	94	426	0.23015	0.23625	0.00383	11590 ± 130	65798
	4	106	516	0.21401	0.20873	0.00421	12585 ± 162	65799
	5	153	752	0.32927	0.18868	0.00356	13396 ± 151	65800
R41115/5	1	71	348	0.12542	0.23637	0.01023	11586 ± 347	65801
	2	85	420	0.09719	0.19938	0.00908	12953 ± 365	65802
R41115/6	1	67	0.04	0.04352	0.26076	0.03460	10797 ± 1065	65803
	2	85	405					
	3	100	479	0.08382	0.21706	0.01364	12271 ± 424	65804
	4	120	580	0.11125	0.15919	0.00886	14761 ± 447	65805
	5	172	838					

Stacked results are shown graphically below (Figure 5.1). (As noted in Table 5.1, R41115/1 is from Gravity Core (GC) 16, R41115/2 is from GC17 and R41115/3 to R41115/6 are from GC18.)

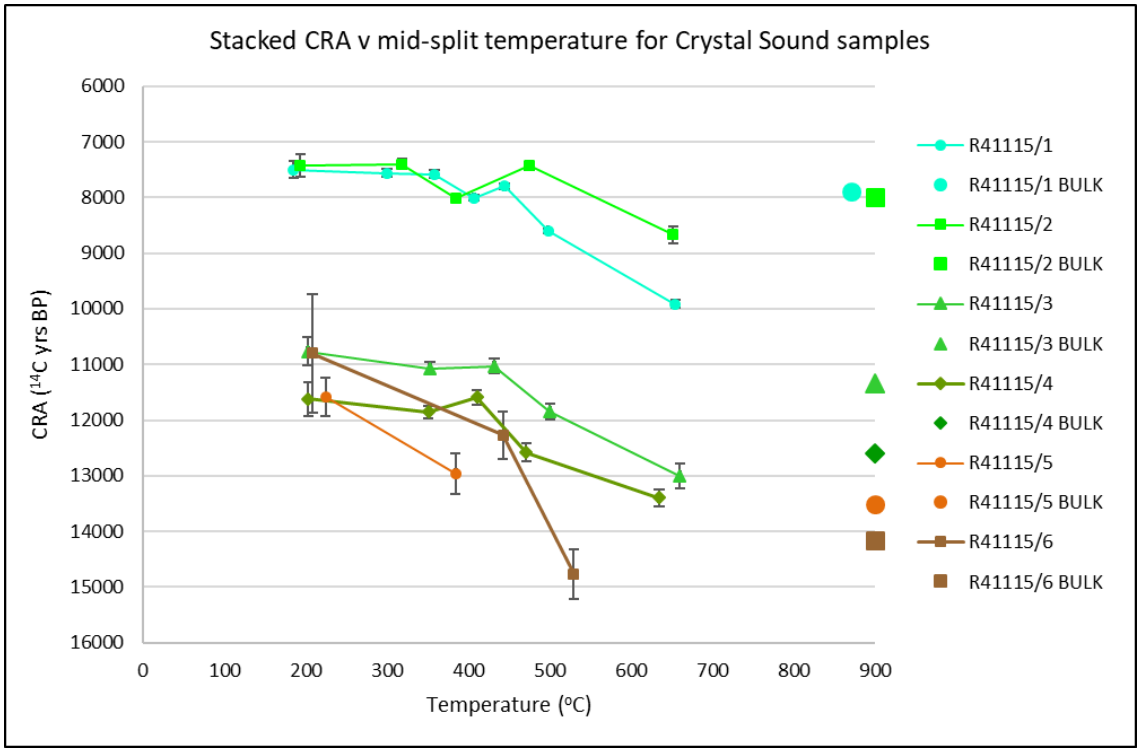

Figure 5.1 CRAs for different-temperature splits for Crystal Sound sediment samples processed through USF RP system. The temperature for each split is the mean temperature for the temperature range over which the split was taken. Bulk-sediment CRAs from the same materials are shown at right. Ages generally increase with the temperatures at which splits are collected. Errors (shown as ± 1 SD) are larger for smaller-sized splits. Results from R41115/1 to R41115/4 runs are shown at larger scale in Figure 5.3 and Figure 5.5.

Bulk sediment ^{14}C ages increase with sample depth. Samples with the shallowest depths, R41115/1 (BS17-GC16 3.18–3.20m) and R41115/2 (BS17-GC17 3.90–3.92m) show the youngest ages from bulk sediment (7896 ± 26 and 7988 ± 26 ^{14}C years BP, respectively). These ages are derived from two different cores, Gravity Cores 16 and 17. Samples were provided without stratigraphic information, so the respective sedimentary horizons from which the samples come cannot be compared or distinguished. While it is possible that the shallower R41115/1 sample is stratigraphically younger, this cannot be reliably established from bulk sediment ages (as discussed at 1.6.3).

Samples from Gravity Core 18 (R41115/3 to R41115/6) are from successively lower stratigraphic levels in the same succession (6.10–6.12m, 6.61–6.63m, 7.43–7.45m, 8.78–8.80m), so can be compared. The bulk sediment ^{14}C ages for these samples (11335 ± 38, 12606 ± 44, 13507 ± 49 and 14155 ± 54 ^{14}C years BP, respectively; see Table 5.2) are both significantly older than the shallower-sample ages and show significant increases in age with

increasing stratigraphic depth. However, these ^{14}C ages are uncalibrated, and calibrated ages (discussed at 1.5.1) could show a change in the sequence, as calibration curves can include intervals of reversal and ambiguity (e.g. marine data in Reimer et al., 2013, Figure 3). (However, age calibration is beyond the scope of this study.)

^{14}C ages for splits from a given sample generally increase with increasing temperature. This is expected from radiocarbon dating of splits from RP processing of a sample. What is particularly relevant is that the ^{14}C ages from the lowest-temperature splits are less than the bulk sediment ^{14}C ages, and the ^{14}C ages from the highest-temperature splits are greater than the bulk sediment ^{14}C ages (Table 5.5 and Figure 5.2). With R41115/5, only Splits 1 and 2 were obtained before the run was abandoned (as noted at 5.3.1 above and in Table 8.1), and the Split 2 age (12954 ± 366 ^{14}C years BP) is younger than the ^{14}C ages from the bulk sediment. In the case of R41115/6, only Splits 1, 3 and 4 were radiocarbon-dated, and of these, the Split 3 age (12271 ± 424 ^{14}C years BP) is less than the bulk sediment ^{14}C ages, while the Split 4 age (14762 ± 447 ^{14}C years BP) is greater.

Table 5.5: CRAs for first split, bulk sediment and fifth split (where obtained and dated) from Crystal Sound samples R41115/1 to R41115/6. Split 1 ages are consistently less than bulk sediment ages, while Split 5 ages are consistently greater than bulk sediment ages. Ages are in ^{14}C years BP. Results are shown graphically at Figure 5.2.

Sample	Core & depth	Split 1 ^{14}C age	Bulk ^{14}C age	Split 5 ^{14}C age
R41115/1	BS17-GC16 3.18–3.20m	7498 ± 160	7897 ± 26	9913 ± 67
R41115/2	BS17-GC17 3.90–3.92m	7429 ± 196	7988 ± 26	8668 ± 151
R41115/3	BS17-GC18 6.10–6.12m	10768 ± 255	11335 ± 38	13003 ± 219
R41115/4	BS17-GC18 6.61–6.63m	11622 ± 310	12606 ± 44	13397 ± 152
R41115/5	BS17-GC18 7.43–7.45m	11587 ± 348	13507 ± 49	
R41115/6	BS17-GC18 8.78–8.80m	10798 ± 1066	14155 ± 54	

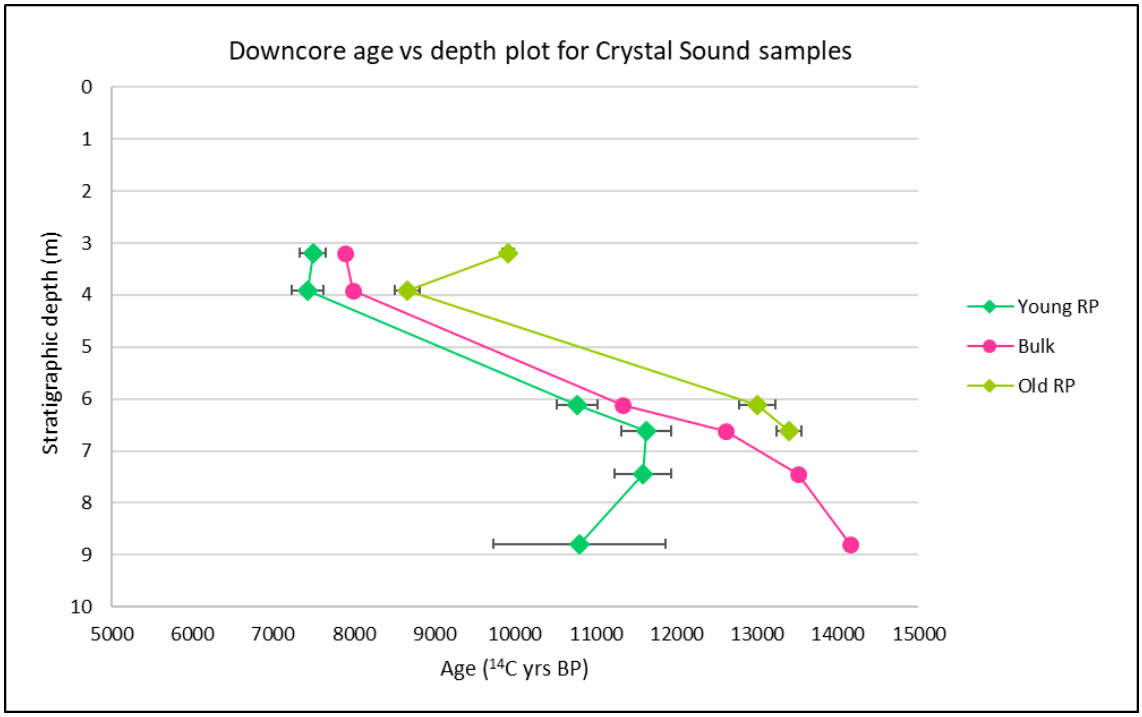

Figure 5.2. Uncalibrated radiocarbon ages for first and last splits for USF RP-processed Crystal Sound samples with bulk sediment ages for the same materials. Fifth splits for R41115/5 and R41115/6 samples were either not obtained or not ^{14}C dated. The particularly large uncertainty for the age for the first split of the R41115/6 (stratigraphically lowest) material reflects its low %TOC (0.12, as recalculated from yield (Table 5.3)), the very small sample size and the associated potential contamination effect.

The picture for radiocarbon ages of intermediate splits is more complex, and less clear-cut. For each sample from which five or more splits were taken, there are apparent age-reversals among increasing-temperature splits, and in some cases, the Split 1 age is not the youngest.

For R41115/1 (Figure 5.4), there are seven splits (as noted at 5.3.1). Among the split-ages, the youngest age is for Split 1 and the oldest is for Split 7, but the ages for Splits 2 and 3 are within the 1 SD error of the Split 1 age, so the Split 1 age is not necessarily the youngest. Split 4, collected over the temperature interval 386 to 427°C, has a greater age than Split 5, collected over the temperature interval 427 to 461°C (Table 5.4; Figure 5.3) so there is an apparent age-reversal at this point in the temperature profile. The implication is that carbon that is more recalcitrant – that is, more resistant to breakdown under pyrolysis – is not always older. Put another way, carbon liberated from a sample at higher pyrolysis temperatures is not always seen to be older than carbon liberated at lower pyrolysis temperatures.

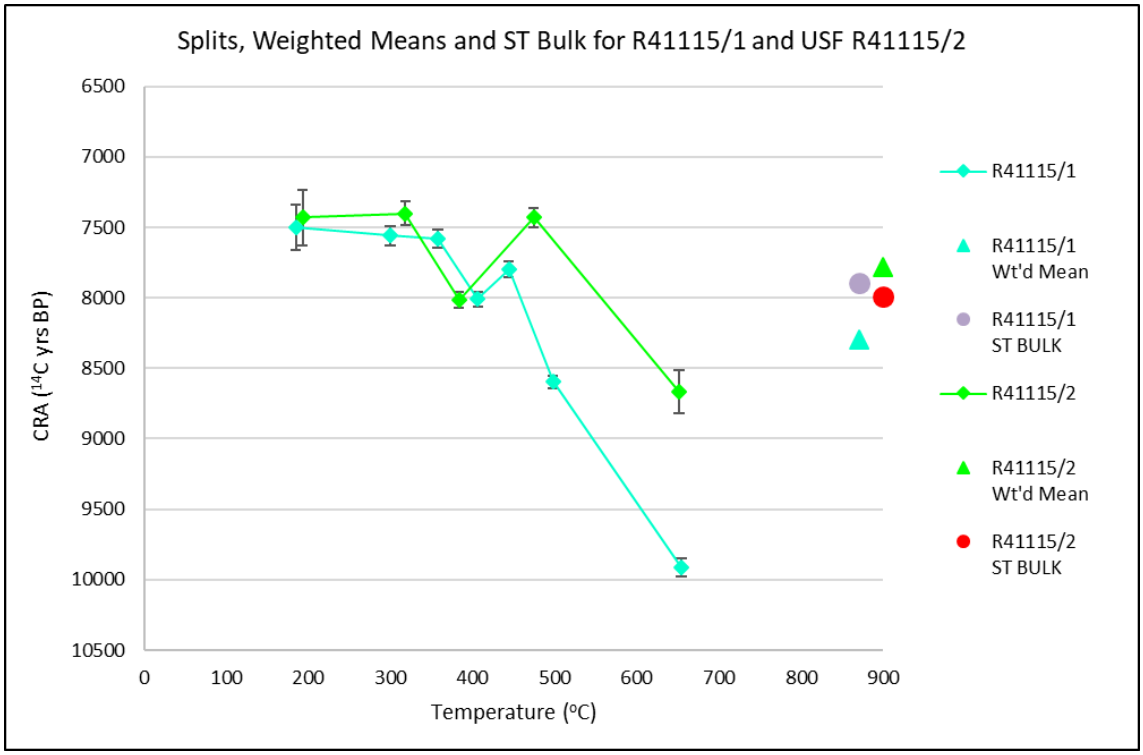

Figure 5.3 CRAs for different-temperature splits from BS17 Gravity Core 16 and 17 samples, with bulk-sediment ages shown at right (circles). Split 1 ages are less than bulk sediment ages and Split 5 ages are greater. Age reversals with increasing temperature are seen in both cases. Also shown at right are weighted means of split ages (triangles; discussed at 5.5).

^{14}C age reversals among increasing-temperature CO_2 fractions have been seen in previous RP processing. Rosenheim et al. (2008) have commented that ^{14}C ages of individual temperature fractions from RP processing of Antarctic marine sediments (NW Weddell Sea) increase "nearly monotonically" with temperature. Among the nine splits collected in their study, Split 7 shows an age reversal (see Figure 5.4; Figure 2.6, above, shows the ages superimposed on the thermograph for the same run). Apparent age reversals among RP splits are also seen from RP processing of high Arctic lagoon and delta sediments (Schreiner et al., 2014, Figures 2(b), (c), (i), (j), and from RP processing of Antarctic Peninsula marine sediments (Subt et al., 2016, Figure 2).

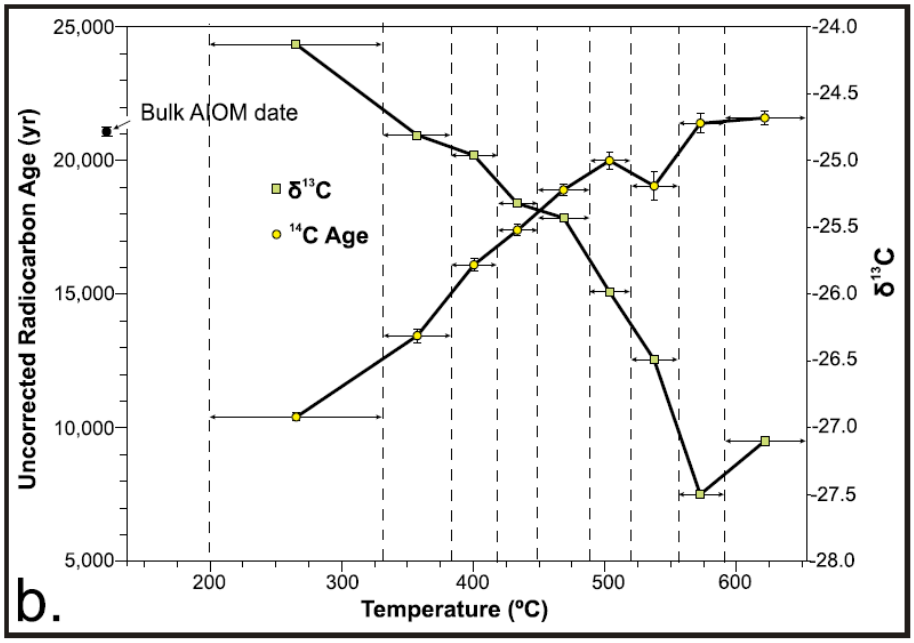

Figure 5.4 CRAs from RP processing of Antarctic marine sediment (NW Weddell Sea; from Rosenheim et al., 2008). Nine splits have been taken, with ages shown by yellow circles, generally trending upwards. The age for Split 7 (520–555ºC) is younger than the age for Split 6 (485–520ºC).

For R41115/2 (Figure 5.3), the youngest ages are for Splits 1, 2 and 4, and these ages cannot be statistically distinguished (to 1 SD, 7429 ± 196, 7400 ± 87 and 7431 ± 71 ^{14}C years BP, respectively). It is possible from this that the lowest-temperature split does have the youngest age, though it is not seen in the plot. The greatest age is for Split 5 (8668 ± 151 ^{14}C years BP), which is greater than the bulk sediment age (7989 ± 27 ^{14}C years BP). However, Split 3 shows a greater radiocarbon age (8016 ± 58 ^{14}C years BP) than Split 4. Again, a reversal is seen in the breakdown-temperature/sediment-age relationship, with the age of the 417 to 532ºC temperature-fraction less than the 350 to 417ºC temperature-fraction age.

Previous radiocarbon-age results from RP processing also show that the lowest-temperature split may not have the youngest age, from RP processing of Mississippi delta river sediment (Rosenheim et al., 2013b, Figure 5(g)) and of high Arctic delta sediment (Schreiner et al., 2014, Figure 2(j)), so again this situation is not unique.

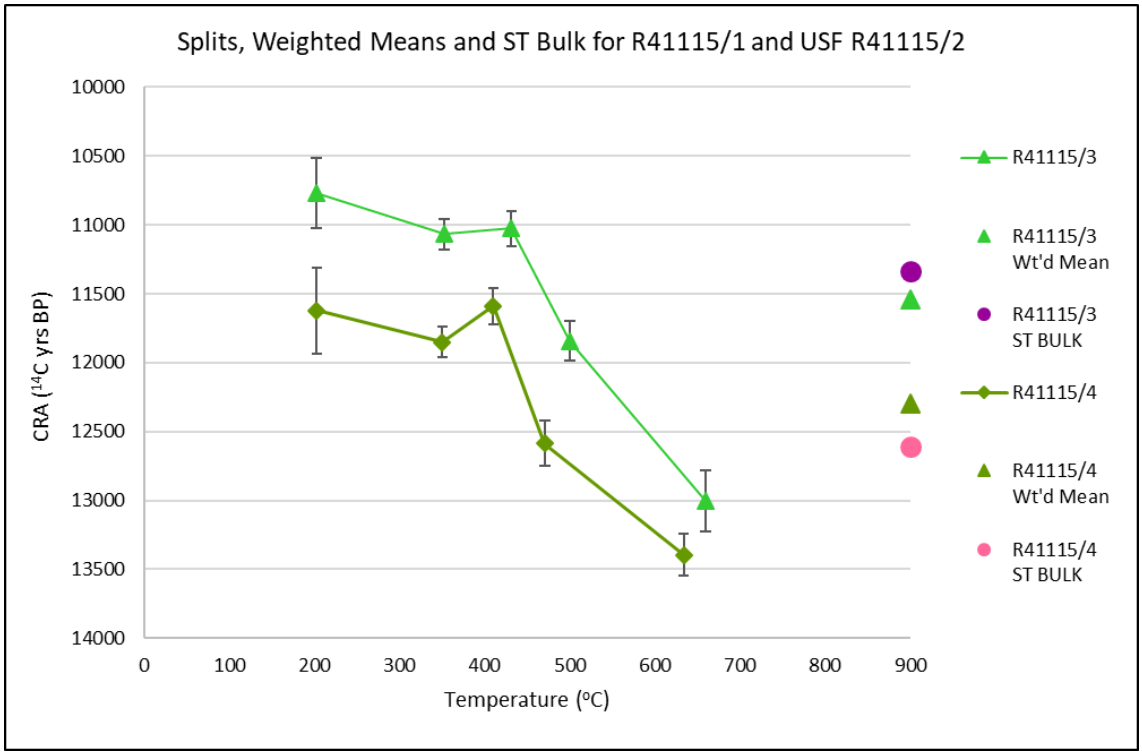

Figure 5.5 CRAs for different-temperature splits from runs with R41115/3 and R41115/4 material. Bulk-sediment ages are shown at right (circles). Split 1 ages are less than bulk sediment ages and Split 5 ages greater. An apparent age reversal for a higher-temperature split is seen with R41115/4, with Split 3 carbon likely to be younger than Split 2 carbon. Also shown at right are weighted means of split ages (triangles; discussed at 5.5).

For R41115/3 (Figure 5.5), the radiocarbon ages for Splits 2 and 3 are within the 1 SD error of the Split 1 age, so the Split 1 age is not necessarily the youngest (though it is likely to be, given the limited degree of overlap in 1 SD ranges). A slight age reversal is evident for Splits 2 and 3, though the ages are within error (to 1 SD) of each other, so the reversal may be apparent only. The ages for all of Splits 1, 2 and 3 are less than the bulk sediment age, with the Split 4 and 5 ages greater. The expected relationship of increasing age with splits taken at increasing temperatures is generally observed for this sample.

For R41115/4 (Figure 5.5), the ^{14}C ages for Splits 2 and 3 are within the 1 SD error of the Split 1 age, and an apparent age reversal is seen for Splits 2 and 3. However, the 1 SD lower limit for the Split 2 age is 11737 ^{14}C years BP while the 1 SD upper limit for the Split 3 age is 11720 ^{14}C years BP, so the reversal may be apparent only. The Split 4 age is within the 1 SD error of the bulk sediment age, but the Split 5 age is greater.

For R41115/5 (see Figure 5.1), only two splits were obtained; their radiocarbon ages are distinct from each other (at 1 SD), and also distinct from the bulk sediment age, which is greater than either.

For R41115/6 (see Figure 5.1), only Splits 1, 3 and 4 were radiocarbon dated. The size of the splits was small, so the 1 SD error-bars are large. There is a small overlap of likely ages for Splits 1 and 2, with the Split 1 age likely to be younger. To 1 SD, the Split 4 age is greater than the bulk sediment age.

From these USF RP-processed Crystal Sound samples, a broad picture of increasing radiocarbon age with increasing temperature at which splits are taken is seen. Apparent age reversals across a pair of splits are also seen in each of the 5-split samples for which radiocarbon ages were derived, and this effect is most pronounced in the shallowest and most recent samples. This may be because carbon derived from living organisms has had less opportunity to become degraded with time (as compared to the opportunity available for stratigraphically deeper, older samples).

It is also notable that these apparent reversals occur in the temperature continuum around the temperature where carbon is most abundantly produced in the pyrolysis reaction – close to the [CO_2] peaks – and it may be that the responses of more volatile and more recalcitrant carbon are less clearly distinguished during this busy part of the pyrolysis reaction.

It is also possible that something is systematically going awry in USF RP processing at the most active parts of runs. However, the runs for the samples showing the most prominent reversals (DB-1768 for R41115/1, DB-1766 for R41115/2 and DB-1782 for R41115/4) were conducted with help from different USF operators on different days, and it seems unlikely that the same kinds of errors or inconsistencies would arise multiple times at similar points with different individuals involved.

5.3.3 RP splits from RRL processing

The first Crystal Sound sample chosen for processing through the RRL RP system was R41115/2, as it was a sample with relatively high %TOC and without complications (such as R41115/1's seven splits). Once processing of R41115/2 samples had begun, it became the

sediment sample with which most testing was done, so it was the obvious candidate to begin parallel processing with. Due to time constraints, parallel processing of any other Crystal Sound sample became impractical.

RRL Runs 31, 37, 39 and 40 were conducted with R41115/2 material with collection starting at 105°C and a single split being taken at 900°C. The gas collected appeared yellow or pale yellow in each case, following failure of the clean-up chemicals in the oxidation chamber. The gases were therefore transferred by laboratory staff into Pyrex collection tubes containing 200–230mg CuO pellets and 2 strands (~4cm long) of Ag wire and recombusted overnight at 500°C to effect sulphur-species clean-up.

Run 44 with R41115/2 material was for 5 splits. The temperatures at which the 5 splits were to be taken was on the basis of a comparison of thermograph shapes from USF Run DB-1766 and previous clean-handled RRL runs with the same material (see 3.11.7). Due to the inconsistencies seen in thermographs for repeated RRL runs with the material (Figure 3.24), it was decided to take splits not at the same temperatures as in the USF run, but at the same comparative points in the thermographs. This meant making an estimate of where thermograph shapes would most likely cohere. On this basis, it was decided to take splits for Run 44 at 280°C, 340°C, 410°C, 525°C and 900°C. Run 44 was conducted with collection tube pre-loaded with 200–230mg CuO pellets and 2 strands Ag wire, for subsequent recombustion of CO_2. For the largest split, Split 4, the collected gases appeared pale yellow.

The CO_2 from each split from these runs was subsequently graphitised by laboratory staff, with AMS measurements made by laboratory staff, as outlined at 1.4.2 and 1.4.3. Contamination corrections were applied as outlined at 4.2 and 4.3.3 to 4.3.5. The single splits from Runs 31, 37, 39 and 40 and Split 4 from Run 44 were all treated as large-sized samples. Splits 1, 2, 3 and 5 from Run 44 were treated as small-sized samples (in the case of Split 3, as its size was close to the 0.3mgC threshold).

Results from AMS measurements of RRL RP-processed R41115/2 samples are presented in Table 5.6. For small-sized samples, corrected $F^{14}C'$ is calculated, as outlined at 4.3.5.

Table 5.6: RRL radiocarbon age determinations for RP processed R41115/2 samples.

Run	Split	Split temp. (°C)	Mass (mgC)	$F^{14}C$	$F^{14}C$' (for small samples)	$F^{14}C$ / $F^{14}C$' error	CRA (^{14}C yrs BP)	±	NZA
31	1	900	1.0532	0.36455		0.00297	8105	65	67618
37	1	900	0.9887	0.36493		0.00290	8097	63	67619
39	1	900	1.0929	0.36564		0.00279	8081	59	67620
40	1	900	1.1395	0.36596		0.00269	8075	58	67621
44	1	280	0.0995	0.40254	0.41149	0.02142	7133	418	67613
	2	347	0.2733	0.41448	0.41871	0.00723	6993	138	67615
	3	418	0.3201	0.40438	0.40779	0.00606	7205	119	67616
	4	525	0.4095	0.38262		0.00462	7717	96	67617
	5	900	0.1670	0.32983	0.32976	0.01282	8911	312	67614

5.4 Comparison of RRL bulk ST and bulk RP results

In each of RRL RP Runs 31, 37, 39 and 40, carbon produced from pyrolysis of R41115/2 sediment between 105°C and 900°C was collected in a single split. Radiocarbon ages from these samples are effectively for bulk sediment which has been RP-processed. All samples were large-sized, ~1mgC at graphitisation. Results are shown in Table 5.6 and in Figure 5.6.

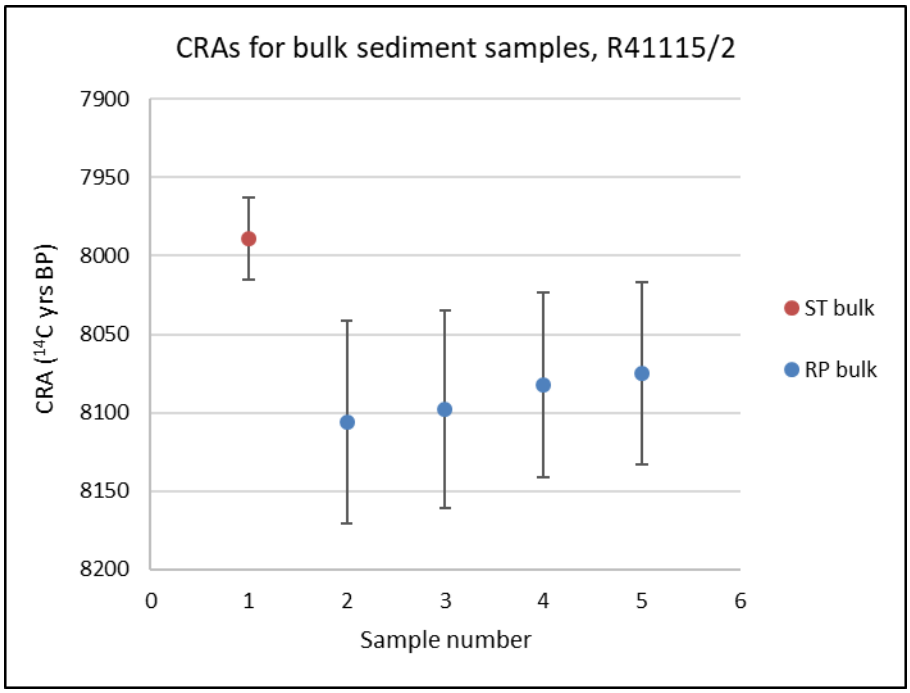

Figure 5.6 Comparison of CRAs from ST combustion (red) and RP processing of bulk sediment samples of R41115/2 material (blue). Runs 31, 37, 39 and 40 are shown as samples

2, 3, 4 and 5 respectively. Radiocarbon ages for the RP-processed samples show good reproducibility, differing from the age for the ST-only sample by ~100 ^{14}C years.

^{14}C ages from the single-slit RP runs agree well with each other. The mean CRA from these four runs is 8090 ± 61 ^{14}C years BP. This is close to the bulk sediment age from ST combustion-only of the same material of 7988 ± 26 ^{14}C years BP. The run showing the age closest to this is Run 40. The minimum difference between the 1 SD ages from Run 40 (8075 ± 58 ^{14}C years BP) and ST combustion-only is 3 ^{14}C years (8017 – 8014). The maximum difference between the same 1 SD ages is 171 ^{14}C years (8133 – 7962).

The differences in ages may be due to dead carbon contamination consistently introduced during RP processing. There is evidence of such DC contamination in the relatively large d value (4.3µgC) obtained from RP processing of small samples (discussed at 4.3.4). Alternatively, the ST combustion-only age may include modern carbon contamination. At the age-range involved, it takes comparatively less modern carbon contamination than dead carbon contamination to shift a radiocarbon age by a similar amount. For example, to move a radiocarbon age from 8000 to 8100 ^{14}C years BP would require the introduction of 0.7% of pure dead carbon, while to move the age the other way, from 8100 to 8000 ^{14}C years BP, would require the introduction of 0.4% of pure modern carbon (using calculation methods utilised by RRL spreadsheets). Further, it is generally easier to contaminate a sample with modern carbon during laboratory handling (e.g. from skin or an eyelash) than with dead carbon (e.g. from the dry ice used for trapping water in the vacuum line, if there was a leak in the line near one of the traps).

Given the agreement between the ages from the single-split RP runs, if there is an outlier among these five ages, it is likely to be the ST combustion-only age. It is more likely that one sample was contaminated than that four samples were independently contaminated. It is plausible, however, that there has been contamination in both directions – a relatively consistent amount of DC contamination in the RP runs, and MC contamination in the ST combustion.

The replication of ^{14}C ages for Runs 31, 37, 39 and 40 indicates that RRL RP processing is itself reliable, at least where a single split is taken from the whole run. Appreciable variability is seen between the thermographs for these RP-processed "bulk sediment" runs (Figure 3.24). Peak [CO_2] values occur in Runs 31 and 37 at distinctly different temperatures, 418°C and 360°C, respectively. For Runs 39 and 40, they occur at 379°C and 398°C. The different [CO_2] peaks probably reflect a spread in peak pyrolysis activity from run to run, yet the radiocarbon ages are in close agreement. So at least for runs where carbon fractions of varying ages are effectively mixed, with a single resultant age being produced, variation in thermograph shape is not relevant.

5.5 Weighted means of split ages from RP runs compared to bulk sediment ages from ST combustion

For runs with R41115/1 to R41115/4 material, RP split-ages weighted according to the proportion of CO_2 collected for each split have been summed to give weighted means (Table 5.7) and are shown in Fig 5.8 alongside results from the USF run and ST combustion of bulk sediment from the same materials. Individual split ages are in Table 5.4.

Table 5.7: Comparison of $F^{14}C$ and CRA values from ST combustion of bulk sediment and from summed weighted means of individual split values. For RRL, ** indicates Runs 31, 37, 39 and 40, which had single splits taken from whole runs. The RRL Bulk $F^{14}C$ and Bulk CRA values are the mean values from these runs. These values are distinguished from the other $F^{14}C$ and CRA values in that they are ST combusted after RP processing, while the other ST values are from ST combustion only.

Sample	Run number	Bulk $F^{14}C$ (from ST)	Bulk CRA (from ST)	Σ split weight fraction * $F^{14}C$	Weighted mean CRA
R41115/1	USF 1768	0.3742 ± 0.0012	7897 ± 26	0.3558 ± 0.0004	8300 ± 9
R41115/2	USF 1766	0.3699 ± 0.0012	7988 ± 26	0.3796 ± 0.0007	7782 ± 15
R41115/2	RRL **/44	0.3653 ± 0.0028 **	8090 ± 61 **	0.3920 ± 0.0031	7521 ± 64
R41115/3	USF 1769	0.2439 ± 0.0012	11335 ± 38	0.2380 ± 0.0013	11531 ± 45
R41115/4	USF 1782	0.2082 ± 0.0011	12606 ± 44	0.2164 ± 0.0016	12295 ± 60

In each case, there is a disparity between weighted mean ages and bulk sediment ages. For R41115/1 and R41115/3, the bulk sediment ages are greater than the weighted mean ages. For R41115/2 and R41115/4, the weighted mean ages are greater than bulk sediment ages.

In the case of R41115/1 (Fig 5.3), the largest of the seven splits taken were the last two, accounting for 41% of the total mass of C (cf. split masses in table 5.4), so it is unsurprising that the sum of weighted split ages (8300 ± 9 ^{14}C years BP) is skewed towards the ages of the last two splits. The bulk sediment age (7897 ± 26 ^{14}C years BP) is substantially younger, sitting between the Split 4 age (8007 ± 51 ^{14}C years BP) and the Split 5 age (7798 ± 56 ^{14}C years BP).

For R41115/2 (Fig 5.3), the largest split is Split 3 (31% of the total mass of C), and the age for this split (8016 ± 58 ^{14}C years BP) is indistinguishable from the bulk sediment age (7988 ± 26 ^{14}C years BP). Three splits (including the higher temperature Split 4) are associated with a younger age and only one split (Split 5) with an older age, and the weighted mean age (7782 ± 15 ^{14}C years BP) is seen to be younger than the bulk sediment age. In this case, the minimum 1 SD difference between the weighted mean and bulk sediment ages is 165 ^{14}C years (7962 – 7797).

For R41115/3 (Fig 5.5), Split 2 is largest (25% of the total mass of C), with Split 1 at ∼15% and Splits 3 to 5 each at ∼20% of the total mass of C. With this reasonably evenly distributed range of masses, the weighted mean age and bulk sediment age both fall between the ages of Splits 3 and 4, and are not greatly separated – at 1 SD, by a minimum of 113 ^{14}C years (11486 – 11373).

For R41115/4 (Fig 5.5), Split 5 is largest (27% of the total mass of C), with 45% of the total mass of C shared between the last two splits. In this case, the bulk sediment age (12606 ± 44 ^{14}C years BP) is indistinguishable from the age for Split 4 (12585 ± 162 ^{14}C years BP). The weighted mean age (12295 ± 60 ^{14}C years BP) is younger than the bulk sediment age by at least 207 ^{14}C years at 1 SD (12562 – 12355).

Among the RRL runs with R41115/2 material (Fig 5.8), the single-split runs (31, 37, 39 and 40) which include C from the whole temperature range (105^{o}C to 900^{o}C) give a mean “bulk” age of 8090 ± 61 ^{14}C years BP. This is close to the ST combustion-only age for bulk sediment from the same material (7988 ± 26 ^{14}C years BP). At 1 SD, the minimum difference between the mean “bulk” and ST combustion-only ages is only 15 ^{14}C years (8029 – 8014), while the maximum difference is 189 ^{14}C years (8151 – 7962). So the ages are relatively similar. In the

case of RRL Run 44, the weighted mean age (7521 ± 64 ^{14}C years BP) is appreciably younger than the USF DB-1766 weighted mean age (7782 ± 15 ^{14}C years BP) – at 1 SD, by a minimum of 182 ^{14}C years (7767 – 7585) and a maximum of 361 ^{14}C years (7797 – 7463). Visually, the separation between the early split ages from the RRL and USF runs is similar to the separation between the weighted mean ages. The weighted mean age from RRL Run 44 is also separated by ~500 ^{14}C years BP from the bulk sediment ages (with the RRL single-split run ages and the ST-combustion-only age considered together). Among the split masses for RRL Run 44, 57% of the total derives from Splits 3 and 4, and the weighted mean age falls between the split-ages for these two splits.

The largest disparity between the weighted mean age and the bulk sediment age is seen in the case of the USF R41115/1 run, where split sizes are least evenly distributed. Where split sizes are most evenly distributed, for the USF R41115/3 run, the disparity between the weighted mean age and the bulk sediment age is smallest.

In a comparison of ages from ST combustion of bulk sediment and weighted means of splits from an RP run of the same material, Rosenheim et al. (2013a) found that weighted mean ages and bulk sediment ages were indistinguishable. In their study, the sizes of most splits within runs were quite similar (Rosenheim et al., 2013a, Table 1). They concluded that all the organic carbon from a sample is utilised in RP processing (Rosenheim et al., 2013a).

The same conclusion can be drawn from the "bulk" results from RRL single-split Runs 31, 37, 39 and 40 compared to the ST combustion-only age from the same material (Figure 5.6). From this study, comparison of bulk sediment ages and weighted mean ages for multiple-split RP runs shows that the two values do not agree with each other. Nor is one kind of age seen to be consistently younger or older than the other. From the evidence, it appears that weighted mean ages can be skewed away from bulk sediment ages in either direction, depending on the distribution of split sizes.

5.6 Comparison of USF and RRL RP results

The only Crystal Sound sample parallel processed on both the USF and RRL RP systems was R41115/2, so at present a comparison of system performance is on the basis of one run per system. Results are shown in Figure 5.7.

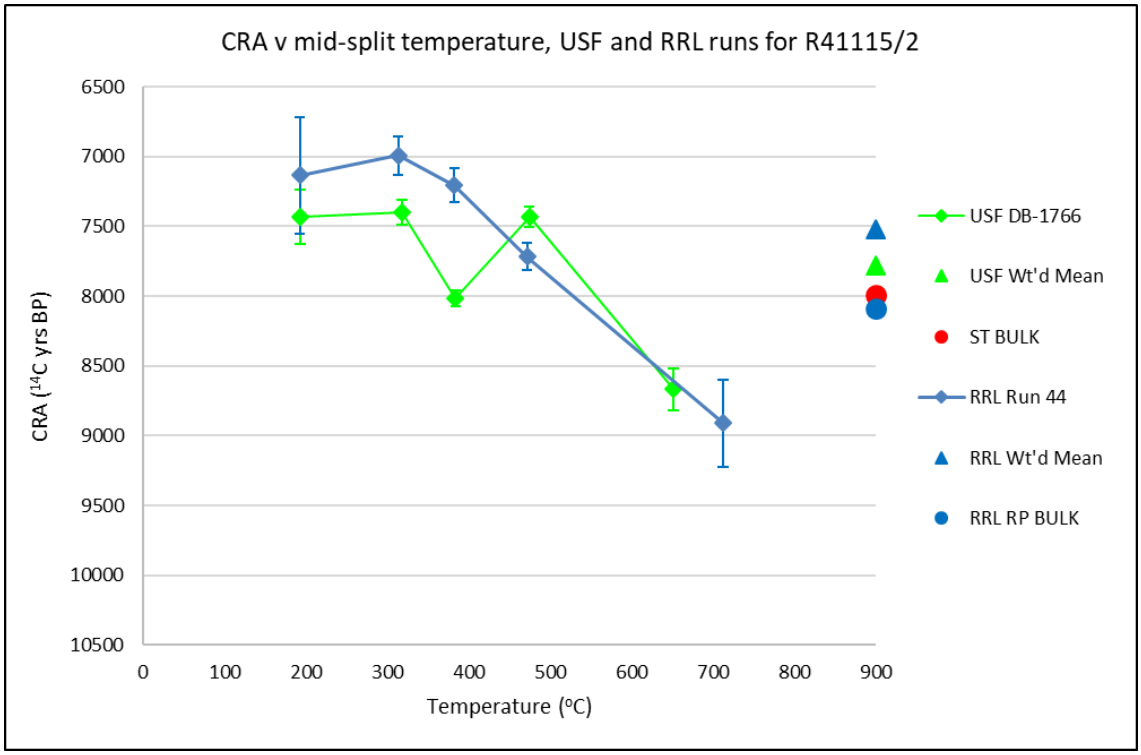

Figure 5.7 Comparative results for USF and RRL RP processing of R41115/2 material for 5 splits. The ages for the lowest and highest temperature splits are in good agreement with each other. The large error bars for these ages reflect the size (weight of carbon at graphitisation) of these splits.

Broad agreement is seen between the results. The youngest-aged splits are younger than the bulk sediment ages, and oldest-aged splits are older. Two bulk sediment ages are considered for this comparison: the ST-only bulk sediment age (7988 ± 26 ^{14}C yrs BP; Table 5.2) and the mean of the RP-bulk sediment ages (8090 ± 61 ^{14}C yrs BP; see 5.4, above). In the USF run, three split-ages are younger than the ST bulk value (though one deviates from the expected order) and four are younger than the RP bulk value. For the RRL run, four split-ages are younger than both ST and RP bulk values. The weighted mean age from RRL Run 44 splits is ~260 ^{14}C years younger than the corresponding USF age, reflecting the generally younger ages for RRL splits.

There are large uncertainties for the radiocarbon ages for the smallest splits, Splits 1 and 5 for each run. The smaller the size of the splits, the larger the influence of contamination on their radiocarbon ages and therefore the larger error bars. Despite the magnitude of the error bars, the overlapping confidence intervals for the ages of the end-member CO_2 fractions are a positive indication that their ages are similar.

The radiocarbon ages for RRL Splits 2 and 3 cannot be distinguished from the age for Split 1, though Split 3 is likely to be older than Split 2, as can be seen from the small degree of overlap between the 1 SD age-ranges for these two splits. The smaller uncertainty for Split 4 among the RRL Run 44 splits are because this split was sized at 0.41mgC, so above the 0.3mgC threshold for a small sample, therefore MCC and DCC were not applied.

There is a deviation between the ^{14}C ages for the central splits from the USF and RRL runs. This may be due to differences in the way the systems operate. In particular, the way heat is transmitted to samples in the differently-oriented furnaces is likely to differ, and this may affect pyrolysis reaction rates, so that although splits are taken at comparable thermocouple temperatures in the two systems, they may be sampling the products of slightly different parts of the pyrolysis reaction.

We have evidence of consistent operation of the RRL RP system where single-split runs are concerned (see Figure 5.6). In this case the samples are large, and the uncertainties in radiocarbon ages are correspondingly smaller. Further, the whole of the volatilised carbon which has been oxidised to CO_2 is measured as a single sample. If there are differences within and between runs, for example in pyrolysis reaction rates and the amount of carbon volatilised in a particular temperature interval, they are not reflected in the bulk-sediment radiocarbon ages that result.

It is expected that at present results from the USF RP system will be more reliable than results the RRL RP system, as the USF system and operating protocols are well-established and corrections for contamination from processing are well constrained. By contrast, contamination corrections for the RRL system are currently based on few results, obtained as issues occurred. Consequently, the USF results should be considered to be more precise. However, despite the large uncertainties attached to the radiocarbon ages for the five splits

from RRL Run 44, particularly with Splits 1 and 5, the expected age-progression with increasing temperature is more clearly seen from the RRL run than from the USF run with the same material. Currently a single run from each system is available for comparison, so no firm conclusion can be drawn as to which set of results are more accurate. These initial results are indicative only.

The results show that the RP method is relevant with the right lithological type of material, particularly sediment including carbon contemporaneous with the age of deposition and carbon from a differently-aged source. Crystal Sound core material is an example, with the sediment including both carbon originating from the contemporaneous pelagic water column and reworked carbon coming from a nearby glacimarine sedimentation source. Close to the surface, the lithology is likely to be diatom ooze, indicative of open water conditions. Given the high sedimentation rates for diatom oozes (e.g. ~20cm/kyr near Ross Island, McKay et al., 2008), the influence of reworking is expected to be relatively minimal in deposits of this kind. Further downcore, where sediments represent deglaciation phases, glacimarine sediment supply is likely contaminated by reworked carbon (Andrews et al., 1999). The RP method is particularly useful where there is enough non-reworked carbon to be measured in low temperature splits, as seen with R41115/1 to R41115/4 materials. Where there is less contemporaneous carbon, dating low temperature splits becomes more problematic, as seen with R41115/5 and R41115/6 materials. Here, there is a trade-off between split size and ^{14}C age uncertainty.

6 Conclusion: The present state of the RRL RP capability

A ramped pyrolysis radiocarbon dating capability has been established at RRL, GNS Science, Lower Hutt, New Zealand, at least in prototype form. This has required the design, construction and testing of a ramped pyrolysis system, including:

- a gas delivery system to provide inputs of UHP He and O_2
- a furnace system to pyrolyse material and oxidise liberated carbon
- a CO_2 detection system to monitor the amount of CO_2 produced
- a vacuum line system to collect and isolate the CO_2.

Testing of the ramped pyrolysis system was conducted to identify problems. CO_2 traces and repeatability were tested. ^{14}C ages were measured from different-temperature CO_2 aliquots and contamination was diagnosed from the processing of blanks and standards through the system.

The major technical issues identified were:

- adequate control of the pyrolysis furnace temperature ramp
- prolonged pressure disturbances when switching between CO_2 collection branches of the vacuum line
- clean handling / contamination (modern and dead carbon inputs)
- thermograph variability
- removal of sulphur from pyrolysis products to enable graphitisation of CO_2.

Remaining problems are:

- the large volume of the collection branches of the vacuum line system, making it difficult to take splits rapidly
- difficulty of manually manipulating valves in a controlled and timely manner
- failure of sulphur clean-up chemicals in oxidation chamber after ~30 runs, meaning a further clean-up step was required for samples processed
- sulphur contamination present in the RP line downstream of furnaces

- difficulty in constraining the amount of modern and dead carbon contamination introduced during RP processing, due to limited number of blanks and standards currently processed

A number of questions have arisen during testing and development which could be further explored:

- Is the amount of CO_2 collected compromised when catalyst wires become "tired"? Tests could be conducted to determine how often catalyst wires need to be refreshed.
- What is the optimal lifetime of clean-up chemicals located in the oxidation chamber? This knowledge is needed to fully realise the improvement of including sulphur clean-up within RP processing itself.
- Does CuO in the oxidation chamber absorb room air between runs, adding modern carbon contamination? Can the amount of CuO used in collection tubes as an oxygen source for recombustion (if required) be reduced from ~200mg to the ~40mg size used at USF?
- Do flow rates affect thermograph shape? Flow rates could be deliberately altered to test this influence.

Despite these remaining questions and issues, a functional RP system was designed and built in the course of this study. Radiocarbon ages have been determined for splits taken at increasing temperatures from sample material from Crystal Sound, Antarctic Peninsula, with samples being RP-processed at both USF and RRL. Radiocarbon ages for splits from RP-processing of this material generally increase with increasing temperature, reflecting the early breakdown under pyrolysis of the freshest organic components, and the breakdown at higher temperatures of older, more degraded organic components within the same material. A broad correspondence has been found for ages obtained from parallel RP-processing of the same material through the USF and RRL RP systems. This provides confidence that the new RRL RP capability can be used to provide better estimates of sedimentation ages than can be derived from bulk sediment samples alone.

Further work is required to resolve existing problems with the RRL RP system. Re-design of the two-branch CO_2 collection system to minimize the volume in which pyrolysis gases are initially captured would be beneficial. Refinement of the valves used to switch trapping states and transfer gases in the vacuum line would also be useful. The line needs to be checked for sulphur contamination, with parts cleaned or replaced as necessary. If the CO_2 collection system is re-designed or major parts replaced, a new set of background checks with blanks and standards to assess contamination introduced by RP processing would be required.

Whether or not modifications are made to the system, the number of background blanks and standards processed will increase over time, enabling more accurate assessment of contamination introduced by RP processing. This will allow for reduction of the uncertainties in radiocarbon ages for splits.

7 References

Andrews, J.T., Domack, E.W., Cunningham, W.L., Leventer, A., Licht, K.J., Timothy Jull, A.J., DeMaster, D.J., and Jennings, A.E. 1999. Problems and Possible Solutions Concerning Radiocarbon Dating of Surface Marine Sediments, Ross Sea, Antarctica. *Quaternary Research* 52:206–216.

Anderson, E.C., Libby, W.F., Weinhouse, S., Reid, A.F., Kirshenbaum, A.D. and Grosse, A.V. 1947. Natural radiocarbon from cosmic radiation. *Physical Review* 72(10):931-936.

Anderson, E. C. and Libby, W. F. 1951. World-wide distribution of natural radiocarbon. *Physical Review* 81(1):64-69.

Anderson, J.B., Conway, H., Bart, P.J., Witus, A.E., Greenwood, S.L., McKay, R.M., Hall, B.L., Ackert, R.P., Licht, K., Jakobsson, M. and Stone, J.O. 2014. Ross Sea paleo-ice sheet drainage and deglacial history during and since the LGM. *Quaternary Science Reviews* 100:31-54.

Arnold, J.R. and Libby, W.F. 1951. Radiocarbon dates. *Science* 113:111-120.

Baisden, W.T., Prior, C.A., Chambers, D., Canessa, S., Phillips, A., Bertrand, C., Zondervan, A. and Turnbull, J.C. 2013. Radiocarbon sample preparation and data flow at Rafter: accommodating enhanced throughput and precision. *Nuclear Instruments and Methods in Physics Research B* 294:194–8.

Baroni, C. and Hall, B.L. 2004. A new Holocene relative sea-level curve for Terra Nova Bay, Victoria Land, Antarctica. *Journal of Quaternary Science* 19(4):377-396.

Bentley, M.J., O Cofaigh, C., Anderson, J.B., Conway, H., Davies, B.J., Graham, A.G.C., Hillenbrand, C., Hodgson, D.A., Jamieson, S.S.R., Larter, R.D., Mackintosh, A., Smith, J.A., Verleyen, E., Ackert, R.P., Bart, P.J., Berg, S., Brunstein, D., Canals, M., Colhoun, E.A., Crosta, X., Dickens, W.A., Domack, E., Dowdeswell, J.A., Dunbar, R., Ehrmann, W., Evans, J., Favier, V., Fink, D., Favier, C.J., Glasser, N.F., Gohl, K., Golledge, N.R., Goodwin, I., Gore, D.B., Greenwood, S.L., Hall, B.L., Hall, K., Hedding, D.W., Hein, A., Hocking, E.P., Jakobsson, M., Johnson, J.S., Jomelli, V., Jones, R.S., Klages, J.P., Kristoffersen, Y., Kuhn, G., Leventer, A., Licht, K., Lilly, K., Lindow, J., Livingstone, S.J., Masse, G., Mcglone, M.S., McKay, R.M., Melles, M., Miura, H., Mulvaney, R., Nel, W., Nitsche, F.O., O'Brien, P.E., Post, A.L., Roberts, S.J., Saunders, K.M., Selkirk, P.M., Simms, A.R., Spiegel, C., Stolldorf, T.D., Sugden, D.E., Van Der Putten, N., Van Ommen, T., Verfaillie, D., Vyverman, W., Wagner, B., White, D.A., Witus, A.E. and Zwartz, D. 2014. A community-based geological reconstruction of Antarctic Ice Sheet deglaciation since the Last Glacial Maximum. *Quaternary Science Reviews* 100:1–9.

Berkman P.A. and Forman, S.L. 1996. Pre-bomb radiocarbon and the reservoir correction for calcareous marine species in the Southern Ocean. *Geophysical Research Letters* 23(4):363–366.

Chen, W.H., Wang, C.W., Kumar, G., Rousset, P. and Hsieh, T.H. 2018. Effect of torrefaction pretreatment on the pyrolysis of rubber wood sawdust analyzed by Py-GC/MS. *Bioresource Technology* 259: 469-473.

Coplen, T.B. 1994. Reporting of stable hydrogen, carbon, and oxygen isotopic abundances. *Pure and Applied Chemistry* 66:273-276.

Corran, R., Norris, M., Turnbull, J.C., Zondervan, A. and Phillips, A. *in prep.* Organic sample pretreatment for radiocarbon measurement at the Rafter Radiocarbon Laboratory.

Craig, H. 1953. The geochemistry of the stable carbon isotopes. *Geochimica et Cosmochimica Acta* 3(2):53-92.

Craig, H. 1954. Carbon 13 in Plants and the Relationships between Carbon 13 and Carbon 14 Variations in Nature. *The Journal of Geology* 62(2):115-149.

Craig, H. 1957. Isotopic standards for carbon and oxygen and correction factors for mass-spectrometric analysis of carbon dioxide. *Geochimica et Cosmochimica Acta* 12(1):133-149.

de Vries, H. 1958. Variation of Radiocarbon in Plants, Shells, and Snails in the Past 4 Years. *Science* 128:250-251.

Domack, E.W., Taviani, M. and Rodriguez, A. 1999. Recent sediment remolding on a deep shelf, Ross Sea: implications for radiocarbon dating of Antarctic marine sediments. *Quaternary Science Reviews* 18:1445-1451.

Donahue, D.J., Linick, T.W. and Jull, A.J.T. 1990. Isotope-Ratio and Background Corrections for Accelerator Mass Spectrometry Radiocarbon Measurements. *Radiocarbon* 32:135-142.

Eglinton, T.I., Aluwihare, L.I., Bauer, J.E., Druffel, E.R. and McNichol, A.P. 1996. Gas chromatographic isolation of individual compounds from complex matrices for radiocarbon dating. *Analytical Chemistry* 68(5):904-912.

Eglington, T.I., Benitez-Nelson, B.C., Pearson, A., McNichol, A.P., Bauer, J.E. and Druffel, E.R.M. 1997. Variability in radiocarbon ages of individual organic compounds from marine sediments. *Science* 277:296–299.

Fahrni, S.M., Southon, J.R., Santos, G.M., Palstra, S.W.L., Meijer, H.A.J. and Xu, X. 2017. Reassessment of the $^{13}C/^{12}C$ and $^{14}C/^{12}C$ isotopic fractionation ratio and its impact on high-precision radiocarbon dating. *Geochimica et Cosmochimica Acta* 213:330-345.

Fernandez, A., Santos, G.M., Williams, E.K., Pendergraft, M.A., Vetter, L. and Rosenheim, B.E. 2014. Blank Corrections for Ramped Pyrolysis Radiocarbon Dating of Sedimentary and Soil Organic Carbon. *Analytical Chemistry* 86(24):12085-12092.

Gao, N., Li, A., Quana, C., Du, L. and Dua, Y. 2013. TG–FTIR and Py–GC/MS analysis on pyrolysis and combustion of pine sawdust. *Journal of Analytical and Applied Pyrolysis* 100:26–32.

Godwin, H. 1962. Half-life of radiocarbon. *Nature* 195:984.

Golledge, N.R., Kowalewski, D.E., Naish, T.R., Levy, R.H., Fogwill, C.J. and Gasson, E.G.W. 2015. The multi-millennial Antarctic commitment to future sea-level rise. *Nature* 526:421-425.

Gordon, J.E. and Harkness, D.D., 1992: Magnitude and geographic variation of the radiocarbon content in Antarctic marine life: Implications for reservoir corrections in radiocarbon dating. *Quaternary Science Reviews* 11:697-708.

Gurfinkel, D.M. 1987. An assessment of laboratory contamination at the Isotrace Radiocarbon Facility. Radiocarbon 29:335-346.

Hoefs, J. 2015. *Stable isotope geochemistry*. Springer.

IPCC. 2014: *Climate Change 2014: Synthesis Report. Contribution of Working Groups I, II and III to the Fifth Assessment Report of the Intergovernmental Panel on Climate Change* [Core Writing Team, R.K. Pachauri and L.A. Meyer (eds.)]. IPCC, Geneva, Switzerland, 151 pp.

Jennings, A.E., Xiao, J., Licht, K.J. and Andrews, J.T. 1995. Benthic foraminiferal assemblages from the western Ross Sea: Approximately 30,000 years ago to present. *Antarctic Journal of the United States* 30(5):26-28.

Jo, Sang-Hee ; Kim, Ki-Hyun ; Kim, Yong-Hyun. 2016. A novel quantitation method for phthalates in air using a combined thermal desorption/gas chromatography/mass spectrometry application. *Analytica Chimica Acta*, 944:29–36.

Libby, W.F. 1946. Atmospheric helium three and radiocarbon from cosmic radiation. *Physical Review* 69(11–12):671-672.

Libby, W. F. 1956. Radiocarbon dating. *American Scientist* 44(1):98-112.

Licht, K.J., Jennings, A.E., Andrews, J.T., and Williams, K.M., 1996, Chronology of late Wisconsin ice retreat from the western Ross Sea, Antarctica: *Geology* 24:223–226.

Licht, K.J. and Andrews, J.T. 2002. The ^{14}C Record of Late Pleistocene Ice Advance and Retreat in the Central Ross Sea, Antarctica. *Arctic, Antarctic, and Alpine Research* 34(3):324-333.

Lisiecki, L.E. and Raymo, M.E. 2005. A Pliocene-Pleistocene stack of 57 globally distributed benthic δ18O records. *Paleoceanography* 20:PA1003.

Litherland, A.E. 1980. Ultrasensitive mass spectrometry with accelerators. *Annual Review of Nuclear and Particle Science* 301:437-473.

Lorrey, A.M., Boswijk, G., Hogg, A., Palmer, J.G., Turney, C.S.M., Anthony M. Fowler, A.M., John Ogden, J. and Woolley, J.M. 2018. The scientific value and potential of New Zealand swamp kauri. *Quaternary Science Reviews* 183:124–139.

Marra, M.J., Alloway, B.V. and Newnham, R.M. 2006. Paleoenvironmental reconstruction of a well-preserved Stage 7 forest sequence catastrophically buried by basaltic eruptive deposits, northern New Zealand. *Quaternary Science Reviews* 25:2143–2161.

McKay, R.M., Dunbar, G.B., Naish, T.R., Barrett, P.J., Carter, L., and Harper, M. 2008. Retreat history of the Ross Ice Sheet (Shelf) since the Last Glacial Maximum from deep-basin sediment cores around Ross Island: *Palaeogeography, Palaeoclimatology, Palaeoecology* 260:245–261.

McKay, R.M., Golledge, N.R., Maas, S., Naish, T., Levy, R., Dunbar, G. and Kuhn, G. 2016. Antarctic marine ice-sheet retreat in the Ross Sea during the early Holocene. *Geology* 44:7-10.

Mosola, A.B. and Anderson, J.B. 2006. Expansion and rapid retreat of the West Antarctic Ice Sheet in eastern Ross Sea: possible consequence of over-extended ice streams? *Quaternary Science Reviews* 25 (17–18):2177-2196.

Nier, A.O. and Gulbransen, E.A. 1939. Variations in the relative abundance of the carbon isotopes. *Journal of the American Chemical Society* 61:697-698.

Ohkouchi, N., Eglinton, T.I. and Hayes, J.M., 2003. Radiocarbon dating of individual fatty acids as a tool for refining Antarctic margin sediment chronologies. *Radiocarbon* 45:17–24.

Ohkouchi, N. and Eglington, T.I. 2008. Compound-specific radiocarbon dating of Ross Sea sediments: a prospect for constructing chronologies in high-latitude oceanic sediments. *Quaternary Geochronology* 3:235–243

Olsson, I.U. 1970. The use of Oxalic acid as a Standard. In: Olsson, I.U. (Ed.) *Radiocarbon Variations and Absolute Chronology, Nobel symposium, 12th Proc*. John Wiley & Sons, New York. p 17.

Pendergraft, M.A, Dicer, Z., Sericano, J.L., Wade, T.L., Kolasinski, J. and Rosenheim, B.E. 2013. Linking ramped pyrolysis isotope data to oil content through PAH analysis. *Environmental Research Letters* 8:044038.

Pendergraft, M.A. and Rosenheim, B.E. 2014. Varying relative degradation rates of oil in different forms and environments revealed by ramped pyrolysis. *Environmental Science & Technology* 48:10966–10974.

Plante, A.F., Beaupré, S.R., Roberts, M.L. and Baisden, T. 2013. Distribution of radiocarbon ages in soil organic matter by thermal fractionation. *Radiocarbon* 55:1077-1083.

Polach, H.A. 1979. Correlation of 14C activity of NBS oxalic acid with Arizona 1850 wood and ANU sucrose standards. In: Berger, R. and Suess, H.E. (Eds). *Radiocarbon Dating. Proceedings of the 9th International 14C Conference*. University of California Press.

Popescu, M.C., Popescu, C.M., Lisa, G. and Sakata, Y. 2011. Evaluation of morphological and chemical aspects of different wood species by spectroscopy and thermal methods. *Journal of Molecular Structure* 988:65–72.

Reimer, P.J. and Reimer, R.W. 2001. A marine reservoir correction database and on-line interface. *Radiocarbon* 43:461–463.

Reimer, P.J., Bard, E., Bayliss, A., Beck, J.W., Blackwell, P.G., Bronk Ramsey, C., Buck, C.E., Cheng, H., Edwards, R.L., Friedrich, M., Grootes, P.M., Guilderson, T.P., Haflidason, H., Hajdas, I., Hatté, C., Heaton, T.J., Hoffmann, D.L., Hogg, A.G., Hughen, K.A., Kaiser, K.F., Kromer, B., Manning, S.W., Niu, M., Reimer, R.W., Richards, D.A., Scott, E.M., Southon, J.R., Staff, R.A., Turney, C.S. M., Plicht, J.V.D. 2013. IntCal13 and Marine13 radiocarbon age calibration curves 0–50,000 years cal BP. *Radiocarbon* 55: 1869-1887.

Roberts, M.L. and Southon, J.R. 2007. A preliminary determination of the absolute $^{14}C/^{12}C$ ratio of OX-I. *Radiocarbon* 49:441-445.

Robinson, C. and Smith, D.B. 1984. The auto-ignition temperature of methane. *Journal of Hazardous Materials* 8:199–203.

Rosenheim, B.E., Day, M.B., Domack, E.W., Schrum, H., Benthien, A. and Hayes, J.M. 2008. Antarctic sediment chronology by programmed-temperature pyrolysis; methodology and data treatment. *Geochemistry, Geophysics, Geosystems* 9(4):Q04005.

Rosenheim, B.E., and Galy, V. 2012. Direct measurement of riverine particulate organic carbon age structure. *Geophysical Research Letters* 39:L19703.

Rosenheim, B.E., Santoro, J.A., Gunter, M. and Domack, E.W. 2013a. Improving Antarctic sediment ^{14}C dating using ramped pyrolysis: An example from the Hugo Island trough. *Radiocarbon* 55:115-126.

Rosenheim, B.E., Roe, K.M., Roberts, B.J., Kolker, A.S., Allison, M.A. and Johannesson, K.H. 2013b. River discharge influences on particulate organic carbon age structure in the Mississippi/Atchafalaya River System. *Global Biogeochemical Cycles* 27: 154–166.

Rosman, J.R. and Taylor, P.D. 1998. Isotopic compositions of the elements (technical report): commission on atomic weights and isotopic abundances. *Pure and Applied Chemistry* 70:217–235.

Rozanski, K., Stichler, W., Gonfiantini, R., Scott, E.M., Beukens, R.P., Kromer, B. and Vanderplicht, J. 1992. The IAEA C-14 intercomparison exercise 1990. *Radiocarbon* 34:506–519.

Salvi, C., Busetti, M., Marinoni, L., and Brambati, A. 2006. Late Quaternary glacial marine to marine sedimentation in the Pennell Trough (Ross Sea, Antarctica). *Palaeogeography, Palaeoclimatology, Palaeoecology* 231:199–214.

Santos, G.M., Southon, J.R., Griffin, S., Beaupre, S.R. and Druffel, E.R.M. 2007. Ultra small-mass AMS ^{14}C sample preparation and analyses at KCCAMS/UCI Facility. *Nuclear Instruments and Methods in Physics Research B* 259:293−302.

Santos, G.M. and Ormsby, K. 2013. Behavioral variability in ABA chemical pretreatment close to the ^{14}C age limit. *Radiocarbon* 55:534–544.

Schreiner, K.M., Bianchi, T.S. and Rosenheim, B.E. 2014. Evidence for permafrost thaw and transport from an Alaskan North Slope watershed. *Geophysical Research Letters* 41:3117–3126.

Sharp, Z. 2001. *Principles of Stable Isotope Geochemistry*. Pearson Prentice Hall.

Southon, J.R. and Magana, A.L. 2010. A comparison of cellulose extraction and ABA pretreatment methods for AMS 14C dating of ancient wood. *Radiocarbon* 52:1371–1379.

Stuiver, M. and Suess, H.E. 1966. On the relationship between radiocarbon dates and true sample ages. *Radiocarbon* 8:534-540.

Stuiver, M. and Robinson, S.W. 1974. University of Washington Geosecs North Atlantic carbon-14 results. *Earth and Planetary Science Letters* 23:87–90.

Stuiver, M. and Polach, H.A. 1977. Reporting of C-14 data—discussion. *Radiocarbon* 19:355–363.

Stuiver, M., Pearson, G.W. and Braziunas, T. 1986. Radiocarbon age calibration of marine samples back to 9000 cal yr BP. *Radiocarbon* 28:980–1021.

Stuiver, M. and Braziunas, T.F. 1993. Modeling atmospheric 14C influences and 14C ages of marine samples to 10,000 BC. *Radiocarbon* 35:137–89.

Subt, C., Fangman, K.A., Wellner, J.S. and Rosenheim, B.E. 2016. Sediment chronology in Antarctic deglacial sediments: Reconciling organic carbon ^{14}C ages to carbonate ^{14}C ages using Ramped PyrOx. *Holocene* 26(2):265–273.

Subt, C., Yoon, H.I., Yoo, K.C., Lee, J.I., Leventer, A., Domack, E.W. and Rosenheim, B.E. 2017. Sub-ice shelf sediment geochronology utilizing novel radiocarbon methodology for highly detrital sediments. *Geochemistry, Geophysics, Geosystems* 18(4):1404-1418.

Suess, H.E. 1955. Radiocarbon concentration in modern Wood. *Science* 122:415-417.

Taylor, R.E. 1987. *Radiocarbon dating: an archaeological perspective*. Academic Press.

Trumbore, S.E., Sierra, C.A. and Hicks Pries, C.E. 2016a. Radiocarbon Nomenclature, Theory, Models, and Interpretation: Measuring Age, Determining Cycling Rates, and Tracing

Source Pools. In: Schuur, E.A.G., Druffel, E.R.M. and Trumbore, S.E. (Eds). *Radiocarbon and Climate Change: Mechanisms, Applications and Laboratory Techniques*. Springer.

Trumbore, S.E., Xu, X., Santos, G.M., Czimczik, C.I., Beaupré, S.R., Pack, M.A., Hopkins, F.M., Stills, A., Lupascu, M. and Ziolkowski, L. 2016b. Preparation for Radiocarbon Analyisis. In: Schuur, E.A.G., Druffel, E.R.M. and Trumbore, S.E. (Eds). *Radiocarbon and Climate Change: Mechanisms, Applications and Laboratory Techniques*. Springer.

Turnbull, J.C., Lehman, S.J., Miller, J.B., Sparks, R.J., Southon, J.R. and Tans, P.P. 2007. A new high precision $^{14}CO_2$ time series for North American continental air. *Journal of Geophysical Research* 112:D11310.

Turnbull, J.C., Zondervan, A., Kaiser, J., Norris, M., Dahl, J., Baisden, T. and Lehman, S. 2015. High-Precision Atmospheric 14 CO 2 Measurement at the Rafter Radiocarbon Laboratory. *Radiocarbon* 57:377-388.

Urey, H.C., Lowenstam, H.A., Epstein, S. and McKinney, C.R. 1951. Measurement of paleotemperatures and temperatures of the Upper Cretaceous of England, Denmark and the Southeastern United States. *Bulletin of the Geological Society of America* 62: 399-416.

Wang, S., Dai, G., Yang, H. and Luo, Z. 2017. Lignocellulosic biomass pyrolysis mechanism: A state-of-the-art review. *Progress in Energy and Combustion Science* 62:33–86

Williams, E.K., Rosenheim, B.E., Mcnichol, A.P. and Masiello, C.A. 2014. Charring and non-additive chemical reactions during ramped pyrolysis: Applications to the characterization of sedimentary and soil organic material. *Organic Geochemistry* 77:106-114.

Williams. P.T. and Besler, S. 1996. Influence of temperature and heating rate on the slow pyrolysis of biomass. *Renewable Energy* 7(3):233–250.

Xu, X.M., Trumbore, S.E., Zheng, S.H., Southon, J.R., McDuffee, K.E., Luttgen, M. and Liu, J.C. 2007. Modifying a sealed tube zinc reduction method for preparation of AMS graphite targets: Reducing background and attaining high precision. *Nuclear Instruments & Methods in Physics Research Section B-Beam Interactions with Materials and Atoms* 259:320–329.

Yamane, M., Yokoyama, Y., Miyairi, Y. and Suga, H. 2014. Compound-Specific ^{14}C Dating of IODP Expedition 318 Core U1357A Obtained Off the Wilkes Land Coast, Antarctica. *Radiocarbon* 56:1009-1017.

Yang, H., Yan, R., Chen, H., Lee, D.H., Zheng, C., 2007. Characteristics of hemicellulose, cellulose and lignin pyrolysis. *Fuel* 86:1781–1788.

Yokoyama, Y., Anderson, J.B., Yamane, M., Simkins, L.M., Miyairi, Y., Yamazaki, T., Koizumi, M., Suga, H., Kusahara, K., Prothro, L. and Hasumi, H. 2016. Widespread collapse of

the Ross Ice Shelf during the late Holocene. *Proceedings of the National Academy of Sciences* 113(9):2354-2359.

Zhao, C., Jiang, E. and Chen, A. 2017. Volatile production from pyrolysis of cellulose, hemicellulose and lignin. *Journal of the Energy Institute* 90:902–913.

Zondervan, A., Hauser, T., Kaiser, J., Kitchen, R., Turnbull, J.C. and West, J.G. 2015. XCAMS: the compact 14C accelerator mass spectrometer extended for 10Be and 26Al at GNS Science, New Zealand. *Nuclear Instruments and Methods in Physics Research B* 361:25–33.

8 Appendix

Table 8.1: Summary of USF RP system runs and maintenance during visit for this study, May 2018. Each USF RP run is uniquely identified by a run number, for this visit beginning with DB-1765 (DB for "Dirt Burner"; run numbering is continuous from initial runs at Woods Hole).

Date	Run / Action	Sample / Part	Aim / Issue – Notes	Result
7/5/2018	Maintenance	CO_2 analyser	CA-10 analyser showing too much fluctuation in [CO_2] readings (>20ppm)	Replaced
7/5/2018	Maintenance	CO_2 trap	Inlet tube broken during CO_2 analyser replacement by falling part	Replaced
7/5/2018	DB-1765	graphite	Blank run for 1 split – collection from 650°C; split taken at 1008°C	Successful
8/5/2018	DB-1766	R41115/2	Run for 5 splits	Successful
9/5/2018	DB-1767	R41115/1	Run for 5 splits – contamination spike to 400ppm at 185°C; leak at insert	Failed run
10/5/2018	DB-1768	R41115/1	Run for 5 splits – 7 splits obtained; pre-determined %TOC incorrect (low)	Successful
11/5/2018	DB-1769	R41115/3	Run for 5 splits	Successful
11/5/2018	DB-1770	Ox-I	Run for 1 split – taken at 153°C	Successful
14/5/2018	DB-1771	R41115/6	Run low %TOC sample for as many splits as possible – 5 small splits obtained	Successful
14/5/2018	DB-1772	R41115/6	Run for 1 split, for combining with split 1 from run 1771	Successful
14/5/2018	DB-1773	R41115/6	Run for 1 split, for combining with run 1771 split 1 – data file inadvertently accessed, stopping data collection	Failed run
15/5/2018	DB-1774	Ox-I	Run for 1 split – taken at 154°C	Successful
15/5/2018	DB-1775	Ox-I	Run for 1 split – taken at 147°C	Successful
15/5/2018	DB-1776	graphite	Blank run for 1 split – collection from 570°C; split taken at 1000°C	Successful
16/5/2018	DB-1777	R41115/4	Run for 5 splits – thermocouple failure after 3 splits	Failed run
16/5/2018	Maintenance	Thermocouple	For temperature controller	Replaced
16/5/2018	DB-1778	R41115/4	Run for 5 splits – temperature ramp failure after 3 splits; blown fuse	Failed run
16/5/2018	Maintenance	Fuse	For temperature controller	Replaced
16/5/2018	Test run	Fuse	Temperature ramp failure; blown fuse	Replaced
17/5/2018	Maintenance	Furnace	Furnace appears compromised – new furnace & reactor required	Replaced
17/5/2018	Cleaning run	Reactor	Baked at 525°C for 30 min	Cleaned
17/5/2018	DB-1779	R41115/5	Run for 5 splits – after 2 splits, O_2 bubbles observed in CO_2 trap	Failed run
17/5/2018	Maintenance	O_2 mass flow controller	Delivering O_2 at 30mL/min, not the 4mL/min flow required	Replaced
18/5/2018	DB-1780	Flow test	Test total flow at vent = 47mL/min	Acceptable
18/5/2018	DB-1781	graphite	Blank run for 1 split – collection from 630°C; split taken at 1011°C	Successful
18/5/2018	DB-1782	R41115/4	Run for 5 splits	Successful

Table 8.2: Summary of RRL RP system runs and maintenance from November 2018 to April 2019, with runs identified by number.

Date	Run / Action	Sample / Part	Aim / Issue – Notes	Result
15/11/2018	1	ROTO17-3C	Shape run for 1.26mgC – [CO_2] peak 611ppm at 65 mins/353^{o}C	Successful
22/11/2018	Maintenance	CuO strands	Visible outside oxidation chamber – downstream Ag wire plug more closely tangled & reinserted	Repositioned
22/11/2018	Maintenance	He and O_2 gas flows	Checked – Porter regulator pressures adjusted	Satisfactory
22/11/2018	2	ROTO17-3C	Run for 1.2mgC – splits at 60, 90, 120 mins	Successful
30/11/2018	3	ROTO17-3C	Run for 1.2mgC – splits at 300, 500, 700^{o}C – part of split 1 lost when non-condensable gases not released before transfer to cold finger; transferred back to CO_2 trap [R. Venturelli (USF) visiting]	Largely successful
30/11/2018	4	ROTO17-3C	Run for 5 splits – splits at 300, 450, 600, 700^{o}C [R.V. visiting]	Successful
6/12/2018	5	R41115/2	Run for 5 splits – splits at 286, 350, 417, 532, 771^{o}C (as at USF) – thermograph shows strong [CO_2] oscillations	Successful
12/12/2018	Maintenance	Cold finger	Calibration → volume = 9.6	Calibrated
11/1/2019	6	R41115/2	Shape run for 1.2mgC – hysteresis still prominent in thermograph	Successful
15/1/2018	Maintenance	Temperature controller	Proportional cycle time changed for 4 sec to 0.5 sec	Adjusted
16/1/2019	Maintenance	CuO strands	Visible beyond furnace – changed; new Ag plug inserted to Ni brace to cajon to prevent Ag moving	Replaced
16/1/2019	Maintenance	Pyrolysis thermocouple	Position changed from mid-furnace to between furnace bore & reactor glass at sample location	Repositioned
18/1/2019	7	R41115/2	Shape run for 1.2mgC – smooth temperature ramp, thermograph shape also smooth	Successful
22/1/2019	8	R41115/2	Shape run for 1.2mgC – shape close to USF shape	Successful
23/1/2019	9	R41115/2	Shape run for 1.2mgC – sample reground at weighing, yield ↑ 10%; shape close to USF shape	Successful
25/1/2019	10	R41115/3	Shape run for 1.2mgC – thermograph peak poorly defined	Successful
29/1/2019	11	R41115/3	Shape run for 1.2mgC – apparent contamination spike at ~235^{o}C, thermograph shape close to USF's	Successful

30/1/2019	12	R41115/2	Run for 5 splits – splits at 48, 62, 85, 108, 150 mins – furnace accidentally turned off	Failed run
1/2/2019	13	R41115/2	Repeat of Run 12 – splits at 48, 62, 85, 108, 150 mins – no dry ice available, so made slush USF way, using alcohol & lN$_2$	Successful
5/2/2019	14	Kauri blank	Run for 0.5mgC, 1 split at 850^{o}C – sample lost during transfer – apparent leak in vacuum line	Failed run
12/2/2019	Maintenance	Vacuum line	Leak at valve M sealed with melted quartz blob	Leak sealed
12/2/2019	Maintenance	He and O_2 gas flows	Checked – Porter regulator pressures adjusted	Satisfactory
13/2/2019	15	Kauri blank	Run for 0.5mgC, 1 split at 900^{o}C – yield 144%; water present?	Successful
15/2/2019	16	Kauri blank	Run for 0.5mgC, 1 split at 700^{o}C – yield 151%; water present?	Successful
20/2/2019	17	Kauri blank	Run for 0.5mgC, 1 split at 800^{o}C – CO_2 transferred through extra water trap after cold finger, but no pressure reduction, yield 162%; then run through combustion processing line, yield 136%; water present?	Successful
22/2/2019	18	Kauri blank	Run for 0.2 mgC, 1 split at 700^{o}C – yield 148%; water present?	Successful
25/2/2019	19	Quartz wool plug only	Contamination test, run to 900^{o}C – 0.1mgC collected, shape has peaks at about 130, 240 & 330^{o}C	Contamination found: conclude all previous runs contaminated
25/2/2019	20	Clean-handled insert only	Contamination test, run to 900^{o}C – tiny initial hump, thermograph otherwise flat	No contamination found
27/2/2019	21	Qz wool pre-baked inside insert	Contamination test, run to 900^{o}C – thermograph flat	No contamination found
1/3/2019	22	Clean-stored qz wool only	Contamination test, run to 900^{o}C – tiny peak (19ppm) at ~62^{o}C, thermograph otherwise flat	Tiny handling contamination found
4/3/2019	23	OX-I standard	Run to 900^{o}C for 0.5mgC – giant peak, with 3 subpeaks (Facilities checking gas tanks during run); yield 129%	Successful
5/3/2019	24	OX-I standard	Run to 250^{o}C for 0.5mgC – yield 111%	Successful
5/3/2019	25	OX-I standard	Run to 250^{o}C for 0.2mgC – sample lost at transfer from cold finger	Failed run
6/3/2019	26	OX-I standard	Run to 250^{o}C for 0.2mgC – 2 subpeaks; yield 105%	Successful

7/3/2019	27	Kauri blank	Run to 700ºC for 0.5mgC – CO_2 collection from pyrolysis furnace switch-on, yield 130%	Successful
8/3/2019	28	OX-I standard	Run to 250ºC for 0.1mgC – yield 123%	Successful
11/3/2019	29	Kauri blank	Run to 705ºC for 0.5mgC – for 1st attempt at this run, thermocouple not positioned correctly, so run re-started with pyrolysis furnace temperature at 59ºC – CO_2 collection from 105ºC, yield 118%	Successful
12/3/2019	30	Clean-stored qz wool only	Contamination test, run to 900ºC – CO_2 collection from 105ºC	No contamination
13/3/2019	31	R41115/2	Run for 1.2mgC, 1 split at 900ºC – collection from 105ºC, yield 106% – gas appeared yellow	Successful, but sulphur contamination
14/3/2019	Maintenance	Clean-up chemicals	Fresh catalyst wires & clean-up chemicals loaded into clean reactor & oxidation chamber	Clean-up chemicals replaced
14/3/2019	Maintenance	He and O_2 gas flows	Checked – no adjustment to Porter regulators needed	Satisfactory
14/3/2019	32	Qz wool only	Conditioning run to 900ºC – steep spike to 700ppm within 4 mins of combustion furnace on, 2nd spike to 250ppm after 8 mins, slight humps at ~300ºC & ~400ºC – 0.22mgC collected	Clean-up chemicals conditioned
15/3/2019	33	Run 32 insert & qz wool	Contamination test, run to 900ºC – thermograph flat	No contamination
18/3/2019	34	Kauri blank	Run for 0.5mgC, 1 split at 900ºC – collection from 105ºC, yield 128%	Successful
19/3/2019	35	Kauri blank	Run for 0.5mgC, 1 split at 800ºC – collection from 105ºC, yield 129%	Cancelled at graphite – bad seal?
20/3/2019	36	Kauri blank	Run for 0.2mgC, 1 split at 900ºC – collection from 105ºC, yield 136%	Successful
21/3/2019	37	R41115/2	Run for 1.2mgC, 1 split at 900ºC – collection from 105ºC, yield 99% – gas appeared pale yellow	Successful, but sulphur contamination
22/3/2019	Maintenance	Clean-up chemicals	Fresh clean-up chemicals loaded into oxidation chamber, Ag wire loaded as dense plugs, 1 upstream & 3 downstream of CuO	Clean-up chemicals replaced
25/3/2019	38	Qz wool only	Conditioning run to 900ºC – [CO_2] spike to 200ppm at ~3mins from combustion furnace on, 2nd tiny spike at 5 mins, & tiny handling peak 10ppm at 14 mins (pyrolysis furnace temperature 125ºC)	Clean-up chemicals conditioned
26/3/2019	39	R41115/2	Run for 1.2mgC, 1 split at 900ºC – for 1st attempt at this run, thermocouple not positioned correctly, so run re-started;	Successful, but sulphur contamination

			collection from 110ºC, yield 106% – gas appeared yellow	
27/3/2019	40	R41115/2	Run for 1.2mgC, 1 split at 900ºC – collection from ambient, yield 106% – gas appeared yellow	Successful, but sulphur contamination
28/3/2019	41	OX-I standard	Run to 900ºC for 0.5mgC to check for S contamination – collection from ambient, gases collected colourless, yield 116%	Successful, but failed in graphite: line contaminated
29/3/2019	42	Kauri blank	Run for 0.1mgC, 1 split at 705ºC – collection from 105ºC, yield 207%	Successful
1/4/2019	43	Qz wool only	Contamination test, run to 900ºC – thermograph flat	Successful
2/4/2019	44	R41115/2	Run for 5 splits – splits at 280, 340 (taken at 347), 410 (taken at 418), 525, 900ºC – samples collected into tubes each loaded with 200-230mg CuO & 2 Ag wires – gases pale yellow for largest split (4)	Successful – samples for recombustion
3/4/2019	45	Kauri blank	Run for 0.1mgC, 1 split at 900ºC – collection into tube pre-loaded with CuO & Ag wire, yield 214%	Successful – sample for recombustion
4/4/2019	46	Kauri blank	Run for 0.2mgC, 1 split at 705ºC – collection into tube pre-loaded with CuO & Ag wire, yield 147%	Successful – but potentially dirty CuO used
4/4/2019	47	Kauri blank	Run for 0.2mgC, 1 split at 800ºC – collection into tube pre-loaded with CuO & Ag wire, yield 163%	Successful – but potentially dirty CuO used
5/4/2019	48	Kauri blank	Run for 0.1mgC, 1 split at 800ºC – collection into tube pre-loaded with CuO & Ag wire, yield 254%	Successful – but potentially dirty CuO used
8/4/2019	49	Kauri blank	Run for 0.5mgC, 1 split at 900ºC – collection into tube pre-loaded with CuO & Ag wire, yield 132%	Successful – but potentially dirty CuO used
9/4/2019	50	Kauri blank	Run for 0.5mgC, 1 split at 800ºC – collection into tube pre-loaded with CuO & Ag wire, yield 128%	Sample lost during graphitisation
10/4/2019	51	Kauri blank	Run for 0.5mgC, 1 split at 800ºC – collection into tube pre-loaded with CuO & Ag wire, yield 134%	Successful – but potentially dirty CuO used